People's Democratic Republic of Algeria
Ministry of Higher Education and Scientific Research
Ferhat Abbas-Setif1 University
Faculty of Sciences
Department of Physics

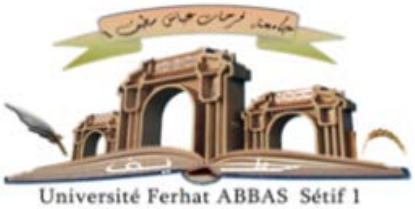

Thesis Submitted for the Degree of Doctor 3rd Cycle LMD of Physics in Physics and Subatomic Engineering

Title:

Thermoluminescence dating of terracotta bricks and study of clay provenance at the site of the antic roman city "Cuicul-Djemila" of Setif

Presented by: **BOUDRAA Lahcene**

Board of Examiners:

Pr. BOUCENNA Ahmed	University of Setif1	President
Pr. KHARFI Fayçal	University of Setif1	Thesis Director
Pr. AMRANI Naima	University of Setif1	Examiner
Dr. ANNANE Salim	University of Algiers 2	Examiner
Mr. SELLAMI Mohamed Tewfik	Djemila Site Museum-Setif	Invited

-January 27, 2021-

Acknowledgment

Throughout the writing of this dissertation, I have received a great deal of support and assistance.

Firstly, I would like to express my sincere gratitude to my thesis director **Prof. Fayçal Kharfi** for the continuous support of my doctoral study and related research, for his patience, motivation, and immense knowledge. His guidance helped me in all the time of research and writing of this thesis. I could not have imagined having a better advisor and mentor for my doctoral study.

Besides my thesis director, I would like to thank my thesis committee: Prof. A. Boucenna, Prof. N. Amrani, Dr. S. Annane and Mr. M.T. Sellami, for their insightful comments and questions.

My sincere thanks also go to Mr. M. Bouhzam and, Mr. M.T. Sellami, from the Archaeological Museum of Djemila-Setif, for their precious support and for having accepting to give me the opportunity to work on Cuicul-Djemila site.

I would also like to extend my thanks to all laboratories that helped us to perform the necessary analysis.

Finally, I wish to thank my classmates, my work colleagues, and everyone who supported me.

Dedication

This thesis is dedicated to my beloved family.

Sincere thanks and gratitude are addressed to my family members. I would like to remember the root of my inspiration "my mother" who has enormous efforts and prayer behind all of my success.

My wife deserve special mention for her support, patience, sacrifice and love throughout the period of this work

Content

Chapter III: Cuicul-Djemila antic Roman City: Historical and urban development

Chapter IV: Thermoluminescence dating of Cuicul Roman city and study of the construction terra-cotta material provenance

List of Figures

List of Tables

List of Acronyms

A.D.: Anno Domini.

CB: Conduction Band.

CCD: Charge Coupled Device.

CW: Chemin de Wilaya.

EMCCD: Electron Multiplication Charge Coupled Device.

ESR: Electron Spin Resonance.

eV: Electronvolt.

FB: Forbidden Band.

FTD: Fission Track Dating.

GLSL: Green Light Stimulated Luminescence.

HF: Hydrogen fluoride.

HPGe: High-Purity Germanium.

ICP-MS: Inductively Coupled Plasma Mass Spectrometry.

IR: Infrared.

IRSL: Infrared Stimulated Luminescence.

keV: Kiloelectronvolt.

LED: Light-emitting Diode.

MAAD: Multiple Aliquot Additive Dose.

MARD: Multiple Aliquot Regenerative Dose.

MeV: Megaelectronvolt.

OSL: Optically Stimulated Luminescence.

PMT: Photomultiplier Tube.

PSL: Photon Stimulated Luminescence.

RN: Route Nationale.

SAAD: Single Aliquot Additive Dose.

SAR: Single Aliquot Regeneration.

SD: Standard Deviation.

TIMS: Thermal Ionization Mass Spectrometry.

TL: Thermoluminescence.

TLD: Thermoluminescent Dosimeter.

TSL: Thermally Stimulated Luminescence.

UNESCO: United Nations Educational, Scientific and Cultural Organization.

VB: Valence Band.

WN: Weight Normalization.

XRD: X-Ray Diffraction

XRF: X-Ray Fluorescence.

INTRODUCTION

Introduction

Archaeological dating is the process of assigning a chronological value (date) to an event or object from the past. Without the ability to date archaeological sites and elucidate the specific historical contexts found there, archaeologists would not be able to study development and cultural change with its continuity over time. No wonder, then, that so much effort has gone into developing increasingly sophisticated and precise scientific methods for determining when events have occurred in the past.

In archaeology, dating methods are subdivided into two main categories: chronometric ones (called "absolute") and relative ones. Luminescence dating belongs to the first category; it refers to age-dating methods that employ the phenomenon of luminescence to determine the amount of time that has elapsed since the occurrence of a given event. Generally, the term luminescence dating is a collective reference to numerical age-dating methods that include thermoluminescence (TL) and optically stimulated luminescence (OSL) dating techniques. Thermoluminescence refers to the one which uses heating as a source of stimulation. The potential applications of TL and the present day progress on research in this field allow it to become indispensable in dating of ancient potteries, ceramics, bricks and it has been established as an important technique in archaeological dating.

Cuilcul is one of the most beautiful ancient roman cities in Algeria. It is located near the town of Djémila, in Sétif. This ancient city was listed by UNESCO as a World Heritage Site in 1982. The settlement of *Cuicul* was built and developed for about four centuries between the second and the sixth century. The final urban development plan of the city spreads out is mainly characterized by the extension of the old city originally built on the northern part of the spur to a new city that extends to the south. Although the historical development of the city has been described by several historians, hardly any rigorous scientific studies have been conducted at the site to confirm them.

In this thesis project, it was a question of using XRF analysis and archaeological dating by thermoluminescence to place certain events and archaeological objects in their real historical context and, thus, to avoid any controversy regarding their origin. This work constitutes, in fact, a scientific reconstitution of a part of the history of the development of this ancient city by dating bricks made from terracotta and by studying the origin of their construction material (Clay) as a second objective of this work. Moreover, an accurate construction timeline map has been successfully established for the whole city by thermoluminescence dating.

This manuscript is organized into four chapters: three theoretical ones reserved for the presentation of the methods and techniques used, and a final experimental one dedicated to the presentation of the results obtained as well as their interpretations. The first chapter is, therefore, reserved for archaeological dating in its general aspect. The second chapter presents the technique of archaeological dating by thermoluminescence used in the framework of the thesis project. In the third chapter, the studied archaeological site, in this case the ancient city *Cuicul*-Djemila, is presented. Finally, in the fourth chapter, the results of the archaeological dating by thermoluminescence and of the study carried out on the provenance of the clay used in the manufacture of a certain brick of a wall near the *Caracalla's* arch are presented. A timeline map showing the chronology of the development of the city was also established by archaeological dating by thermoluminescence dating of numerous samples of bricks taken from the entire site after a meticulous urban subdivision of the city into different zones.

CHAPTER I :

Archaeological Dating

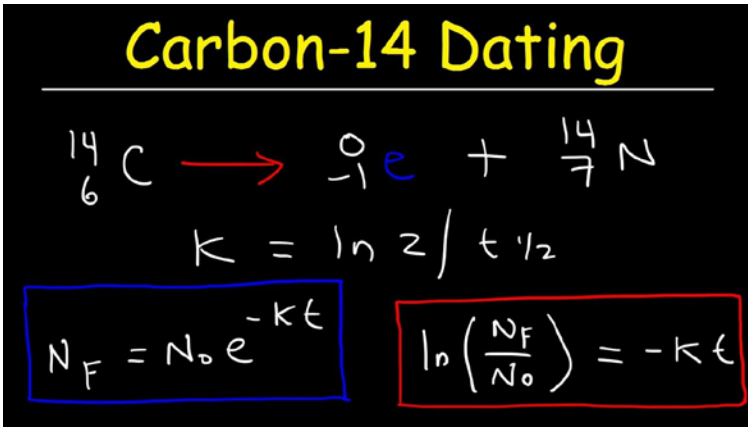

I.1 Introduction

Archaeological dating represents the attribution of a date to the age of an event, an object (document, fossil, geological layer), an action, a soil, etc. It is an essential element in the study of an archaeological site. In fact, it makes it possible to locate the site in a given chronological period and to determine the duration of its occupation. The precision and nature of the chronology are variable and depend on the methods used. We can distinguish two types of dating methods: absolute dating methods and relative dating methods [1.2]. The first give the date of the sample without taking into account the context (which then intervenes in the interpretation of the results); they make it possible to obtain calendar dates, regardless of the degree of accuracy of the date (the day, the year, century, millennium) and its precision (dating range). The latter, on the other hand, are based on the analysis of comparative data. They can also be based on a global analysis of the material found on the site, taking into account the evolution of this material. This approach allows ordering the most common events relative to each other on a relative timescale. However, the relative dating methods do not offer any precision on the absolute age expressed in number of years of the object to be dated [3].

Absolute dating methods require sample processing in the laboratory. They provide quantified results for estimating the real age of the objects to be dated or the occupation of an archaeological site, with greater or lesser precision depending on the method used [4].

I.2 Dating methods

I.2.1 Relative dating methods

I.2.1.1 Stratigraphy

Stratigraphy was before the 1950s, one of the only ways to date a site. The principles of stratigraphy in archeology are borrowed from geology, which very early on made it possible to relate the spatial positioning of layers and their temporal relationships. The study of strata, their succession, their content, allows them to be reorganized in chronological sequences [3]. Usually, each stratum is isolated into a separate chronological unit that incorporates the artifacts found in that layer of soil. On the other hand, dating using stratigraphy of the sites is sometimes based on the objects discovered in the soil strata. Indeed, certain objects of which we know the exact or approximate age are called "guiding fossils". Their presence on archaeological sites helps date soil layers, other artifacts and related events, and thus refines the chronology of a site.

Stratigraphy obeys four fundamental laws [5]:

1- The law of superposition: in a series of superimposed layers, and if no disturbance has disrupted the order of the deposits since their constitution, the upper layer is the most recent, and the lower the oldest. (This is the principle on which the chronological significance of stratigraphy is based.)

2- The law of original horizontality: any layer deposited in an unconsolidated form will tend to form a horizontal surface. The layers that are currently found with a sloping surface were therefore initially horizontal or lie in accordance with the contours of a pre-existing settling basin. This law of geological origin is more difficult to apply to human actions, which can generate deposits of voluntary slopes or deposits of lenticular forms.

3- The original law of continuity: the edges of a layer, unless they rest on an obstacle, naturally tend to adopt a wedge shape. Consequently, if a layer has a vertical front, it is the result of an accidental interruption. We must then look for the missing part or explain its absence. It is from this principle that the stratigraphic correlation results.

4- The law of stratigraphic succession: a stratigraphic unit takes place in the stratigraphic sequence between the oldest of the layers which surmount it and the most recent of the underlying layers and with which the stratigraphic unit is in direct contact.

However, the reoccupation of a space can sometimes cross-older layers. This method is nevertheless very reliable when it comes to dating objects or events in undisturbed stratigraphic levels.

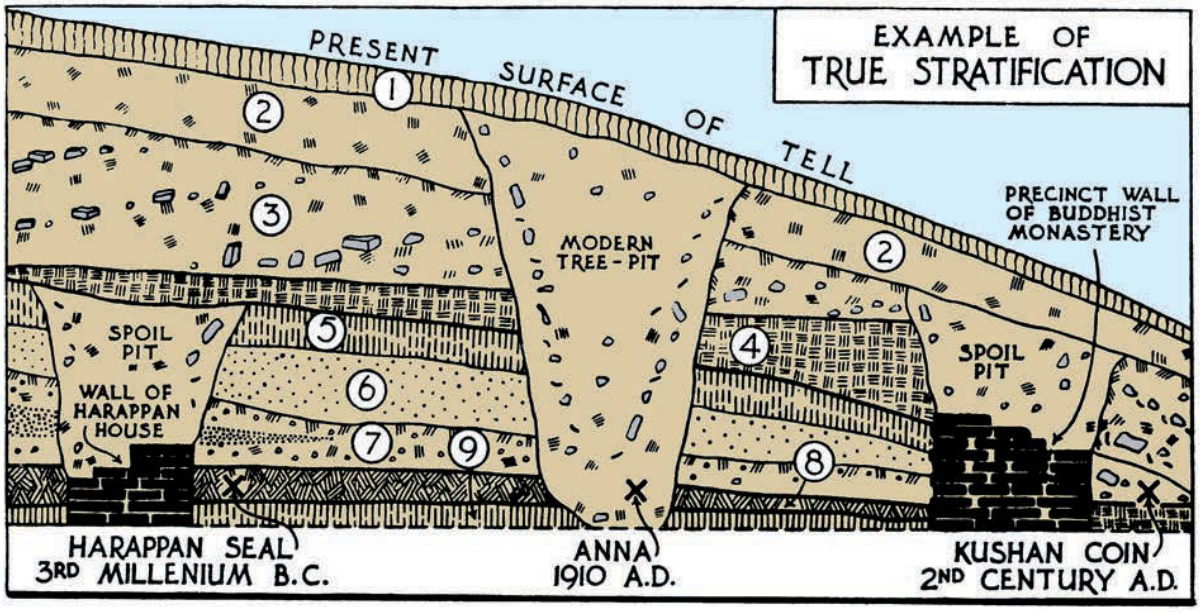

Fig I.1: Example of true stratification; drawing of a section across a tell or mound. Pit disturbance makes dating difficult, but the Harappan seal, for example (age known from similar seals found elsewhere), lies in an undisturbed context in layer 8, and can therefore help date that layer and the wall against which the layer abuts [3].

I.2.1.2 Typochronology

Typochronology is a method of comparing objects with each other, in order to classify them according to their resemblance or their difference, and to relate them to a given context or period. Frequently used when absolute dating methods cannot be used, this technique generally makes it possible to distinguish the cultural period to which a site or an object belongs, without however specifying the date of occupation.

This method is particularly applicable to material found most abundantly at sites such as ceramics. It can be done between multiple sites or within the same site or region. The typology then allows relative dating of the same objects found in excavation, i.e. a dating by type. These types are aggregates of diagnostic attributes recorded at a particular sample site at a particular time. Similarity is therefore based on the quality or quantity of diagnostic attributes that the types and data seem to share [6]. The dating of these objects can help to date a site or to illustrate the influence of a culture or its preference for a type of tool in a cultural area or at a given period.

The typological method requires, after the classification of objects, a detailed description of them according to the classes. This description should be short, expressive, but comprehensive. In the description it is necessary to show (1) the distribution, (2) the period in which the types, genera, groups and categories are known. The description of the categories must precede the description of the group; the description of the group that of the categories; the description of categories that of types. The description of each higher class should appear as a deductive introduction to the description of the immediately subordinate class. The description should be accompanied by schematic type distribution maps, to show the area of distribution of each type, and the interrelation of areas of different types between them [7].

Once the typology has been established, it can be combined with absolute dating methods which allow it to be marked with precise chronological references.

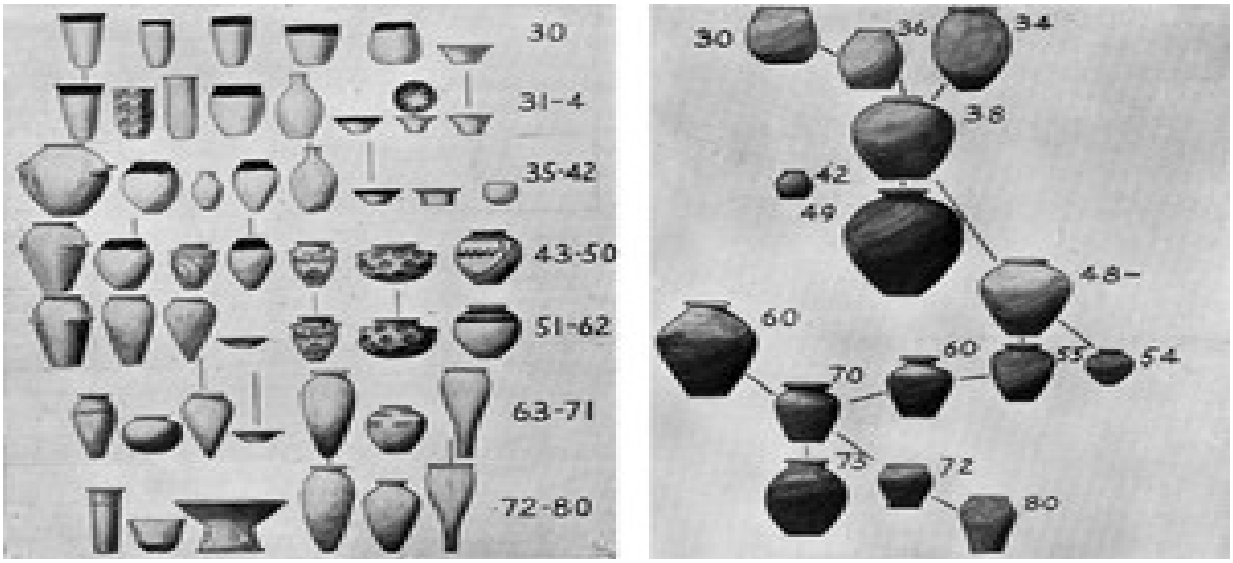

Fig I.2: Two graphic representations of Petrie's chronological ordination of archaeological types. On the left, a summary of diachronic trends articulated in seven successive stages. Some forms of diagnostic vessels show continuity between adjacent stages. Rather, the graphs on the right are an attempt at genealogical sorting. Petrie's hypothesis was one of unilinear and unidirectional change over time [6].

I.2.1.3 Seriation

Invented at the end of the 20th century by Petrie for the study of 900 predynastic tombs, seriation is a descriptive analytical technique. The aim of this method is to organize comparable units into a single dimension (i.e. along of a row) so that the position of each unit reflects its

similarity to other units, such as the shape or decoration of artifacts. Thanks to statistical methods taking into account the different objects present in a succession or a serial order, we can determine the evolution of the structure and show a chronological succession between the different parts of the latter [3]. Seriation as an archaeological method for deducing relative chronology is reviewed according to its assumptions and the conditions under which it is applicable. From this review, it is concluded that serials can be inferred as chronologies when and only when: (1) comparisons are made using historical classes; (2) the units ordered are of comparable duration; (3) the units ordered come from the same cultural tradition; and (4) when the order is repeated by several independent series [8]. As the operating principle remains the same, this method has benefited from advances in computing to allow automated processing of statistical calculations and make the process faster and more complete. Like any statistical tool, seriation must respond to hypotheses and depends on serial samples. The results, therefore, only have statistical significance in the restrictive sense of the term and it is therefore desirable to combine seriation with other methods.

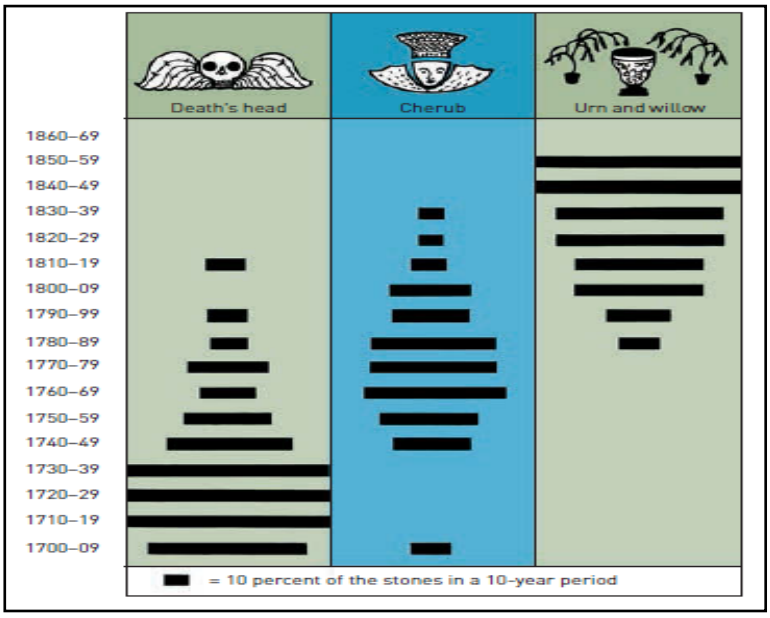

Fig I.3: Frequency seriation: changes in the popularity (or frequency) of three tombstone designs, from 1700 to 1860. Rises and falls in popularity have produced the characteristic battleship-shaped curve for the fluctuating fortunes of each design. As elsewhere in New England, the Death's head design (below; peak popularity 1710–1739) was gradually replaced by the cherub (peak 1760–1789) which in turn was replaced by the urn and willow tree (peak 1840–1859) [3].

I.2.2 Absolute dating methods

I.2.2.1 Dendrochronology

It was the American physicist and astronomer A.E. Douglass who, at the beginning of the 20th century, laid the foundations for modern dendrochronology [9, 10]. It is based on the study of annual growth rings and their precise dating. When the climate imposes on the vegetation a period of activity and a period of rest during the same calendar year, and outside the tropical context, the trees develop each year at the periphery of their trunk under the bark, a growth ring whose main physical characteristics are the width and density of the wood. The values of these characteristics vary during the life of the tree depending on internal factors (genotype, age) and external factors (climates, soil, altitude, exposure, topography, human interventions) [11, 12, 3]. The result is that sequences of rings common to several trees of the same species that have grown in the same area constitute a chronological reference point capable of synchronizing series of rings and therefore of relatively dating different pieces of wood [13].

- ✓ **Principle:**

The principle of the method is to draw a curve which indicates the thickness of each ring, in order to compare it subsequently with other curves called reference curves, to go back in time. To obtain these reference curves, the curves of several trees are established, and then an average is taken; by overlapping between trees which partly lived at the same time, we gradually go back in time. The sequence obtained for the sample is calibrated to the reference curve of the species for the region under consideration and dating is obtained for the sample [14, 15].

Dendrochronology requires four conditions:

1. The trees studied must have lived in regions subject to a seasonal rhythm inducing the formation of an annual layer of wood called a ring. Woody plants living in equatorial regions form rings, the periodicity of which is not well known; they are therefore unusable by the dendrochronologist.

2. The thickness of the rings must be limited by one or more external factors. If the external conditions satisfy all the ecological requirements of the tree, the rings will form series of constant thickness unsuitable for providing information.

3. These limiting factors must vary in intensity from one year to another according to series which are not reproducible over time, in such a way that the succession of variations in the thickness of the rings is also not reproducible.

4. The action of the limiting factors must be exerted in an identical way on trees having the same ecological requirements and distributed over sufficiently large areas.

The synchronization of different samples is based on the search for a visual concordance between the curves representative of the different chronologies and on the use of statistical tests, parametric or nonparametric, applied to the numerical series. Various types of devices, more or less modern and automated, allow these measurements, with an accuracy ranging from 1/10 to 1/100 mm. The samples studied are sometimes cores, most often at 1.30 m from the ground (non-destructive samples, not requiring tree felling), sometimes washers taken from the trunks at varying heights.

- ✓ **Application:**

Dendrochronology, thanks to the information which can be drawn from it, finds its place in a journal open to the multidisciplinary aspects of Quaternary research including archeology.

Scientists have spent years identifying growth ring sequences for different species. It is now possible to go back hundreds or even thousands of years to the present [3].

However, it should be noted that we can only determine the date of the tree's felling and not its date of use. In addition, to achieve this dating, the last ring must be present but it is often very difficult to read. It is thus possible to carry out dating to the nearest year. Dating can also be difficult because dark circles can be missing. In addition, dark circles can appear due to climatic accidents, human actions or insects.

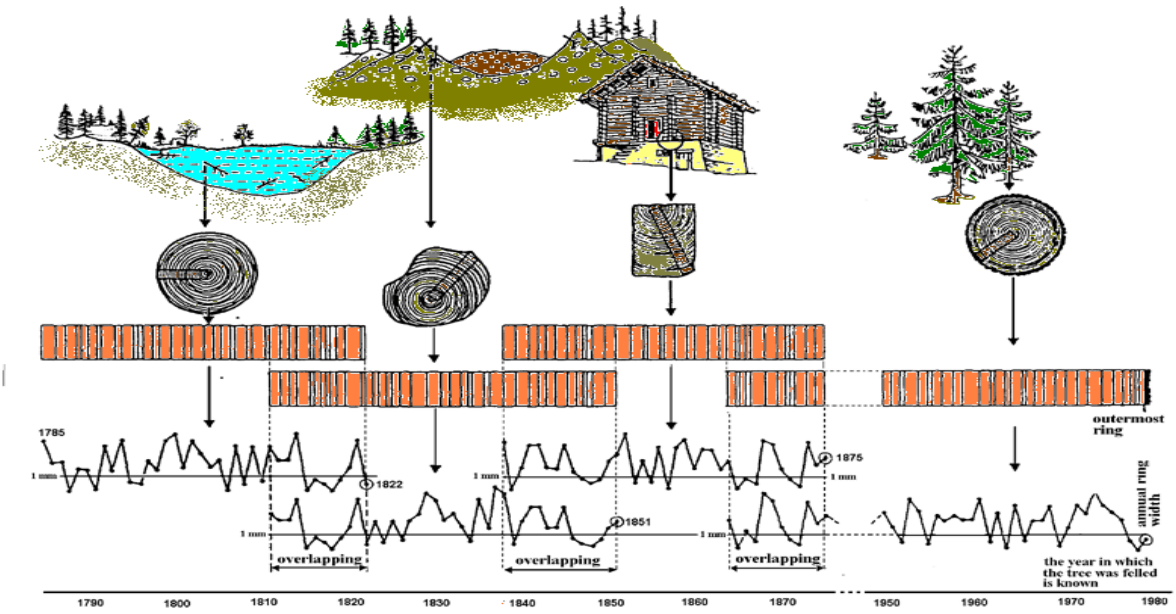

Fig I. 4: Schematic showing how crosses referencing works in dendrochronology. This is a reproduction of a figure from Schweingruber [2].

I.2.2.2 Isotopic and radiometric methods

The most important absolute dating methods are based on the phenomenon of radioactive decay. These methods use the regular variation of the proportion of radioactive isotopes relative to the stable isotopes contained in a body, over time. This variation is based on a known exponential decay law, the half-life: this is the time during which half of the nuclei of a radioactive isotope have disintegrated. It does not depend on any external influence, be it physical, chemical or biological.

I.2.2.2.1 Carbon-14 dating

Carbon-14 dating appeared around the 1940s thanks to the activities carried out in the United States by Libby [16], in order to use the properties of ^{14}C in the dating of organic matter. This technique is based on the measurement of the radiological activity of Carbon-14 contained in these materials. It allows determining the time interval since the death of the organism to date [3].

✓ **Principle:**

After formation, the carbon-14 atoms combine rapidly with oxygen to form carbon dioxide molecules, which behave in chemically almost the same way as ordinary carbon dioxide. There is rapid mixing in the atmosphere and through photosynthesis, there is an entry into plant life. The entire atmosphere, biosphere and oceans contain ^{14}C and are known as the carbon exchange reservoir. The concentration ratio between Carbon-14 atoms and non-radioactive carbon atoms are about the same throughout this reservoir and it remains approximately constant over time. This concentration ratio represents the level of equilibrium which is established, on a global scale, between loss by radioactive decay and production by cosmic rays. In a dead organic matter, that is to say that no longer exchanges its carbon with the reservoir, the quantity of Carbon-14 assimilated then decreases exponentially over time while that of Carbon-12 remains constant [4]. Dating is based on the comparison of the ratio between the amounts of Carbon-12 and Carbon-14 contained in a sample with that of a standard reference sample. From this comparison, we deduce the "Carbon-14 age" of the sample that we are trying to date. This age is then translated into real age (or “calendar age”), by comparing it to a standard curve, produced by researchers using numerous additional measurements. The 14C/12C isotope ratio can be measured in two different ways. Either by counting the beta particles resulting from the decay of 14C, this radioactivity is proportional to the number of 14C atoms, which can thus be determined. Either by measuring the isotope ratio by mass spectrometry; the sample is reduced to graphite or CO2 gas, analyzed in a mass spectrometer. This technique allows the measurement of a very small number of carbon atoms, so it has an advantage over beta counting when only very small amounts of sample are available, or the sample is old and contains little of 14C [17,3].

✓ **Application:**

The samples analyzed generally consist of organic material found at archaeological sites, such as charcoal, wood, seeds, plant remains, and human or animal bones.

The precise measurement of a sample's ^{14}C activity is affected by counting errors, background cosmic radiation, and other factors that contribute to an element of measurement uncertainty. This means that the radiocarbon dates are invariably accompanied by an estimate of the error attached to each radiocarbon date [3].

Note that in 5 730 years, half of the ^{14}C atoms will have disappeared (half-life of ^{14}C), therefore, the further we advance in time, the lower the quantity of Carbon-14 in the sample and becomes less in less measurable. This method therefore makes it possible to date objects up to 50,000 years old [3].

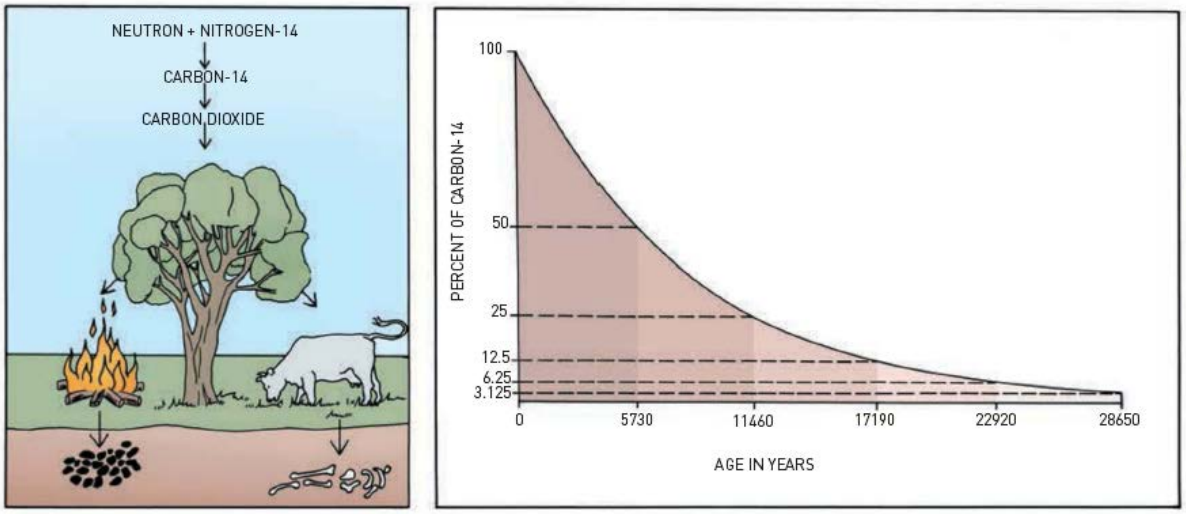

Fig I.5: Radiocarbon dating. Left: radiocarbon is produced in the atmosphere and absorbed by plants through carbon dioxide, and by animals through feeding off plants or other animals. Right: after death, the amount of 14C decays at a known rate, 50 percent after 5730 years. Measurement of the amount left in a sample gives the date [3].

I.2.2.2.2 Potassium-Argon dating

Potassium-argon (K-Ar) dating is a radiometric dating method that determines the age of a rock sample by measuring the amount of argon-40 (40Ar) and potassium-40 (40K) from the solidification of a fully degassed magma. It is used to date minerals in metamorphic and volcanic rocks [18].

- ✓ **Principle:**

With a half-life of 1250 million years, Potassium-40 represents about 0.012% of natural potassium. It is a radioactive isotope that decays to give Calcium-40 and Argon-40. It's the accumulation of this later which is the basis of this dating method [4]. In the case of the 40K/40Ar couple, the initial quantity of the isotope resulting from the radioactive decay is zero. Indeed, during an eruption, the rock loses Argon-40, which is called degassing. Over time, the Argon-40 produced by the radioactive decay of Potassium-40 will therefore accumulate again

in the rock while the Potassium-40 gradually disappears. To apply this method, we therefore assume that the rock analyzed did not contain argon at the time of its formation. The age is calculated by measuring the isotopic ratios of the argon which appears during the reaction [19.20]. By measuring the quantities of 40K potassium matter and 40Ar argon in a sample, we can calculate the age t of the rock or mineral analyzed using the following chronometric formula [21]:

$$t = \frac{1}{\lambda\beta+\lambda\varepsilon} \ln\left[\left(\frac{\lambda\beta+\lambda\varepsilon}{\lambda\varepsilon}\right)\frac{40Ar}{40K} + 1\right] \qquad (I.1)$$

With:

λ_β: The decay constants of 40Ca = 4.962 10-10 yr^{-1}

λ_ε: The decay constants of 40Ar = 0.581 10-10 yr^{-1}

A more sensitive variation of the method, which requires a smaller sample, is known as argon-argon laser fusion dating (40Ar/39Ar dating). A stable isotope of potassium, 39K, is converted to 39Ar by neutron bombardment of the sample to be dated. The two isotopes of argon are then measured by mass spectrometry after their release by laser fusion. Since the 40K/39K ratio in a rock is constant, the age of the rock can be determined from its 40Ar/39Ar ratio [3].

- ✓ **Application:**

This method is mainly used to date deposits of magmatic rocks, rich in potassium, in particular volcanic ash found on certain excavation sites. It allows a dating of 100,000 years to several tens of millions of years [22].

The main limitations of the technique are that it can be used only to date sites buried by volcanic rocks, and that it is rarely possible to achieve accuracy better than ± 10 percent [3].

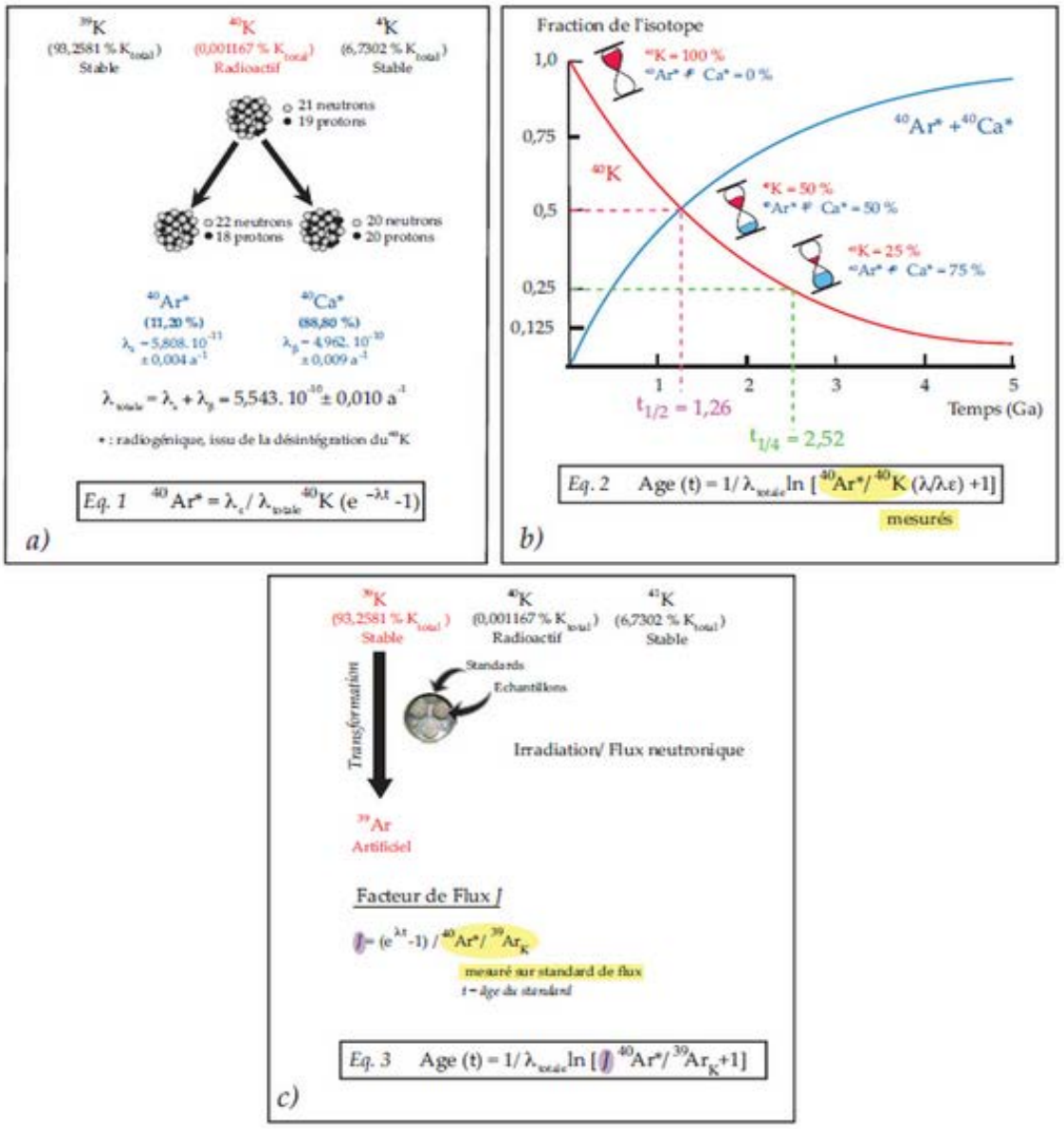

Fig.I.6: A/ Diagram showing the proportion of the different isotopes of potassium in nature, the decay constant of Steiger and Jäger (1977) as well as the equation relating to the radioactive decay of 40K in 40Ar. B/ Diagram illustrating the radioactive decay of 40K to 40Ar as well as the relative age equation. C/ Diagram illustrating the transformation of 39K to 39Ar resulting from neutron activation. The equation for the flow factor J is integrated into the age equation [23].

I.2.2.2.3. Uranium-Thorium dating

The uranium-thorium dating method is a radiometric dating method that makes it possible in particular to measure the age of certain carbonate formations of animal or sedimentary origin. This dating method is based on the radioactive decay of uranium isotopes.

- ✓ **Principle:**

Two radioactive isotopes of uranium (238U and 235U) decay in a series of stages into daughter elements. Two of these daughter elements, thorium (230Th) and protactinium (231Pa), themselves also decay with useful half-lives for dating. The natural isotopes of uranium are soluble in water, while the daughter's products are not. This means, for example, that only the isotopes of uranium are present in the water and is incorporated into the material forming from it, such as the skeletons of corals, shells or calcite forming on the wall cave then, the radioactive clock is started. At the time of their formation, they contain only water-soluble 238U and 235U and are therefore free of the insoluble isotopes 230Th and 231Pa. Thus the amounts of daughter isotopes increase over time as the original uranium decays, and by measuring the daughters/parent ratio, typically 230Th/238U, and age can be determined. Isotopes are measured by counting alpha emissions; each isotope emits alpha radiation of a characteristic frequency [3].

- ✓ **Application:**

The method is currently used in rocks rich in calcium carbonate, often those deposited by the action of surface or underground water around sources rich in lime or by infiltration in limestone caves.

This method allows dating up to 500,000 years using a mass spectrometer. Under favorable circumstances, the method results in dates with an associated standard error of ± 12,000 years for a 150,000 year-old sample, and around ± 25,000 years for a 400,000 year sample. These numbers can be drastically reduced by using thermal ionization mass spectrometry (TIMS) to directly measure the amounts of each isotope present. Such precision dates may, for example, have an associated uncertainty of less than 1000 years for a sample of 100,000 years [4].

U-series dating has been used successfully in conjunction with other methods such as potassium-argon [4].

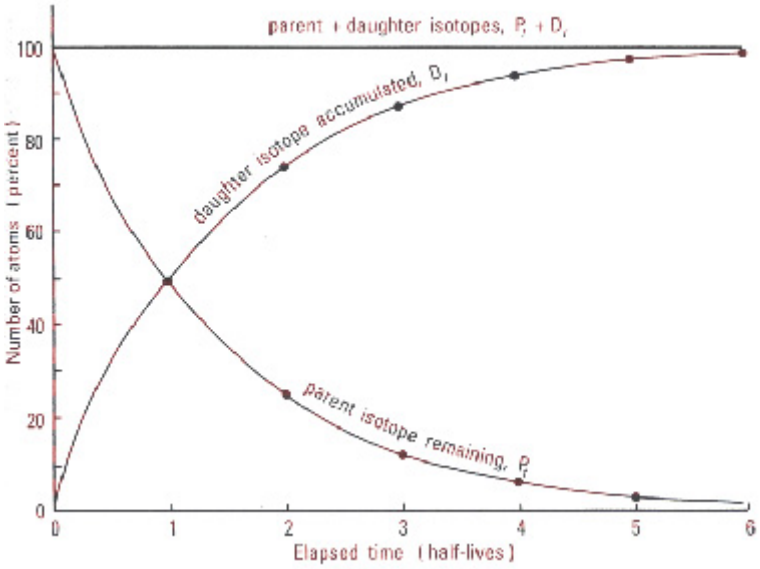

Fig I.7: Decay of a radioactive parent isotope (P_t) and the corresponding accumulation of its daughter isotope (D_t). In a closed system, the sum of the parent and daughter isotopes ($P_t + D_t$) at any time equals the original amount of the parent isotope. (source: http://www.biblicalcatholic.com/apologetics/p64.htm).

I.2.2.2.4 Fission-track dating

Fission-track dating (FTD) is one of the isotopic methods which appeared in the early sixties, with the work of Price and Walker (1963). Since then, this method has undergone rapid development and shown great flexibility in use since it adapts as well to the dating of very recent geological and archaeological materials, as to the analysis of fission events recorded in the oldest rocks [24, 25].

It is based on the recording by minerals and glasses of the damage produced locally by the spontaneous fission of Uranium-238. Natural glasses are characterized by the presence of uranium content of the order of a few ppm, generally distributed homogeneously throughout the volume, a characteristic which makes these materials a medium of choice for FTD dating. As irradiation damage is sufficiently stable at the temperatures prevailing at the earth's surface, it is possible to use it in dating by the fission-track method.

The uranium fission-track method provides two types of information: an age and its uranium content. FTD requires only light and easy-to-use instrumentation.

✓ **Principle:**

In nature, more than 99% of uranium exists as 238U and less than 1% as 235U. 238U is a radioactive isotope which decays by spontaneous fission, while 235U is an essentially radioactive isotope which fission by neutron capture. During their fission, these two isotopes produce two daughter atoms, called "fission fragments", releasing the energy of about 200 MeV. These fragments are ejected in two opposite directions. When the phenomenon occurs in a mineral, this recoil induces local disorganization of the crystal lattice by ionization of the atoms along their path. As they move away from each other, these fragments thus lose their energy and are quickly stopped. Solid non-conductive or semiconductor detectors of high resistivity, like most minerals, glasses and plastics, can record the passage of fission fragments. This recording is a function of the sensitivity of the solid detector. The path of these fission fragments reveals a zone of linear damage of a very small diameter, less than a hundred angstroms, this is called the latent trace [26]. Price and Walker have shown that it is possible to make these traces visible under optical microscopy using an appropriate chemical attack, enlarging their diameter to a fraction of a micron [27]. It is the traces thus revealed that are used for dating.

The density (number per unit area) of traces of spontaneous fission in the material to be dated is a function of its age and its uranium content. The determination of age by fission-tracks requires the measurement of the density of fossil traces and the uranium content. Since Uranium-235 can crack under the influence of thermal neutrons, the 235U content in the material to be dated is determined through exposure in a nuclear reactor [28].

✓ **Application:**

In archeology, this method has been used mainly for dating occupation sites and studying obsidian trade routes. It presents a wide field of application to quaternary problems; since it applies equally well to the treatment of geological problems than to earth-space relationships and to the evolution of the species and human civilizations (dating of ancient deposits of fossil humans, archaeological objects and sites), giving ages up to two billion years [3].

For dating within the quaternary, the need to reset the fission-track chronometer limits its application, on the one hand to volcanic rocks, on the other hand to sufficiently heated materials,

that is to say where all the pre-existing traces were annealed: stones from ovens and hearths, ceramics, impacted rocks.

For the dating of continental volcanism, the trace method is often used in conjunction with that of K-Ar [29]. It has the advantage of a simple and inexpensive implementation. Its limitations come mainly from the need to find phases sufficiently rich in uranium. The trace method does not only allow dating of objects from traces of spontaneous fission of ^{238}U. It can also be used for this purpose from traces of induced fission of ^{235}U. It can then be used either as a relative dating technique (fossils), or as a back-up technique for another dating method (thermoluminescence).

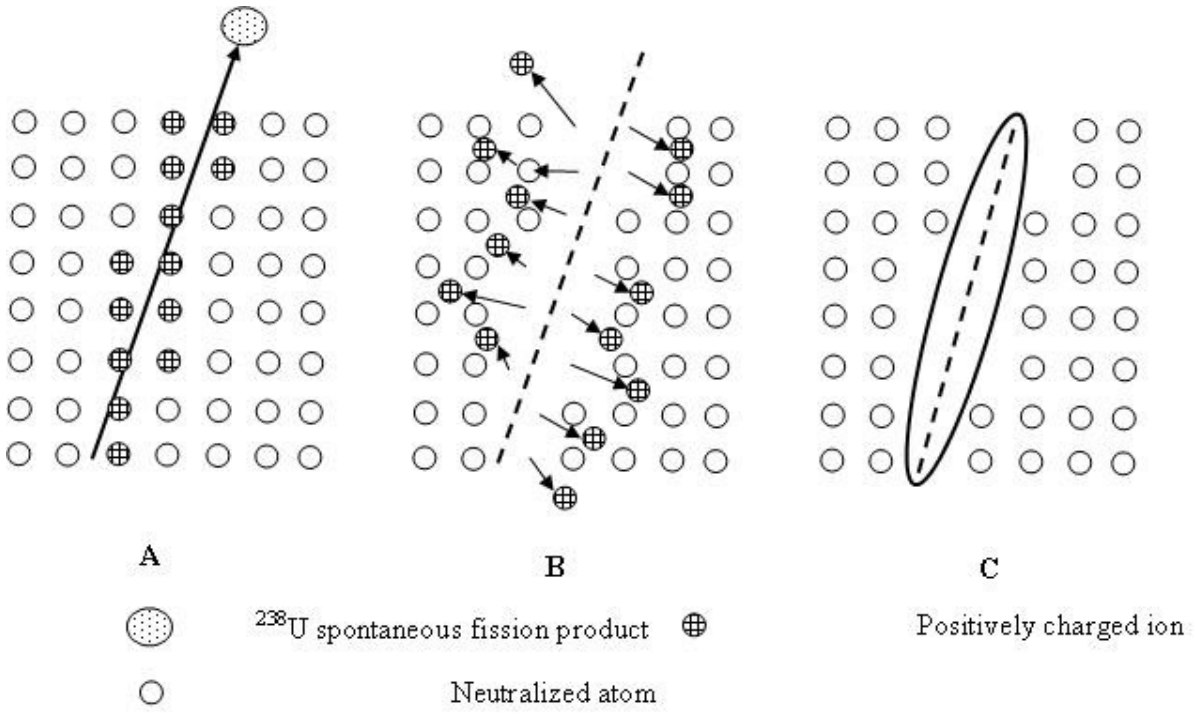

Fig I.8: Track formation in a simple crystalline solid: A/ the atoms have been ionize by the massive charges particle which has just passed; B/ the mutual repulsion of the ion has separated them and forced them into the lattice; C/ observable track after etching (source: https://sites.google.com/site/mansourftt/usedtechniques).

I.2.2.3 Solid state physics methods

I.2.2.3.1 Stimulated luminescence

Luminescence dating is a method used to determine the time that has passed since the last exposure to sunlight or the last heating of a piece of pottery. It is based on the emission of light

when the material is heated or illuminated and can be applied to materials that contain quartz or feldspar. Therefore, this method is widely used for environmental dosimetry and dating of archaeological materials.

- ✓ **Principle:**

Stimulated luminescence dating is based on the phenomenon of accumulation over time of electrons trapped under the effect of natural radioactivity in defects in minerals such as quartz and feldspars. These act as dosimeters, recording the amount of radiation to which they have been exposed. Such minerals are able to store within their crystal structure a small proportion of the energy supplied by radiation, due to the decay of radioactive elements in their environment, and cosmic radiation. This energy accumulates as exposure to radioactive decay continues over time. At a later date, it will be released, in the form of light (luminescence) upon exposure to light or heating, and in this case, the luminescence signal in the grains of the mineral is erased (optical whitening or thermal annealing) until reduced to zero. Once the grains are buried in the sediment away from daylight, the electrons accumulate again under the effect of natural radioactivity. To produce the luminescence signal, electrons trapped and stored in the minerals can be released in the laboratory either by heating (TL thermoluminescence), or by exposure to light (optically stimulated luminescence, OSL). The light emitted when returning to equilibrium is proportional to the number of electron-hole pairs created, itself proportional to the dose received [30].

To calculate an age, two quantities must be determined: the equivalent dose (or paleodose), which corresponds to the amount of energy per unit of mass stored by the mineral since its last heating (or its last exposure to light); and the annual dose, which is the amount of energy per unit mass accumulated in a year by the mineral. Age is determined by dividing the equivalent dose by the annual dose [31]:

$$Age = Paleodose / Annual\ dose \qquad (I.2)$$

- ✓ **Applications:**

Luminescence dating was originally developed for dating pottery [32]. It was then extended to the dating of stones and flint heated in prehistoric sites [33] and volcanic eruptions.

The chronological range accessible by luminescence dating extends from a few years to several hundred thousand years or even 500,000 years [34; 35].

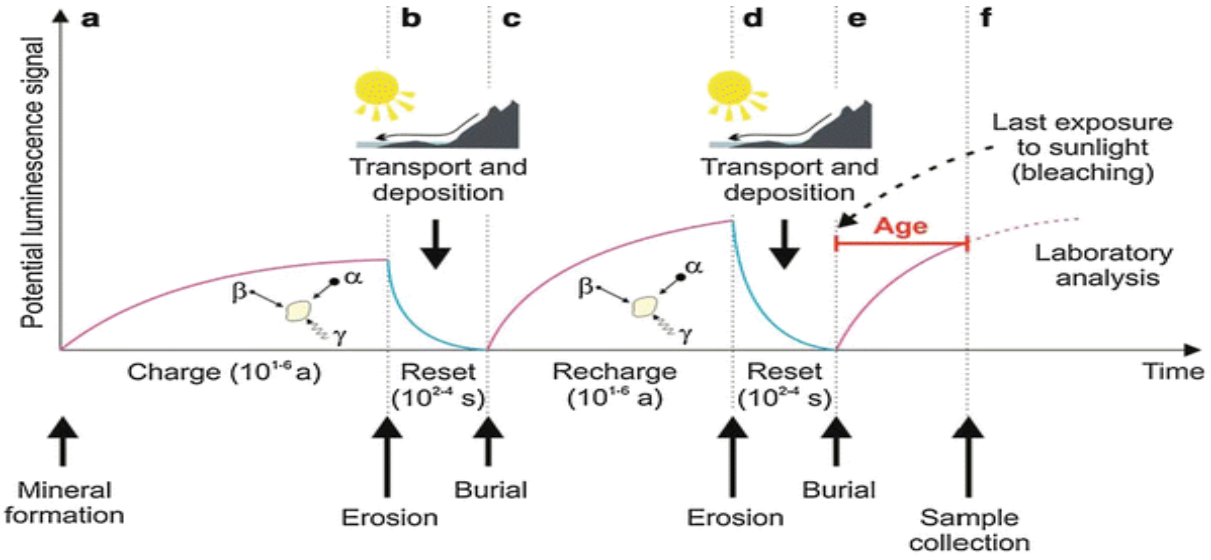

Fig I.9: Processes associated with OSL dating. (a) Luminescence is acquired in mineral grains with exposure to ionizing radiation and trapping of electrons. (b) The luminescence for grains is zeroed by exposure to sunlight with erosion and transport. (c) With burial and exposure to ionizing radiation free electrons are stored in charge defects within grains crystal lattice. (d) Further light exposure of grains with erosion and transport zeros the luminescence. (e) The grains are buried again and luminescence is acquired with exposure to ionizing radiation. (f) Careful sampling without light exposure and measuring of the natural luminescence, followed by a normalizing test dose (Ln/Tn) compared to the regenerative dose to yield an equivalent dose (De). (Source: https://www.baylor.edu/geosciences/index.php?id=955929).

I.2.2.3.2 Electron Spin Resonance (ESR)

Discovered in 1945 by Zavoisky, electron spin resonance (ESR) is today a classic method of analyzing the structure of matter. This technique, also called electron paramagnetic resonance (EPR), is based on a natural phenomenon, which is the accumulation of trapped electrons in certain mineral defects under the effect of natural radioactivity [36].

✓ **Principle:**

The principle of electron spin resonance dating is analogous to that of the luminescence method. The theoretical band model is generally used in solid-state physics to

explain the phenomenon (this model is explained in detail in chapter II). However, a luminescence measurement removes age information from the sample, whereas an ESR measurement can be performed multiple times on the same sample [37].

In order to obtain reliable dating results, an ESR signal must have the following properties: (i) a zeroing effect removes all the ESR intensity previously stored in the sample at the event to be dated, (ii) the signal strength increases steadily with the radiation dose, (iii) the signals must have a stability greater than at least an order of magnitude at the age of the sample, (iv) the number of traps is constant or changes in a predictable way; recrystallization, crystal growth or phase transitions must not have occurred, (v) signals must not show any discoloration, and (vi) the ESR signal is not influenced by sample preparation (grinding , exposure to laboratory light) [38].

The trapped electrons form a specific paramagnetic center which can be measured by ESR spectrometry, giving rise to characteristic ESR lines. ESR measurement does not affect the population of trapped electrons. The intensity of the ESR line is proportional to the number of electrons trapped and the number of electrons trapped in turn results from three parameters: (i) the strength of the radioactivity (dose rate), (ii) the number of traps (sensitivity), and (iii) duration of radiation exposure (age) [37].

ESR age estimate is derived from the following formula:

$$Age = Accumulated\ dose\ (DE) / Dose\ rate\ (D) \qquad (I.3)$$

Measuring the accumulated dose *DE*, which is the radioactive dose the sample has received since its formation, is the actual ESR part of the dating procedure. The dose rate, *D*, is derived from the chemical analysis of radioactive elements in the sample and its surroundings [37].

✓ **Application:**

The field of application of the electron spin resonance (ESR) dating method extends from a few thousand to 1-2 million years ago, thus making it possible to assess the age of numerous geological or quaternary archaeological deposits [39].

ESR spectrometry is much less sensitive than TL and requires fairly heavy equipment, it has the advantage of allowing identification of the observed radical, of giving valuable

information on its position and its environment within the crystal lattice of the mineral studied, and, not being destructive, to multiply the measurements on the same sample.

The two main limitations of ESR dating are: (i) saturation: when all traps are filled, any additional radiation cannot cause a further increase in the number of trapped electrons, and (ii) thermal stability: n electrons 'have a limited likelihood of remaining in the traps. After a certain period of time, 63% of the original population of trapped electrons will have left the traps and recombined with holes. Only if the average lifespan is at least ten times the age of the sample, can the effect of recombination or discoloration be overlooked [38].

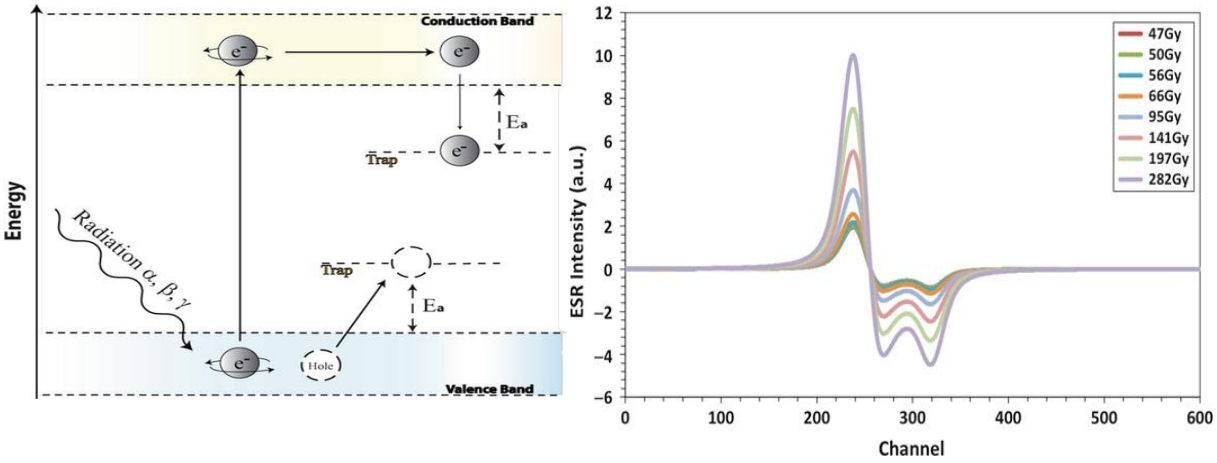

Fig I. 10: (Left) Band model of trapping charges processes under radiation. (Right) Influence of laboratory g-irradiation on the ESR signal. ESR spectra are increasing with irradiation; however, the signal remains qualitatively the same [40].

I.2.2.3.3 Archaeomagnetic dating

Archaeomagnetism was born thanks to the pioneering work of Thellier. Archaeomagnetic dating is based on the recording of variations in the earth's magnetic field by terracotta and volcanic rocks. The materials brought to high temperature acquire, during cooling, a remanent magnetization with a parallel direction and an intensity proportional to the ambient earth's magnetic field. By measuring this remanence, it is possible to determine the direction and strength of the earth's magnetic field as it cools. Conversely, the knowledge of the variation of the earth's magnetic field in the past makes it possible to date the last firing of terracotta; one then speaks of archaeomagnetic dating [41].

For dating, these values are compared to reference curves, called regional secular variation curves, which are constructed from reference data valid in a limited geographical area due to the spatial variation of the earth's magnetic field. The dating results are conditioned by the precision and resolution of the curves, which depend on the number and quality of reference data [42].

✓ **Principle:**

The terrestrial globe has a magnetic field that can be materialized at any point surrounding the earth by its action on the magnetic needle of a compass free to orient itself around its center of gravity. Thus, at a point 0 on the earth's surface, at time t, the earth's magnetic field can be represented by a vector OF whose direction is given by that of the magnetized needle. This tangent vector to the lines of the magnetic field is described by three components: inclination, declination and intensity. The inclination expressed in degrees is the angle of the vector with respect to the horizontal plane; the declination expressed in degrees is the angle between true north and the projection in the horizontal plane of the vector OF. The intensity is expressed in tesla [43].

The principle of laboratory measurements is the determination of a value of the strength of the old magnetic field. The experiments in the laboratory aim to gradually destroy the original magnetization and replace it with new thermo-remanent magnetization acquired under known and controlled field conditions. This magnetization is also proportional to the strength of the applied laboratory field. If the proportionality ratio between magnetization and intensity remains unchanged, it becomes easy to access the intensity of the old field by the following relation [43]:

$$H_{old} = H_{lab} \frac{MARN}{MATR} \qquad \text{(I.4)}$$

With:

H_{old}: the intensity of the old field that we are trying to determine.
H_{lab}: the laboratory field applied to replace the old magnetization.
MARN: The moment of the original thermo-remanent magnetization.
MATR: the moment of the new thermo-remanent magnetization acquired in the laboratory.

The archaeomagnetism study objects fall into two main categories: those found in situ on the place of their last firing, such as the walls of ovens, hearths or burnt floors, and those on the contrary moved from the place of their original firing, such as pottery and architectural terracotta. In the first case, they make it possible to find information relating to both the direction, defined by a declination and an inclination, and the intensity of the magnetic field, while in the second case, only information on the intensity of the old field can be obtained because the firing position of objects in the oven is generally unknown [43].

- ✓ **Application:**

Recent advances have made the method of dating by archaeomagnetism capable of providing dates with an accuracy of ± 20 years for most of the periods up to the present day.

Current applications mainly relate to pottery and building materials such as tiles, bricks, paving tiles, and brickwork elements. Such materials can only be used for archaeomagnetism dating purposes if it is possible to find, from simple technological considerations and common sense, the position they had during their last firing.

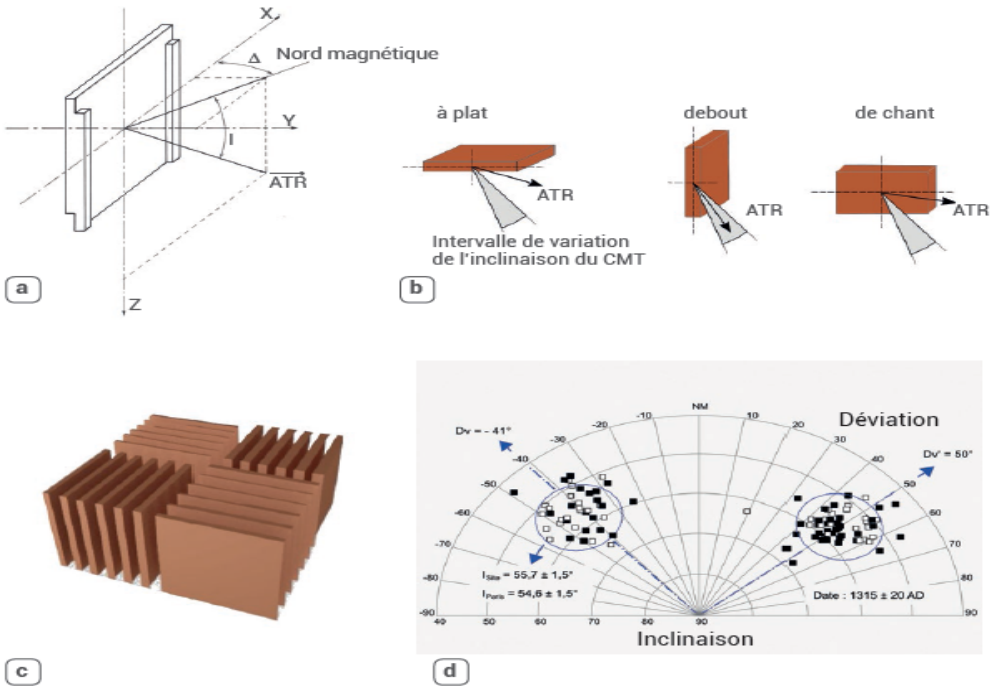

Fig I.11: Analysis of the magnetization of a set of fired bricks. (A) Definition of the angles of inclination (I) and deviation (Δ) on a tile (or brick) fired on edge in a vertical position. (B) Tilt test to restore the baking position (flat, upright or tilting) of a brick in the event of loading into the oven in a z axis according to the vertical. (c) Simplified diagram of how the bricks were stored. (d) Stereogram representing the inclination and deviation of the magnetizations measured on a set of 106 medieval bricks baked on slices in perpendicular rows [44].

Table I.1 shows the chronological domain accessible to the luminescence method and the other absolute dating methods by indicating the nature of the samples to be dated and the principle on which dating's are based. Although there are many methods that are of intersect with luminescence, there are, however, circumstances where these other methods may be useful to fill in gaps or to overcome dating constraints by which the validity and accuracy of luminescence results can be judged, and vice versa. Table I.2 presents further information about the applicability chart of archaeological absolute dating methods. This chart is comparative in either direction; it is intended as a guide to further reading rather than a definitive judgment.

Table I.1: Capabilities of dating by absolute methods

Dating method	Principle	Material	Age
Dendrochronology	Counting tree rings	Wood	thousands of years since the present
Radioactive carbon (14C)	Radioactive decay of 14C	Organic material, carbonates objects	up to 35,000 years old
Potassium-argon (K-AR)	Radioactive decay of potassium to argon	Volcanic rocks	from 100,000 years to several tens of millions of years
Uranium series (U-Th)	Ratio of isotopes of U and Th during radioactive decay	rocks rich in calcium carbonate	50,000 –500,000
Fission tracks	Density of traces of uranium fission in the crystal structure of uranium ores	Titanite and Zircon	300,000 - 2.5 billion
Stimulated luminescence	the energy accumulated in crystal defects	Pottery Heated stones and flint Volcanic eruptions Wind deposits	from a few years to several hundred thousand years or even 500,000
Electron Spin Resonance (ESR)	Magnetic resonance of captured electrons	Quaternary geological or archaeological deposits	from a few thousand to 1-2 million years ago
Archaeomagnetism	the variation of the Earth's magnetic field recorded by magnetic minerals	Baked clay: pottery and building materials	Up to present day

Table.I.2: Chart of the applicability archaeological absolute dating: Closed circle indicates appropriate age range that is good prospect of reliable date, less than closed circles indicates some qualification limitation due perhaps to reliability or to limitation in applicability.

Dating method	Dated Artefact									
	Wood, plant, seeds etc.	Bone, antler, ivory, teeth	Tooth enamel	Shells	Pottery, baked earth	Slag	Burnt flint and stone	Unburnt sediment	Obsidian	Glass
Dendrochronology	●									
Radioactive Carbon (14-C)	●	●	●	◕	○	◕				
Potassium-argon (K-AR)										●
Uranium series (U-Th)		◑	◑	◑						
Fission tracks						◕			●	◕
Stimulated luminescence					●	○	●	●		
Electron Spin Resonance (ESR)		○	◕	◑	○		○			
Archaeomagnetism					◑			◑		

I.4 Conclusion

Nowadays, there is a variety of methods used for determining the ages of materials and which differ according to many parameters including, their physical principles, the nature of the samples to be analyzed, their contexts of discovery…etc. Depending on whether they give a precise age or not, these methods are distinguished between those called relative and those called absolute. The so-called relative dating methods make it possible to organize events chronologically, geological or otherwise. However, they do not give precise dates but can, in fact, represent an approach before absolute dating; which they give precise values of the ages to be determined.

However, dating methods are mutually supportive and often several techniques are used simultaneously in order to arrive at a precise chronology.

Dating by luminescence, and more particularly thermoluminescence, and because of the large age range that it covers, represents a method of choice for the study of the quaternary. Sometimes it is the only method that can be applied in a particular context. Considering the basis and the technical aspects of the method, we were interested in the thermoluminescence technique, compared to the wide range of chronological methods currently available.

References

[1] J.F. Ruiz, M.W. Rowe (2014) Dating Methods (Absolute and Relative). In Archaeology Of Art. In: Smith C. (Eds) Encyclopedia of Global Archaeology. Springer, New York, NY

[2] J.K. Feathers (2014) Dating Techniques In Archaeological Science. In: Smith C. (Eds) Encyclopedia of Global Archaeology. Springer, New York, NY.

[3] C. Renfrew, P. Bahn (2016) Archaeology Theories, Methods, and Practice. Thames and Hudson, London.

[4] M. J. Aitken (1990) Science-Based Dating In Archaeology (Longman Archaeology Series). Routledge, London.

[5] E.C. Harris (1997) Principles Of Archaeological Stratigraphy, Academic Press. London

[6] E. Bortolini (2016) The Oxford Handbook of Archaeological Ceramic Analysis: Typology and Classification. Oxford University Press.

[7] V. A. Gorodzov (1933) The typological method in archaeology, American Anthropological Association, doi.org/10.1525/aa.1933.35.1.02a00070.

[8] R.C. Dunnell (1970) Seriation method and its evaluation. American antiquity, vol 35 : 305-319.

[9] A.E. Douglass (1935) Accuracy in dating II: the presentation of evidence. Tree-ring bulletin 1(3): 19-21.

[10] A.E. Douglass (1936) Climatic cycles and tree-growth Vol III. Carnegie Institution of Washington Publication 289, Washington, DC, USA.

[11] E.R. Cook, L.A. Kairiukstis (1990) Methods of Dendrochronology, Applications In The Environmental Sciences. International Institute for Applied Systems Analysis. Kluwer Academic Publishers, Dordrecht, 394.

[12] S. Payette (2011) La Dendroécologie : Principes, méthodes et applications Informations. Presses de l'université Laval. Québec.

[13] F.H. Schweingruber (1988) Tree Rings Basics and Applications of Dendrochronology, Kluwer Academic Publishers. New York.

[14] M A Valentin. (1979) La Dendrochronologie. Association Française pour l'étude du Quaternaire, Vol 16 : 65-74

[15] M. Becker, J. Bouchon , R. Keller (1988) La dendrochronologie et la xylochronologie : des outils d'analyse rétrospective du comportement des arbres . Revue forestière française, vol. XL, n° spécial diagnostics en forêt », pp. 53-61.

[16] W F. Libby (1955) Radiocarbon dating. University of Chicago Press. Chicago 175

[17] T.E. Törnqvist, B.E. Rosenheim, P. Hu, A.B. Fernandez (2015) Radiocarbon dating and calibration. In book: Handbook of Sea-level, Research Chapter: 23. John Wiley: I. Shennan, A.J. Long, B.P. Horton. New Jersey.

[18] P. Dumesnil (1966) Analyse par Activation de l'Argon : application à la datation par La méthode Potassium-Argon. Thèse. Se. phys. Paris. 1966. No 155. Université de Paris-Centre d'Orsay.

[19] A.M.R. Althoff (1997) Datation des minéralisations d'émeraude du Brésil par les méthodes K-Ar et 40Ar/39Ar. Thèse en Géosciences, Matières Premières. et E.;.nvironriement. Université de Lorraine.

[20] H Guillou, V Scao, S Nomade, B Platevoet,D. Blamart(2019) De La justesse ses ages K-Ar : Exemple de la datation de deux dômes trachytiques tu Gölcük (Turquie),Quaternaire 28/2 : 141-148.

[21] P.Y. Gillot, A. Hildenbrand, J.C. Lefevre, C.A. Livadie (2006) The K/Ar dating method: principle, analytical techniques, and application to holocene volcanic eruptions in southern Italy. Acta vulcanologica, vol 18 (1-2) : 55-66.

[22] C. Cassignol (1979) Quelques Recherches Sur La Méthode Potassium-Argon. Association française pour l'étude du Quaternaire, Vol 16 : 27-33

[23] A. Pereira, S. Nomade, J.J. Bahain, M. Piperno (2017) Datation par 40Ar/39Ar sur monocristaux de feldspaths potassiques : exemple d'application sur le site pléistocène moyen ancien de Notarchirico (Basilicate, Italie). Quaternaire, vol. 28/2 : 149-154.

[24] G. Poupeau, E. Zuleta (1984) Les datations par traces de fission (TF) en archéologie, Principes et méthodes. Centro Brasileiro de Pesquisas Físicas - CNPq/CBPF, Nota de Fisica, CBPF-NF-047/84.

[25] P. Gérard (1979) Les datations par traces de fission de l'uranium : principes et applications aux problèmes du quaternaire. Bulletin de l'association française pour l'étude du Quaternaire 16 : 15-26.

[26] N. Sabit (1995) La datation par traces de fission: aspects méthodologiques et applications thermochronologiques en contexte alpin et de marge continentale. Thèse Géologie appliquée. Université Joseph-Fourier - Grenoble I, 1995.

[27] P.B. Price, R.M. Walker (1962) Chemical Etching of Charged Particle Tracks in Solids. J Appl Phys 33 : 3407–3412.

[28] P. Gérard (1979) Les datations par traces de fission de l'Uranium. Principes et applications aux problèmes du quaternaire. Association française pour l'étude du quaternaire vol 16 n°1-2 : 15-26.

[29] G.A. Izett, C.W. Naeser (1976) Age of the Bishop Tuff of eastern California as determined by the fission-track method. Geology 4: 587–590

[30] L. Bejjit (2017) Développement de la méthode de datation par luminescence (TL/ OSL) au Maroc. Anthropologie : 1-10.

[31] C. Bassinet (2007) Datation par luminescence : recherches méthodologiques et applications au volcanismedans l'environnement de Laschamp, Thèse géologie appliquée. Université Blaise Pascal Clermont-Ferrand II.

[32] J.R. Aitken, J. Biely, D.C. Hill, J.B. O'neill, A.R. Robblee, J. Sell (1963) A Feeding Trial conducted at six different locations. Poultry Sci. 43: 744-751.

[33] H. Valladas (1992) Thermoluminescence dating of flint. Quaternary science review, Volume 11, P. 1-5.

[34] M. Fattahi, S. Stokes (2000) Extending the time range of luminescence dating using RedTL (RTL) from volcanic quartz. Radiation Measurements 32: 479-485.

[35] G.W. Berger, B.J. Pillans P.J. Tonkin (2001) luminescence chronology of Loess-Paleosol sequences from Canterbury south island New Zealand. Journal of Geology and Geophysics: 501-516

[36] J.J. Bahain (1993) Datation par résonance de spin électronique (ESR) de carbonates et d'émail dentaire quaternaires : potentiel et problèmes. Thèse Archéologie et préhistoire. Museum national d'histoire naturelle de Paris.

[37] R. Grun (1993) Electron spin resonance dating in palaeoanthropology. Evolutionary anthropology 172-181

[38] T. Aitken (1997) Chronometric Dating In Archaeology. Plenum Press, New York and Australian National University, Canberra 217-260.

[39] B.J. Jacques, Y. Yuji, F. Christophe, B. Roland (1995) Electron Spin Resonance (ESR) dating of quaternary marine carbonates. Quaternaries 6: 13-19

[40] R. Joannes-Boyau (2014) Electron Spin Resonance (ESR) Dating in Archaeology. In: Smith C. (eds). Encyclopedia of Global Archaeology. Springer, New York, NY.

https://doi.org/10.1007/978-1-4419-0465-2_2447

[41] L. Philippe (1990) La datation archéomagnétique des matériaux de construction d'argile cuite : Apports chronologiques et technologiques. Gallia tome 47 : 321-341.

[42] H Gwenaël (2012) Datation par archéomagnétisme des terres cuites archéologiques en France au premier millénaire Av. J.-C. : étalonnage des variations du champ géomagnétique en direction et intensité. Archéologie et préhistoire. Université Michel de Montaigne - Bordeaux III.

[43] Y. Gallet, A. Genevey, J-C. Margueron (2014) Exemples de chronologie archéomagnétique à mari/tell hariri. Syria supplement 2 : 217-230.

[44] P. Lanos (2019) Physique de l'archéomagnétisme pour la datation de bâtiments du haut moyen âge. Reflets phys. N°63: 54-59

CHAPTER II:

Thermoluminescence Dating

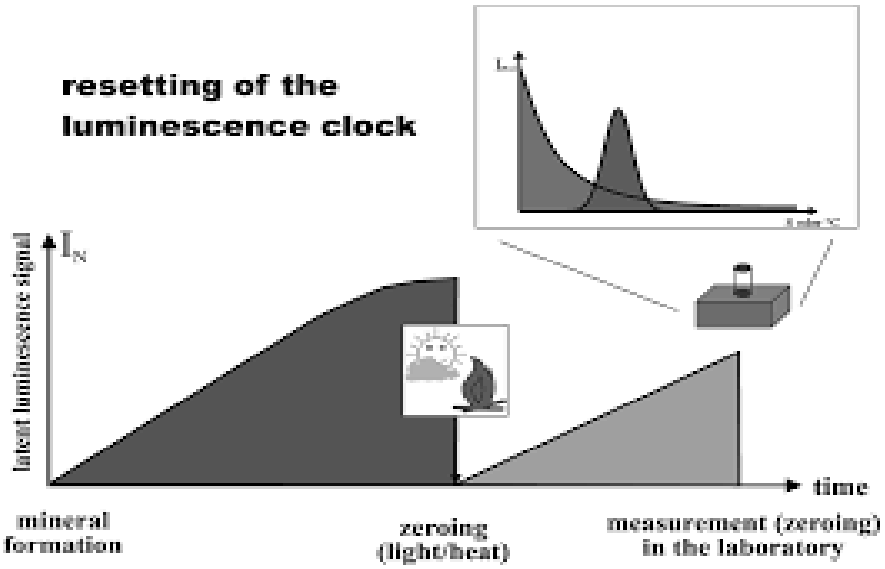

II.1 Introduction

Luminescence dating is among the dating methods prevalent in archeology. It is so called because it is based on the phenomenon of luminescence in semiconductor materials, mainly quartz or feldspar. The cumulative energy from ambient radioactivity by these minerals can be delivered upon exposure to light or heating, and is released as light. These two properties, accumulation and zeroing, are the mainstays of several luminescence dating methods.

The ability of certain minerals to release luminescence when stimulated is not a recent discovery. The first recorded observation of behavior in minerals has been attributed to Robert Boyle, who in 1664 discovered that a diamond could emit light when heated [1,2]. Subsequently, Boyle described the phenomenon as "self-shining" [3]. Throughout the eighteenth, nineteenth, and early twentieth centuries, much activity was devoted to examine the effects of luminescence. Advances in dating materials, however, have been hampered by a limited understanding of the luminescence process and precise ages were difficult to find [4]. Luminescence dating has grown considerably since 1950s. One of the techniques developed on this principle was thermoluminescence. Daniels and Aitken were among the first to develop analysis by this technique in their laboratories [5,6]. At first, it was exclusively limited to the study of terracotta materials such as pottery, and ceramics [7-9]. In 1953, Daniels et al. had proposed that TL of ancient pottery could be used to determine its antiquity [5,6]. The idea was based on the recognition that heating pottery to high temperatures (>500°C) during production had the effect of clearing any previously accumulated energy from the constituent mineral grains. It was in 1964 that Aitken et al. designed a study to determine the relationship between an artefact's TL glow and its age [6]. The positive results noted in these early studies gave impetus to further refinements in TL protocols, and throughout the 1960s and 1970s the dating method gained a foothold in archaeological studies. It then spread to other objects such as burnt stones (flint) [10]. Since the 1980s, luminescence dating has been extended to sediments using optical stimulation techniques (OSL) [11]. Other terms used to describe OSL include optical dating [11] and dating by photon stimulated luminescence or photoluminescence [12].

Thermoluminescence (TL) and Optically Stimulated Luminescence (OSL) have the same working principle; while the first uses heating as an excitation source to extract the stored energy, the second relies on a monoenergetic light source.

With luminescence dating, it is possible to date when and at what temperature an object was heated (making a pottery, a brick, etc.). This last part is still being tested today, but the results are already very conclusive. Luminescence methods can generally be used to date materials ranging in age from a few decades to around 100,000 years. However, ages up to several hundred thousand years have been reported in some studies [13].

In this chapter, the application of luminescence techniques to the dating of archaeological events is examined. In what follows, we will develop in detail the phenomenon of luminescence, by explaining the behavior of electrons by the bands model; before describing the two techniques of luminescence dating mentioned previously, in a general way. The equation of age follows, explaining in detail how to determine the paleodose and the absorbed dose and thus trace the age of an archaeological object, using thermoluminescence dating.

II.2 The phenomenon of luminescence

II.2.1 Mechanism

The phenomenon of luminescence is based on the accumulation of radiation damages in minerals over time, which results from exposure to low levels of ionizing radiation found in nature [14]. The more a mineral is exposed to this radiation flux, the greater the damages caused. The intensity of this damages is therefore a measure of the total dose (the total amount of energy absorbed by ionizing radiation), that the mineral received for a certain period of time, and which is detected in the form of a small amount of light, called luminescence.

Radiation damages, and therefore the latent luminescence signal, can be suppressed or zeroed by exposure to heat or light. For ancient pottery, for example, zeroing took place during its manufacture, when it was fired. Once the zeroing agent is no longer operational, the luminescence signal may begin to build up again.

The latent luminescence signal can also be released in the laboratory using the same zeroing agents, which are heat or light. It will thus be linked to the dose received by the mineral since the last zeroing event. If the rate at which the dose was absorbed is also determined, then an age can be calculated. This refers to the time that has elapsed between the moment that the archaeological object was deposited and the moment of sampling for analysis. This is illustrated in (fig.II.1) [15].

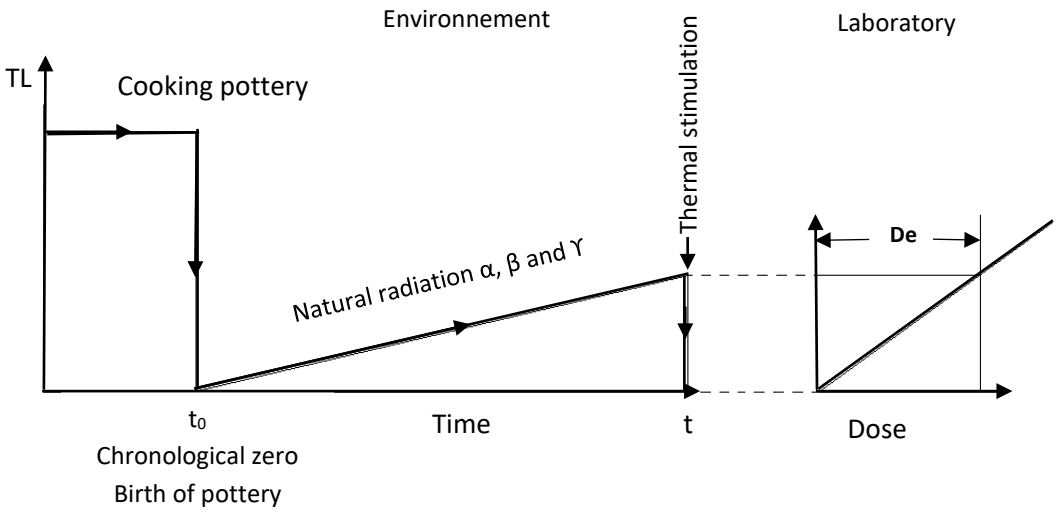

Fig.II.1: Illustration of the basic principle of luminescence dating: first, the signal is reset to zero during the firing of the pottery, then the mineral is irradiated and the natural luminescence signal increases proportionally with the number of charges trapped in crystal defects. This signal is measured in the laboratory and is proportional to the duration of exposure to ionizing radiation.

These phenomena are conventionally described by a band diagram, which represents the possible energy levels of electrons in a crystal (fig.II.2). The lowest energy band in which electrons are linked to atoms is the valence band; the highest energy band in which electrons move freely is the conduction band. The gap between the two is the “Forbidden band gap”. In an ideal crystal, no electron occupies a position in this area [16].

Except that the reality is much more complicated; indeed, all natural crystal carries defects which serve to disrupt the ordered crystal structure and which create energy levels located in the forbidden band gap [17,18].

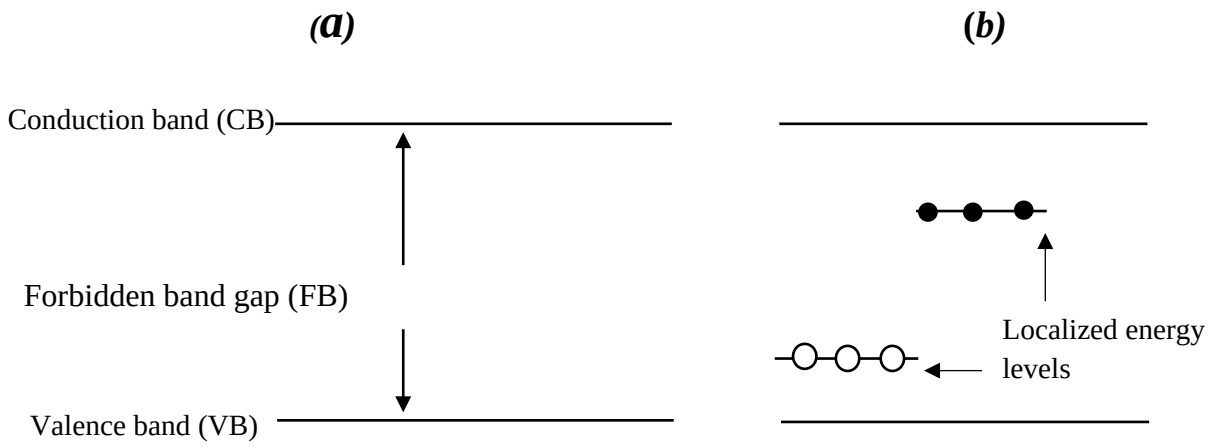

Fig.II.2: Band diagrams: a) perfect crystal, b) natural crystal.

Many types of imperfections are possible, such as impurities (either as substitutions or in interstitial positions), or missing atoms. These defects generate the presence of energy levels in the forbidden gap band. As the conduction and valence bands extend across the crystal, defect states are associated with the defects themselves, and are therefore called localized energy levels. An electron in a localized level may thus not participate in either electrical conduction or the valence processions of atoms, it is said to be "trapped". These traps are the key to the phenomenon of luminescence. In other words, luminescence requires the existence of defects in the lattice.

Natural radioactivity emits a low level of radiation which has an ionizing effect. During the interaction with the crystal, an electron can move from the valence band to the conduction band (Fig.II.3 (a)). For each electron moved, an electron vacuum called a hole is left and the electron and the hole are free to move through the crystal. In this way, the energy of nuclear radiation is absorbed, but can be released again (usually as heat) by recombination. This is the case with most charges, they recombine directly. Another possibility is that the electron and the hole are trapped at the defect centers; some of these defects are located close of the valence band and thus, constitute traps for the positive holes created by the ejection of an electron under the effect of an incident radiation. Others are located near the conduction band and are traps for free electrons ejected from the valence band to the conduction band. In this case, nuclear energy is temporarily stored in the crystal lattice and the system is in a metastable situation (Fig.II.3 (b)). Energy in the form of heat or light is necessary to remove the electrons from the traps and put

the system back into a stable situation; here comes the phenomenon which is at the origin of the production of light. The amount of energy required is determined by the depth of the trap E below the conduction band. This depth therefore, determines how long an electron stays in the trap. To empty deeper traps, more energy will be needed. Moreover, the higher the difference in energy between the conduction band and the trap, the lower the probability of the electron escaping from it. This is formalized by the following equation [18] (in the case of a first order kinetics):

$$p = s \exp(-E/kT) \qquad \text{(II.1)}$$

With:

p: is the escape probability of the electron (in s-1),

s: is the frequency factor (in s-1), specific to the type of trap,

E: is the activation energy (in J); it is the difference in energy between the conduction band and the level of the trap.

k: is Boltzmann's constant, equal to 1.38 x 10-23 J / K,

T: is the temperature (in °K). Note that the higher it is, the greater the probability of ejection.

1/p: corresponds to the stability of the trap, it represents the time necessary for half of the electrons trapped initially to leave their traps.

For dating, we are only interested in traps deep enough (i.e. ~ 1.6 eV or more) that the lifespan is at least several million years.

By exposing the crystal to heat or light, the trapped electrons can absorb enough energy to overpass the barrier to the conduction band (Fig.II.3 (c)). Once excluded, they can be trapped again or recombine with holes in the recombination centers. They are attractive fault sites for electrons. Recombination can results in either the emission of heat (non-radiative recombination) or light (radiative recombination). The fault sites where radiative recombination occurs are called luminescence centers, and the resulting light is referred to as thermoluminescence or optically stimulated luminescence, depending on whether heat or light, respectively, was used to release electrons from the traps. The amount of light emitted is proportional to the amount of electrons stored in the defects, and therefore to the amount of energy absorbed by nuclear radiation. Since energy is absorbed at a certain rate, intensity is related to accumulation time; the more the material is exposed, the more the signal is acquired [16].

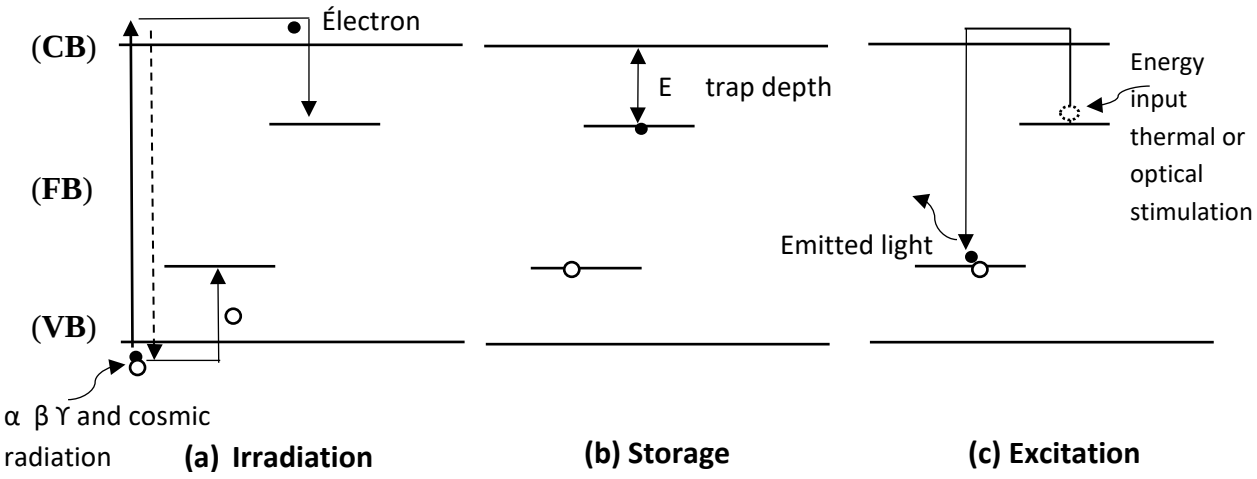

Fig.II.3: Schematic representation of the energy levels of charges in a crystal lattice explaining the phenomenon of stimulated luminescence [16], this is a simplified model: traps with variable energies, photosensitive or not, probability interaction,… etc.
a- A valence electron is excited by ionizing radiation and has enough energy to reach the conduction band, leaving a hole in the valence band. Most of the excited electrons dissipate their energy by immediately recombining with a hole in the valence band; the transition is sometimes accompanied by an emission of photons.
b- Transition of excited electrons into energetic states located under the edge of the band, resulting in electron trapping.
c- By heating the sample, the electron is ejected from the trap and reaches the luminescence centers where they recombine with the holes, resulting in emission of light.

II.2.2 Signal growth and trap stability

The luminescence signals depend on the number of electrons trapped, and therefore increase with the radiation dose received, as long as it is not too large. However, the growth of the luminescence signal with dose is not always linear, as shown in Fig.II.4 for TL.

At low dose, the luminescence signal growth curve shows sometimes a supralinear domain, for which the signal growth increases faster than the dose, while at high dose, saturation of the signal is observed, the causes of which are still discussed, both in TL and OSL. The level of saturation differs depending on the nature of the luminescent material, the stimulation applied (thermal or optical), and the optical window for recording the luminescence signals. It is therefore characteristic of the crystal defects.

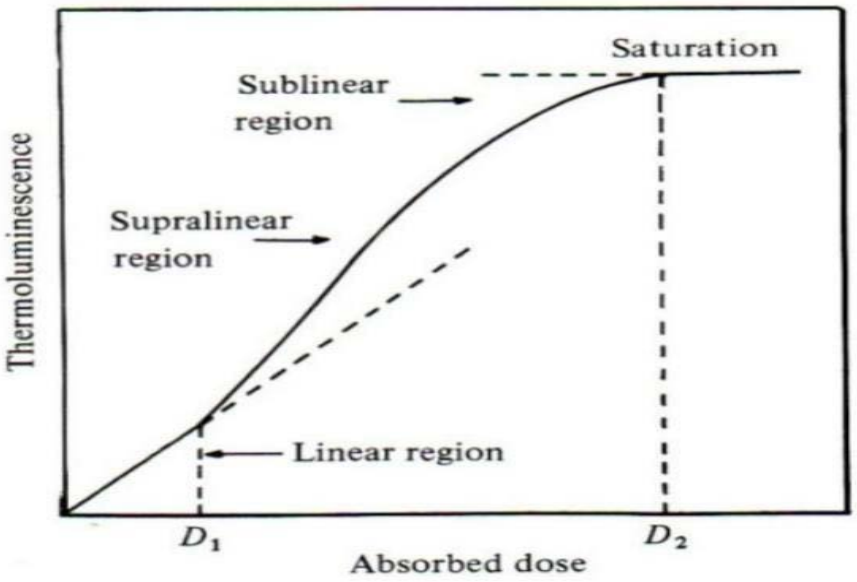

Fig.II.4: Theoretical growth of thermoluminescence according to Aitken (1989) [12].

Now, it is clear that the same production mechanism is responsible for the two luminescence phenomena, TL and OSL [19]; and that the only difference is in the way the electrons are stimulated out of their traps. In the OSL, the electron escapes from its trap following the absorption of a photon of light with a sufficient energy, while in the TL the electron escapes due to the rise in temperature, most often above 450°C. The rate of expulsion depends on the intensity of the stimulating light and the sensitivity of the trap to light and heat.

Intensity refers to the number of photons arriving in a certain time. It is easy to understand that the more photons there are per unit of time, the more electrons will be stimulated out of their traps.

Another phenomenon that can also occur is the *anomalous fading*. It corresponds to the loss of part of the trapped electrons despite the thermal stability of the trap considered satisfactory [20]. Note, however, that this effect can be significant for certain feldspars, but it is negligible for quartz.

The method of stimulated luminescence is therefore based on the ability of materials (crystals) to capture and store energy of radioactive origin in the form of metastable electronic states, and to return in the form of luminescence, during a sufficient supply of energy, such as heating or lighting.

II.3 Basic luminescence measurement equipment and the main approved techniques

II.3.1 The luminescence reader

The basic layout of the equipment used to measure luminescence in archaeological dating is shown in Figure II.5. Luminescence dating systems generally have TL and OSL measurement capabilities [21, 22]. To perform a measurement, samples are usually loaded onto discs of about 1 cm in diameter which rest on an appropriate sample holder. These are then introduced into the device, commonly referred to as a luminescence reader [23] and selectively placed in position for measurement. The luminescence signal of the sample is captured by a photon detection system [11], for example, a photomultiplier tube (PMT) or charge coupled device (CCD) camera after passing through optical filters.

When performing TL measurements, the filters exclude the infrared signals from the heater but allow blue or purple emissions to pass through. In OSL measurements, the wavelengths used for stimulation are rejected by the filters, while the purple and near-ultraviolet wavelengths are usually transmitted. The output of a TL measurement is markedly different from that obtained using OSL stimulation (Figure II.5).

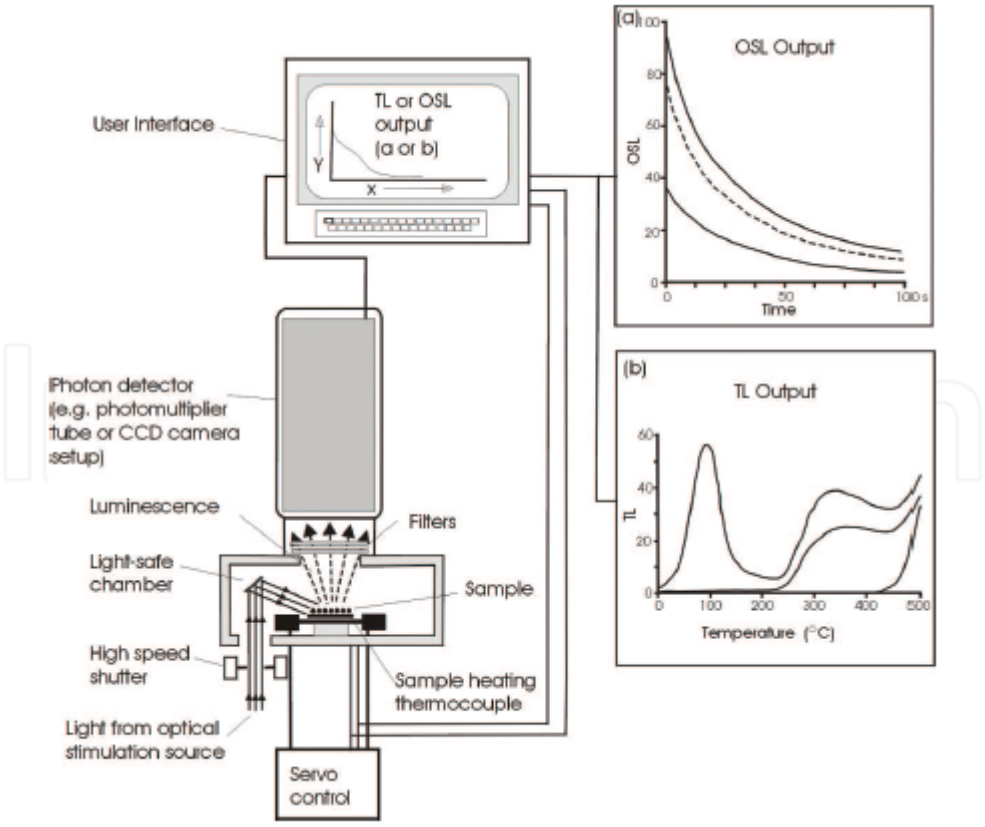

Fig.II.5: Main components of a luminescence reader measuring both TL and OSL signals [24].

For dating studies, the main objective of TL and OSL measurements is to determine the amount of energy that has been stored in the mineral grains of a given material since the start of the event studied. As stated above, two main methods are used to stimulate energy release in luminescence studies. Heating allows TL measurement, while stimulation using a light source is used for OSL measurements.

II.3.2 Thermoluminescence (TL)

The term thermoluminescence (TL) describes the light emitted by a mineral when it is heated. This light comes from the electrons captured and which are released due to thermal stimulation and subsequent recombination. Thus, it is also (and more correctly) referred to as thermally stimulated luminescence (TSL), although this term is not often used.

TL was the only method used in retrospective dosimetry and luminescence dating until the mid-1980s, and was initially developed for dating ceramic, although it was also later used to date volcanic rocks [15], artefacts and heated sediments, as well as aeolian deposits [25]. However,

among the applications mentioned above, only the dating of heated ceramics and artefact remains in use today.

It is important to heat the samples at a constant rate in order to obtain a temperature resolved luminescence curve for the identification of maximum temperatures. Linear heating is normally accomplished using a low mass heating strip, made of high strength alloys and feeding a controlled current through the heating element. Temperature feedback control is performed using a thermocouple welded to a heating strip (Fig.II.5). Normally, heating is controlled by an electronic ramp which can generate various preheating functions and linear heating rates. The maximum temperature normally used for quartz and feldspar dating is 500°C [26]; while the emitted photons are detected by a photomultiplier tube and then counted.

Although, a TL luminescence curve may look like a smooth continuum, it is made up of a number of overlapping peaks derived from the thermal release of electrons from traps of different stabilities. This is because the lifetime of electrons in deep traps is longer than that of electrons in shallow traps. Normally, traps giving light peaks below 260°C are not useful for dosimetry as electrons can be easily drained from these unstable traps, even at ambient temperatures [27]. Stable light peaks suitable for dosimetry generally occur at 300°C or higher [26].

If heating continues, all electron traps will be emptied. A luminescence curve obtained after the first heating of a sample is given in Figure II.6. Heating the sample again shortly after the first heating will produce a different curve. The second curve corresponds to the incandescence which is usually observed when a material is sufficiently heated to a high temperature, therefore from this second heating there will be no luminescence of the trapped electrons that had accumulated at based on ionizing radiation since the last zeroing event.

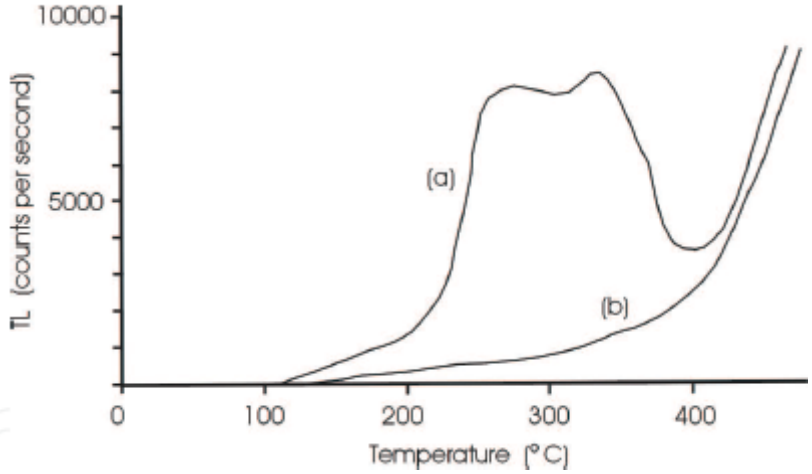

Figure II.6: Illustration of luminescence curves obtained after thermal stimulation. (a) A signal produced after the first heating of a quartz sample with trapped electrons (paleodose). (b) A luminescence curve of the incandescence resulting from the second heating of the sample to an elevated temperature. It is important to note that the incandescence is also achieved above 400 ° C during the first heating [24].

II.3.3 Optical stimulation

The most important breakthrough in luminescence dating in recent years has been the use of optical stimulation (optical dating). This luminescence dating method mainly comprises stimulation by visible light, introduced by Huntley et al in (1985) [11], and that by infrared (IR) discovered by HÜTT et al. (1988) [28]; and may be collectively referred to as photoluminescence or photon stimulated luminescence (PSL). The advantage of any optical method is that only the light sensitive part of the luminescence signal is stimulated, which greatly minimizes the problems of whitening the luminescence signal.

Regardless the type of photostimulation used, optical filters are placed between the sample and the photosensitive surface of the photomultiplier tube to minimize interferences between light from the stimulation source and light emitted by sample [15] (Fig.II.7). When optical excitation begins, latent luminescence in the mineral begins to decay, giving rise to a decay curve recorded by photomultiplier [15] (Fig.II.8).

The term optically stimulated luminescence (OSL) refers to stimulation by visible light. Visible light stimulation is achieved by exposing the sample to a laser beam, light from a filtered halogen lamp, or high power light emitting diodes (LEDs), this latter is the latest and greatest development, and therefore used in the majority of luminescence readers currently

manufactured (Fig.II.7). The width of the excitation waveband differs for different stimulation sources, but all of them are in the green to blue part of the spectrum i.e. between 420-550nm. Quartz and feldspar react both to stimulation in this waveband, although for dating applications, it is primarily used for OSL measurements of quartz [19]. Light of longer wavelengths becomes increasingly ineffective in stimulating OSL in quartz, while wavelengths in the near infrared excite luminescence in feldspars, due to one or more resonances of excitation. Light emissions for quartz using OSL are detected in the ultraviolet range.

In OSL, the signal comes from the recombination of the charge that has been optically released by the electron traps in the crystal. These traps may or may not be the same as those associated with TL peaks. The electron population in the traps is the result of irradiation of the material, and therefore the OSL intensity is related to the absorbed radiation dose. For reasons of experimental convenience, the OSL emitted during the recombination of the destroyed charges is generally measured in a spectral region different from that of the excitation photons. While the TL signal during heating appears as a curve (glow curve) with several temperature peaks representing the different trap levels, the OSL signal during exposure to the stimulating light decreases to a low level when the trapped charge is exhausted (decay curve) (Fig.II.8) [29]. The physical principles of OSL are therefore closely linked to those of TL.

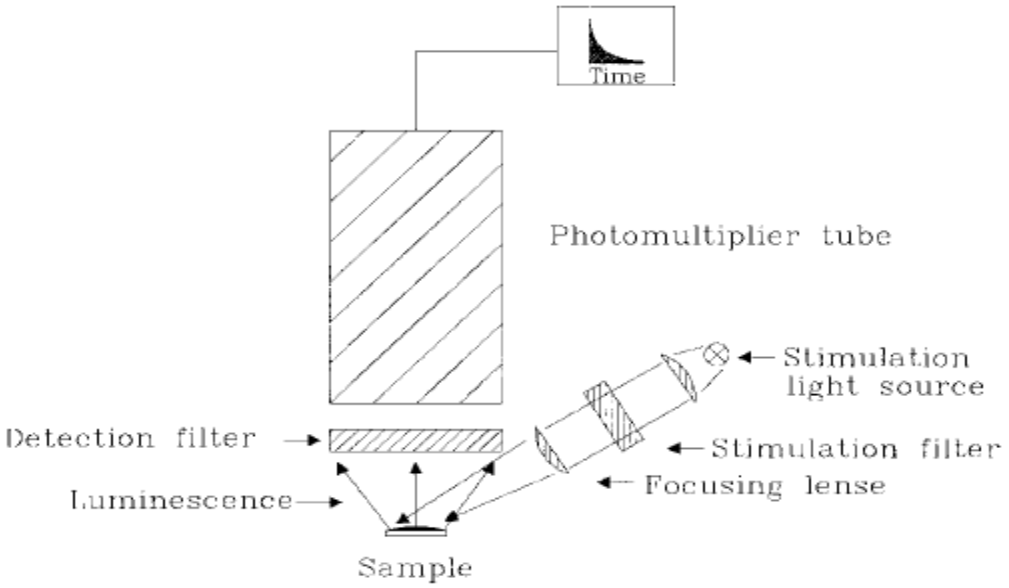

Fig.II.7: Simple diagram of an OSL system with stimulating light source, detection filter, photomultiplier and readout electronics [29].

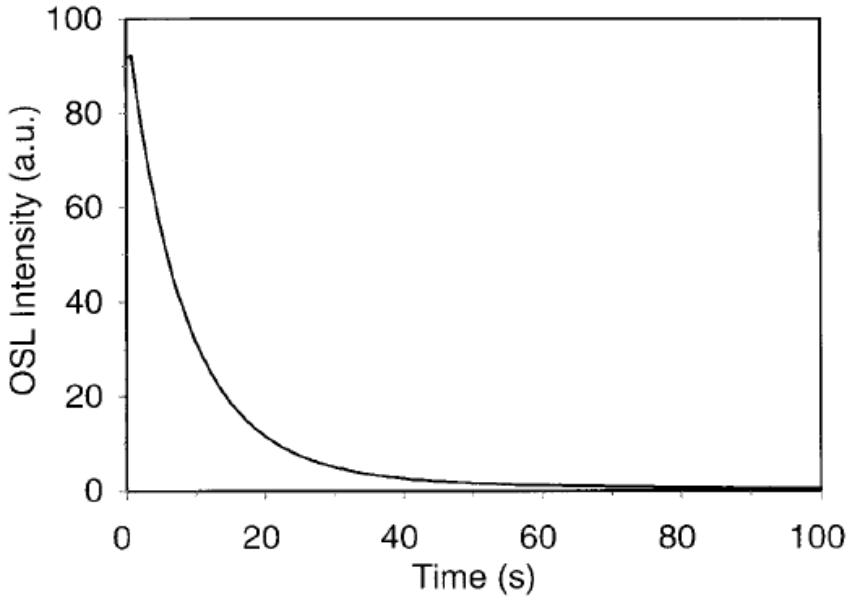

Fig.II.8: Typical OSL decay curve obtained using green light stimulation on a sedimentary quartz sample [29].

II.4 Luminescence dating materials

Materials of archaeological origin dated using luminescence methods must meet a number of characteristics before they can be successfully analyzed. First, the material must consist of a substance that behaves like a dosimeter. Second, the luminescent energy contained in the material must have been reset to zero at some point which now serves as the starting point for counting time. Third, the energy storage in the materials should not have reached saturation at the time of analysis; otherwise, the stored energy would cease to be an accurate measure of the time that has passed.

Luminescence dating mainly uses quartz and feldspar. In the following, the luminescence properties of the two minerals are examined.

II.4.1 Quartz

Quartz is the most common mineral used in luminescence dating because it offers a number of advantages over the alternative. Due to its resistance to chemical weathering and mechanical abrasion, it is very stable on the earth's surface. As a result, it is one of the most abundant minerals in clastic depositional environments. The luminescence properties of quartz are also very stable. In addition, it does not have an internal source of radiation as a major part of its composition. Thus, the ionizing radiation that quartz grains receive in nature usually comes

from an external source, which simplifies the procedures for calculating the dose rate. There are, however, situations where quartz grains may contain very low levels of uranium, but these are rare [30].

• TL properties of quartz:

Natural dose quartz shows peaks of TL at 325°C and 375°C [26]. TL dating generally uses the peak of 375°C which is very stable and would be the result of impurities in the AlO_4 network which serve as hole traps [31]. Under sunlight, the peak of 325°C whitens much faster than the peak of 375°C [32]. Quartz which has been artificially irradiated also shows a peak at 110°C [Fig II.9].

Regarding the missions, heating the quartz above 300°C shows a natural TL emission band around 460–480 nm (blue) and another in the order of 610–630 nm (orange). Laboratory-irradiated quartz has a TL emission band less than 300°C in the region of 360–420 nm.

• OSL properties of quartz:

Quartz has been shown to luminescent when stimulated by wavelengths from any part of the visible spectrum [32]. Most current OSL studies, however, prefer to use blue light for stimulation because of the higher OSL intensities it produces [22]. The emission bands observed in the OSL quartz are of the order of 360 to 420 nm (figure 6), which corresponds to the emissions observed in the TL quartz at temperatures below 300°C [32] (Fig II.9).

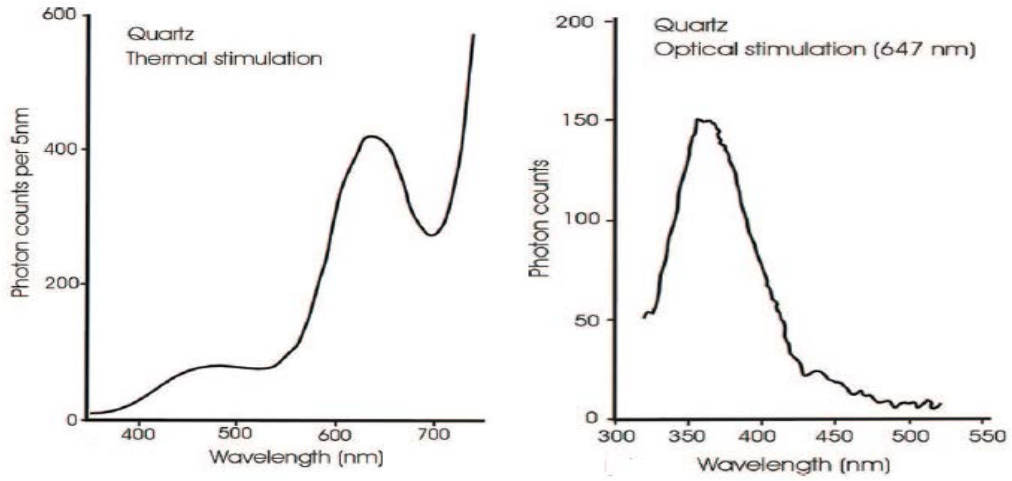

Fig.II.9: Examples of TL (a) and OSL (b) emission spectra [32]. For TL spectra, the sharp increase in emissions beyond 650nm is broadened due to incandescence (rather than electrons expelled from traps).

II.4.1.2 Feldspar

Feldspar is another mineral widely used in OSL dating. It makes up about 60% of the earth's crust and although it passes faster than quartz, it is also a very common mineral on the earth's surface. In terms of chemistry, feldspars are aluminosilicates that form series of solid solutions with potassium (K), calcium (Ca) and sodium (Na) as end members of a ternary system. Since potassium has an isotope that contributes to ionizing radiation in luminescence dating, potassium in K-feldspars should be treated as an internal dose source, in addition to dose inputs from sources external to the grains. Accordingly, when dating feldspars, it is necessary to separate K feldspars from Ca and Na feldspars and analyze them separately.

Compared to quartz, feldspar exhibits a number of attractive luminescence characteristics. First, feldspar emissions are generally brighter than quartz which produces stronger signals. This means that lower doses can be measured during analysis. Second, the internal potassium dose is not sensitive to external influences such as changes in pore water, allowing dose rates to be more accurately determined. Third, feldspar can be stimulated using infrared radiation which allows efficient separation.

• TL properties of feldspar:

Various studies have shown that K-feldspars extracted from sediments produce natural TL signals which peak at 280°C and 330°C [32]. In terms of emission wavelengths, K-rich feldspars have been reported [33] to show maximums in the range 390-440 nm (purple to blue). Conversely, the emissions of some plagioclase feldspars are in the range of 550 to 560 nm (blue-green).

• OSL properties of feldspar:

Optical stimulation of feldspars luminescence has been investigated using visible light. Early studies used lasers that included the 514.5nm wavelength of argon and the 633 nm (red) wavelength of krypton. The emissions were then monitored at shorter wavelengths [11, 34] and were found to be centered around 400 nm [34]. The application of OSL stimulation in feldspars dating, however, has been relatively limited because near infrared stimulation (discussed below) has proven to be a more desirable approach. However, a study [35] comparing green light stimulated luminescence (GLSL) of feldspars with infrared stimulated luminescence (IRSL) reported data suggesting that at 10°C, GLSL signals were more stable than IRSL signals. This would indicate that different types of traps could be involved [16]. In addition to green

and red stimulation, luminescence in the feldspar has been demonstrated using a range of other wavelengths in the region spanning 380–1020 nm [36].

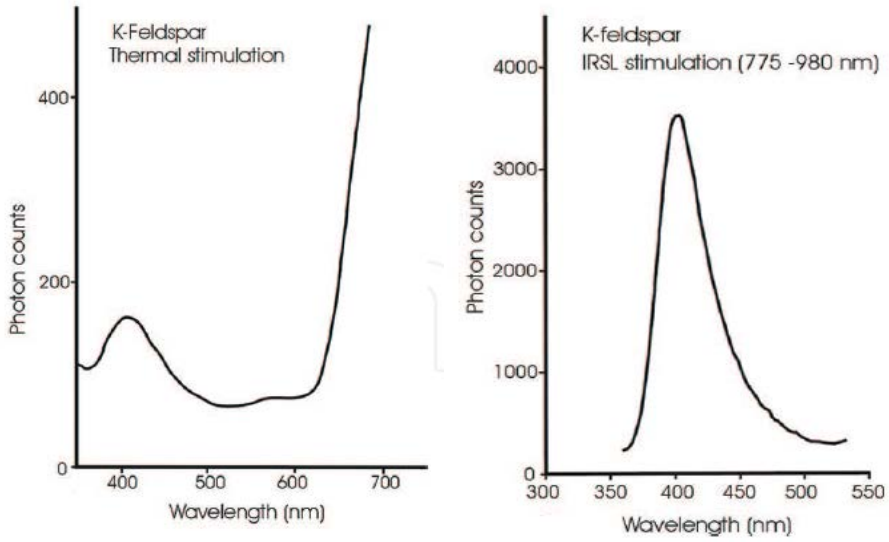

Fig.II.10: Examples of TL (a) and OSL (b) emission spectra [32]. For TL spectra, the large increase in emissions beyond 650 nm is largely due to incandescence (rather than electrons expelled from traps).

Figure II.11 shows the main emission wavelengths for quartz and feldspars used in luminescence dating as well as wavelengths used for stimulation.

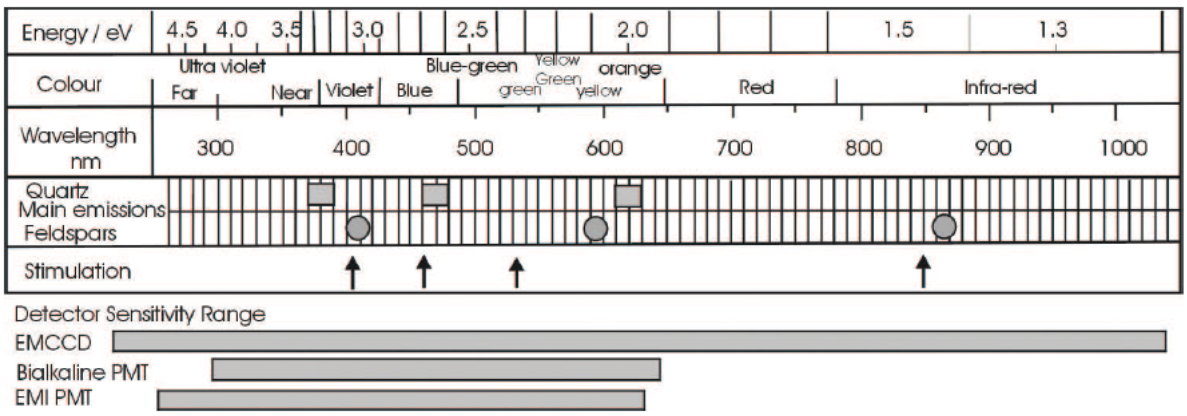

Fig.II.11: Main emission wavelengths for quartz and feldspars used in luminescence dating as well as wavelengths used for stimulation. The sensitivity ranges of some detectors are also indicated. Standard bialaline photomultipliers (PMTs) and PMTs EMI 9235QB do not detect emissions beyond 650 nm, while electron multiplication CCD cameras (EMCCD) can capture the full range [21].

II.5 Lower and upper age limits in luminescence dating:

At present, luminescence dating methods can be used to date samples as young as a few decades [37]. When dating young samples, it is desirable to use mineral grains characterized by high sensitivity to luminescence and that the grains have been completely bleached prior to burial [38]. The maximum ages that can be obtained using luminescence dating methods are ultimately controlled by the fact that the population of electron traps in a given dosimeter is fixed. Figure II.12.a shows such a function expressing the quartz signal. It shows that once a certain dose is reached, the curve lengthens. This dose is the upper limit above which the proportionality between the dose received and the luminescence signal obtained breaks down. Quartz generally saturates with a dose of about 100 to 150 Gy. An approach used in some studies [13, 39] working with high doses is to model the growth curve by combining a linear function and a saturating function as shown in Figure II.12.b [40]. This approach has been used to report quartz ages greater than 200,000–400,000 years. It should be noted that the age limits that can be obtained are ultimately determined by the magnitude of the dose rate, with low dose rates resulting in higher age limits and vice versa. Essentially, with feldspar and quartz dating there are maximum dose limits above which reliable ages cannot be produced due to depletion of electron traps.

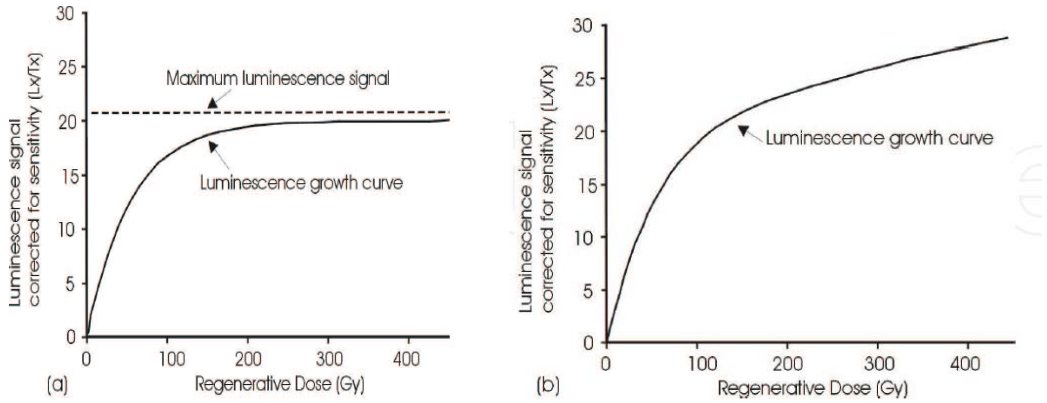

Fig II.12: Examples of growth curves for quartz brought to saturation. (a) Curve constructed using a saturating exponential function of the form $I(D) = I_0 (I - exp - D/D_0)$ where I(D) is the luminescence signal produced by the D dose and I_0 is the maximum intensity of luminescence produced. The parameter D_0 determines the shape of the curve. (b) Since curve (a) seems to underestimate some older ages, the saturating function of (a) is combined with a linear function in (b) [40].

II.6 Thermoluminescence dating

Thermoluminescence is a technique used in the laboratory to produce a luminescence signal. It is based on the principle of heating samples to a temperature set between 450° and 700°C. Indeed, in the case of dating by thermoluminescence, and following its firing, the ceramic has the effect of emptying the traps filled during the geological irradiation (the archaeological zero) [40]. The study in the laboratory later reproduces the old heating, but this time, the light is measured; so we can determine the amount of energy absorbed by the crystals from the old heating by emission of photons, and this amount of energy is called the archaeological dose (or paleodose).

II.6.1 Thermoluminescence signal

Luminescent materials are characterized by different peaks of light emission, which appear during rising heating temperatures at a constant rate. The peaks recorded correspond to the emptying of traps present in the crystal. The higher the temperature at which the peak appears, the greater the depth of the trap in terms of activation energy. The peak appearance temperature also varies depending on the heating rate used. Table II.1 represents the characteristics of the various traps frequently observed in quartz.

Table II.1: characteristics of various traps, frequently observed in quartz. The peak temperatures correspond to temperature rise rates of 2 to 10°C \ sec [30].

Peak (°C)	110	190	240	325	375
Activation Energy (eV)	0.8-0.99	1.42	1.6	1.69	1.66
Frequency factor (s-1)	8 10E+12	3.4 10E+14	9.2 10E+14	1 10E+14	1.5 10E+15
Life time (a) à 15 °C	1.00E-02	0.7 10E+3	340 10E+3	100 10E+6	>10E+8

The area under the peak is an increasing function of the number of traps occupied before stimulation; it is therefore a function of the radiation dose received. Figure II.13 represents the thermoluminescence curve of a recorded quartz sample, during a temperature rise to 5°c /s.

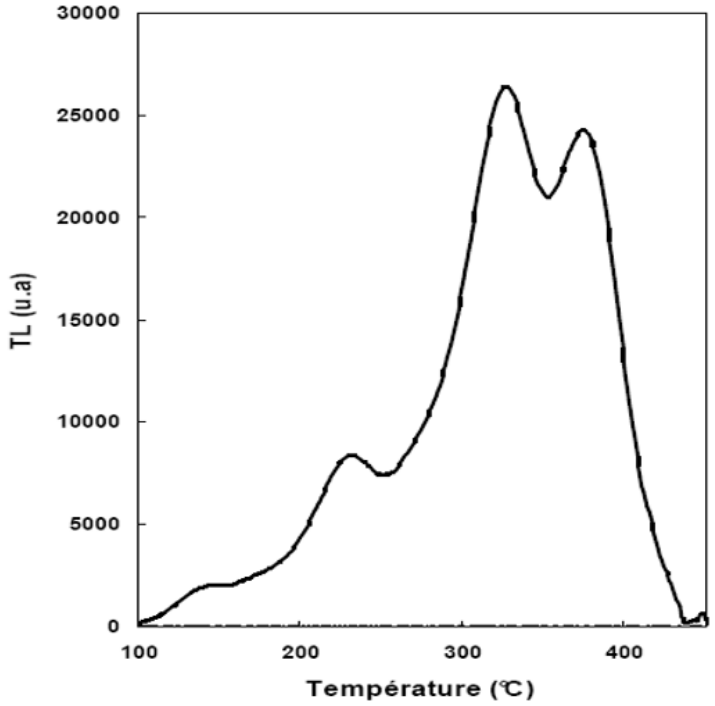

Fig.II.13: Thermoluminescence curve of a quartz sample recorded at a temperature rise of 5°C\s.

II.6.2 Model

A simple model describing the variations in the thermoluminescence intensity as a function of time I(t), has two energy levels, namely an electron trap and a recombination center. If the concentration of trapped electrons is denoted by n(t), and the recombination centers m(t), so:

In a neutral crystal we have:

$$n\,(t) = m(t) \qquad \text{(II.2)}$$

The intensity I(t) emitted during heating is proportional to the rate of recombination. If we suppose that all the recombination are radiatives, I(t) is therefore given by:

$$I\,(t) = -\frac{dm}{dt} = -\frac{dn}{dt} \qquad \text{(II.3)}$$

The average lifetime τ of an electron in a trap is given by:

$$\tau = \frac{1}{p} = s^{-1} exp\,(-\frac{E}{KT}) \qquad \text{(II.4)}$$

In the model of Randall and Wilkins (1945), the probability of trapping an electron during heating is assumed to be negligible. The intensity I(t) is therefore equal to the probability of electrons release per unit time p (for a fixed temperature) multiplied by the number of electrons trapped, hence:

$$I(t) = -\frac{dn}{dt} = n.p = n\ s.exp(-\frac{E}{KT}) \qquad \text{(II.5)}$$

By considering a temperature rise at a constant rate β from the initial temperature T_0, by integrating from t = 0 to t and by noting n_0 the concentration of electrons trapped at t = 0, the resolution of this differential equation leads to the following expression:

$$N(t) = n_0 exp(-\frac{s}{B}\int_{T0}^{T} \exp(-\frac{E}{KT})dt) \qquad \text{(II.6)}$$

The intensity of TL I (T) is then given by [18]:

$$I(t) = n_0\ s exp(-\frac{E}{KT})\ exp\ (-\frac{s}{B}\int_{T0}^{T} exp(-\frac{E}{KT})dt) \qquad \text{(II.7)}$$

If:

$$\frac{dI(t)}{dt} = 0 \qquad \text{(II.8)}$$

Solving the equation II.7 leads to the following relation:

$$\frac{E}{KT} = \frac{s}{B} exp(-\frac{E}{KT}) \qquad \text{(II.9)}$$

In Figure II.14 are represented the change profiles of trapped electron population n, the probability of thermal excitation p and the intensity of thermoluminescence I as a function of the temperature T, when the sample goes through the heating cycle to read the luminescence curve. The initial part of the thermoluminescence curve increases exponentially. In this part, the n population change is not noticeable. On the other hand, the probability of thermal excitation p increases exponentially. The value of n can be considered constant at n_0 in this part. When the number of trapped charges n, is appreciably reduced, the intensity curve TL

stops increasing exponentially. It goes through a maximum before dropping and eventually drops to zero when all traps are emptied.

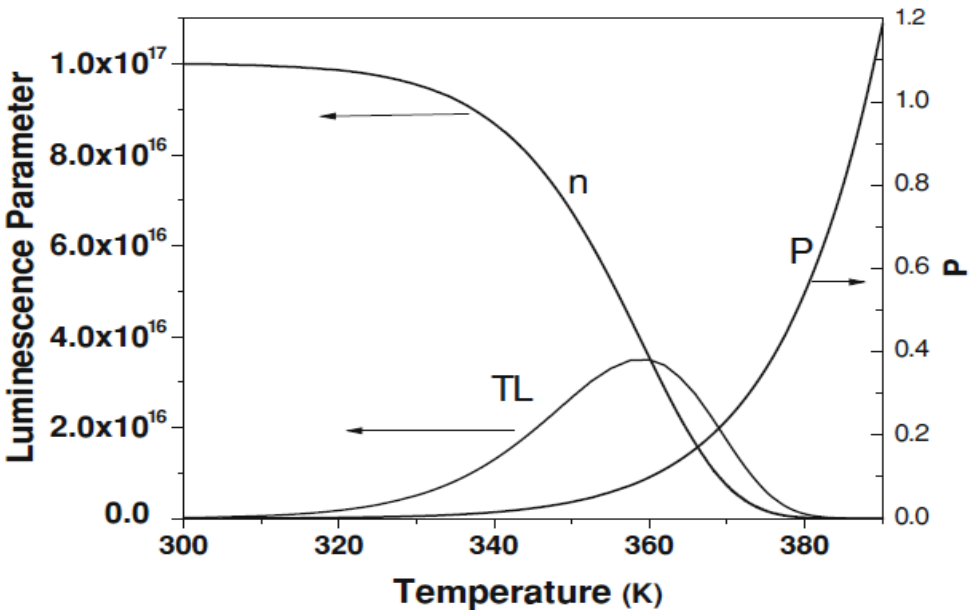

Fig.II.14: Profiles of trapped electrons population n, excitation probability p and the thermoluminescence curve TL as a function of the temperature, during heating. The intensity values plotted in the luminescence curve are 10 times the actual values calculated for a better visibility. The calculations are carried out using the Randall-Wilkins model [18].

II.6.3 The age calculation

Archaeological dating by luminescence-based methods involves evaluating the total dose of energy received since the signal was reset to archaeological zero, by comparing the “natural” signal resulting from natural irradiation and recorded during burial [41], to signals from the same sample induced in the laboratory by the administration of doses of artificial radiation with a calibrated source; and the evaluation of the annual dose rate to which the sample is subjected, or the energy absorbed by the crystals during one year, by measurements of radioactivity in the field and/or in the laboratory.

Indeed, the radiochemical composition in the sample's environment is still changing; which means that the dose rate is likely to change over time as well. It is for this reason that the mean value is determined. With these quantities, it is possible to determine the age of a sample from the last firing according to the fundamental dating equation [16, 41]:

$$Age\ TL\ (an) = \frac{Archaeological\ dose\ (Gy)}{Annual\ Dose(Gy/an)} \qquad \text{(II.10)}$$

With:

- ✓ **Archaeological dose (paleodose):** the amount of energy per unit mass, stored by the crystal since its last heating, measured in Gy. It consists of comparing the natural signal resulting from natural irradiation and recorded during burial, to signals from the same sample induced in the laboratory by the administration of doses of artificial radiation with a calibrated source.
- ✓ **Gy:** Gray symbol, unit of the absorbed dose such that: 1 Gy=1 Joule/Kg.
- ✓ **Annual dose:** the quantity of energy per unit of mass accumulated in a year by the crystal. It is determined by either using the radioelement concentrations of the sample and the landfill medium, or directly using ultra-sensitive dosimeters left at the location where the sample was found for a few months.

II.6.4 Determination of paleodose

Thermoluminescence dating includes estimation of paleodose, or rather equivalent dose (De). This latter can be performed using multiple aliquot or single aliquot techniques.

II.6.4.1 Single aliquot protocol

This protocol is carried out on a single aliquot of the sample on which are carried out all the measurements necessary for the construction of a curve of growth of luminescence as a function of the dose. In this case, the procedure is repeated on several aliquots (one dozen for example), in order to improve accuracy.

II.6.4.2 Multiple aliquot protocol

Multi-aliquot techniques, and in particular those that have been developed for quartz, are the ones that are of direct interest to us in our work; they require the measurement of several aliquots of the mineral. This technique however requires normalization measurements to minimize aliquot-to-aliquot differences in luminescence sensitivity. Although this improves the precision of the measurement, the resulting De is not necessarily more precise [42].

For the two techniques, there are two approaches used: the additive dose and the regenerative dose [16]. For both approaches, a so-called dose-response curve is calculated, reflecting the increase in latent luminescence in mineral grains with the increase in dose [41,32]. In the

additive dose approach, an artificial signal induced in the laboratory is added to the natural signal (Fig.II.15), while in the regenerative dose method, the latent luminescence signal is first removed, and the sample is then irradiated and a laboratory signal regenerated (Fig.II.16).

Regardless of the approach used, the measurement of paleodose involves three different steps: irradiation, preheating and luminescence measurement.

Irradiation is performed to induce a latent luminescence signal in the grains; it is carried out using either beta sources (external or integrated in the luminescence reader) or external gamma sources. During artificial irradiation, all traps, including those unstable for longer periods, capture electrons. To allow comparison with the paleodose absorbed during the burying time, the unstable component of the luminescence signal should be removed and is obtained by heating the sample (between 200°C and 300°C for typically 10s, or more hours at temperatures of about 150°C), causing the expulsion of electrons captured in shallow traps. Once this preheating of the sample is done, luminescence is measured by stimulating the sample with heat.

II.6.4.3 Multiple Aliquot Additive Dose (MAAD) technique

In this approach, a number of aliquots are prepared and divided into groups. From a group, the natural TL signal is measured. The other groups receive known and different doses of radiation in addition to their natural dose, using a source calibrated in the laboratory. All aliquots are then preheated and measured. A plot of the measured luminescence intensity against the added dose gives the dose response or growth curve. The unknown dose is obtained by extrapolating this growth curve to zero luminescence intensity (Fig.II.15). Since the MAAD technique involves an extrapolation, the result depends quite strongly on the choice of the mathematical function (linear, exponential, polynomial, etc.) used to describe the growth of the signal with the dose.

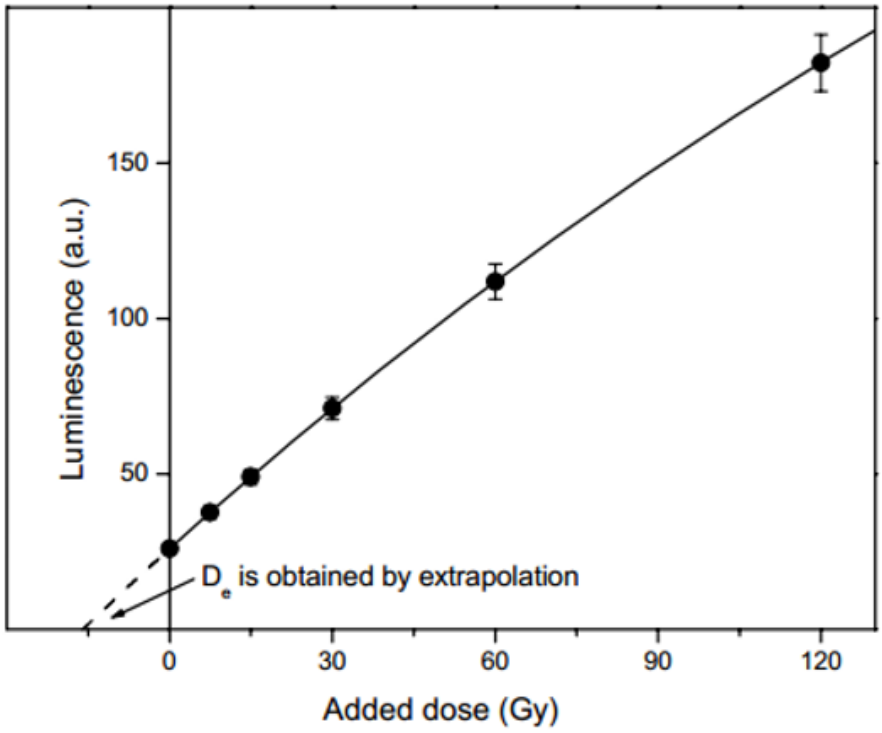

Fig.II.15: Schematic representation of the additive multi-aliquot technique for the determination of the equivalent dose. The function is fitted to these data and is extrapolated to zero luminescence intensity to obtain the equivalent dose.

II.6.4.4 Multiple Aliquot Regenerative Dose (MARD) technique

In this method, all groups of aliquots, except the group reserved for measuring the natural signal, are first heated to remove the naturally acquired luminescence signal. Subsequently, they receive different and known regenerative beta doses. After warm-up, the natural and regenerated TL signals are measured. Regeneration doses are chosen such that the resulting luminescence signals encompass the natural signal. This makes it possible to determine the equivalent dose by interpolation (Fig.II.16), which has the advantage of reducing the uncertainties due to the choice of the adjustment function. The most important disadvantage of this technique is that dosing and heating can alter the luminescence properties of mineral grains. More precisely, a change in sensitivity (luminescence per unit dose) may occur between the measurement of natural TL and the measurement of regenerated TL. This has been observed [43-45] using feldspars, quartz or a mixture of minerals. Heated and regenerated grains may become more sensitive, and will emit more luminescence for the same dose as natural grains. The growth curve will therefore become steeper. This is illustrated in (Fig.II.16). The

occurrence of changes in sensitivity can be recognized by comparing the slope of the regenerated growth curve with that of the additive dose growth curve.

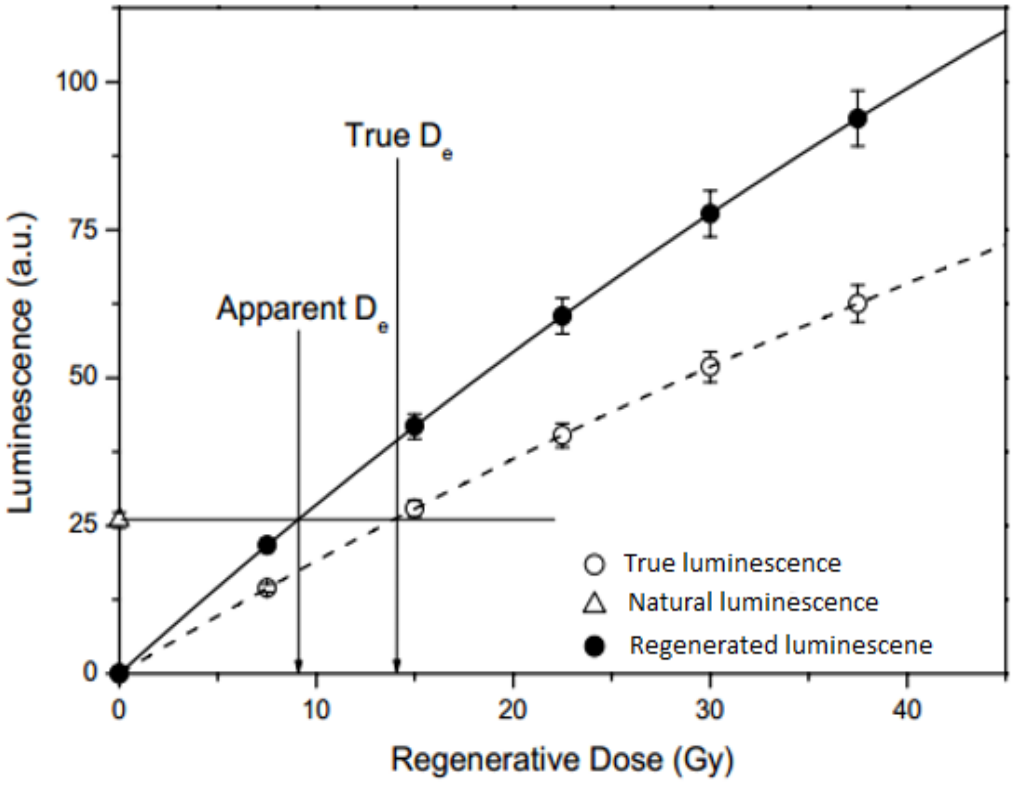

Fig.II.16: Schematic representation of the multiple aliquot regenerative dose technique for equivalent dose determination.

II.6.5 Determination of the annual dose

II.6.5.1 Nature and origin of ionizing radiation

The assessment of the annual dose is an essential step in the dating process. Indeed, it has a direct influence on the final result, and its uncertainty is linearly transferred to its age [46]. However, when determining the dose rate during luminescence dating, it is important to distinguish between the dose absorbed by the soil matrix and that by the grains emitting luminescence. For example, quartz grains separated from the soil contain almost no internal radioactivity and the outer layer of large grains can be etched, thus reducing the contribution of alpha radiation to zero. The annual radiation dose in luminescence dating comes from the

ionizing radiation (γ, β and α radiation) of long-lasting life natural primordial radionuclides present in the sample and its immediate surroundings (235U, 238U, 232Th, 40K) and cosmic radiation [47-51]

Natural uranium and thorium are composed of three radioactive series led by 235U, 238U and 232Th and which end in 207Pb, 206Pb and 208Pb respectively. It is generally assumed that the 238U to 235U ratio is naturally constant. Even though 235U is only 0.72% of the atoms in natural uranium, it contributes about 4.4% of the combined activity of uranium, due to the shorter half-life of 235U compared to 238U. When transforming the U concentration into an annual radiation dose, the constant ratio 238U/235U is taken into account.

When the 235U nucleus undergoes radioactive decay, with the emission of an α particle, the child nucleus formed, 231Th, is also radioactive. This process continues through radioactive descendants until the stable isotope of 207Pb is reached.

Connecting the beginning and the end of the chains, several radioactive descendants of 235U, 238U and 232Th are important because they emit a variety of α, β and γ radiations.

The radioactive decay series of 235U, 238U, 232Th and 40K are shown in Fig.II.17, II.18, II.19 and II.20 respectively [52].

The impact of ionizing radiation on matter is dependent on the characteristics of the emitting source and also on the properties of the matter it passes through; the matter here representing the mineral matrix of an archaeological sample. These types of ionizing radiation have different powers of penetration into the material; the different characteristics of these radiations complicate the evaluation of the dose rate as well as the procedures required for the preparation of the portions to be measured. First, for a given amount of energy absorbed, alpha radiation is much less effective at inducing thermoluminescence than beta and gamma radiation. Second, the mean free path is very different: alpha 0.03 mm; beta 3 mm; gamma 0.3m [16]. In addition, in pottery, there is a considerable heterogeneity in the levels of radioactivity of its constituents. Quartz grains have much lower radioactivity than the clay matrix in which they are embedded, and potassium feldspar grains have higher radioactivity.

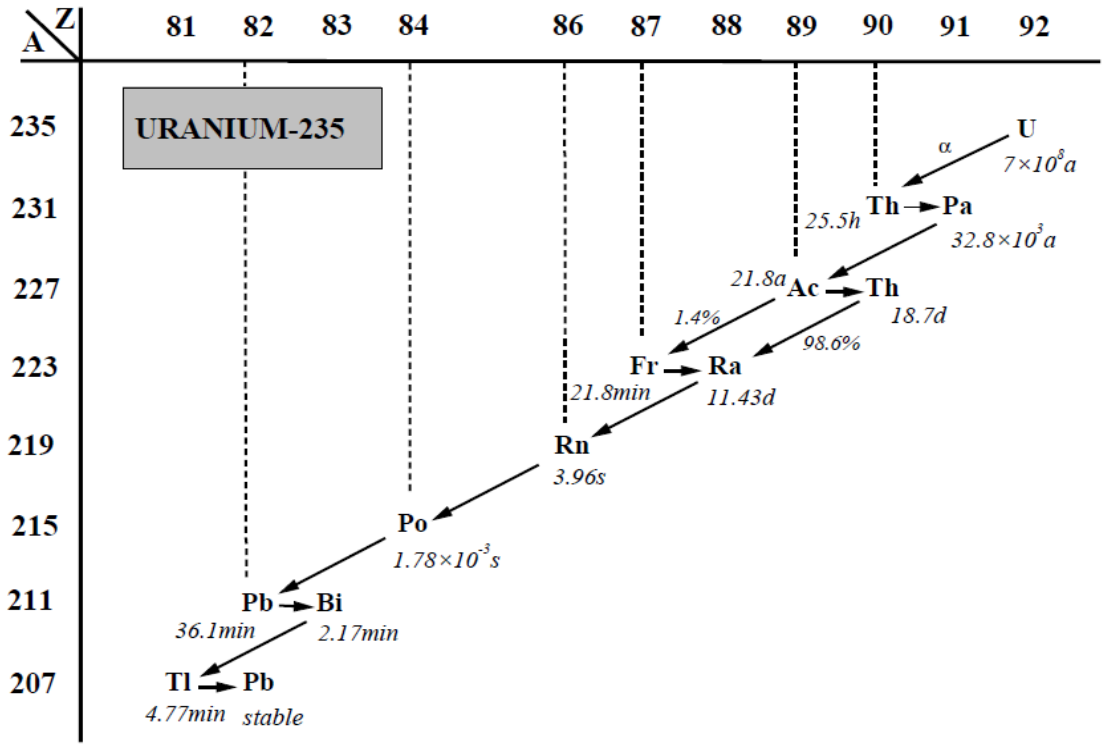

Fig.II.17: Decay chain of ^{235}U (branchings with a probability of less than 1% are omitted).

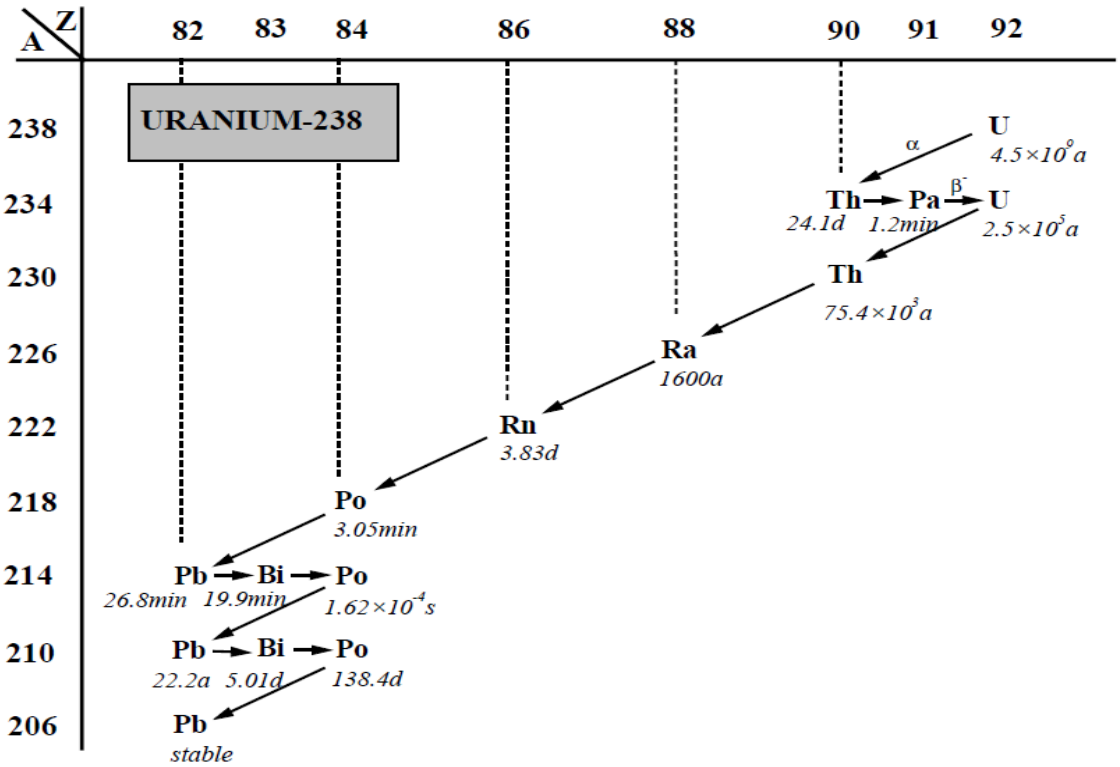

Fig. II.18: Decay chain of 238U (branchings with a probability of less than 1% are omitted).

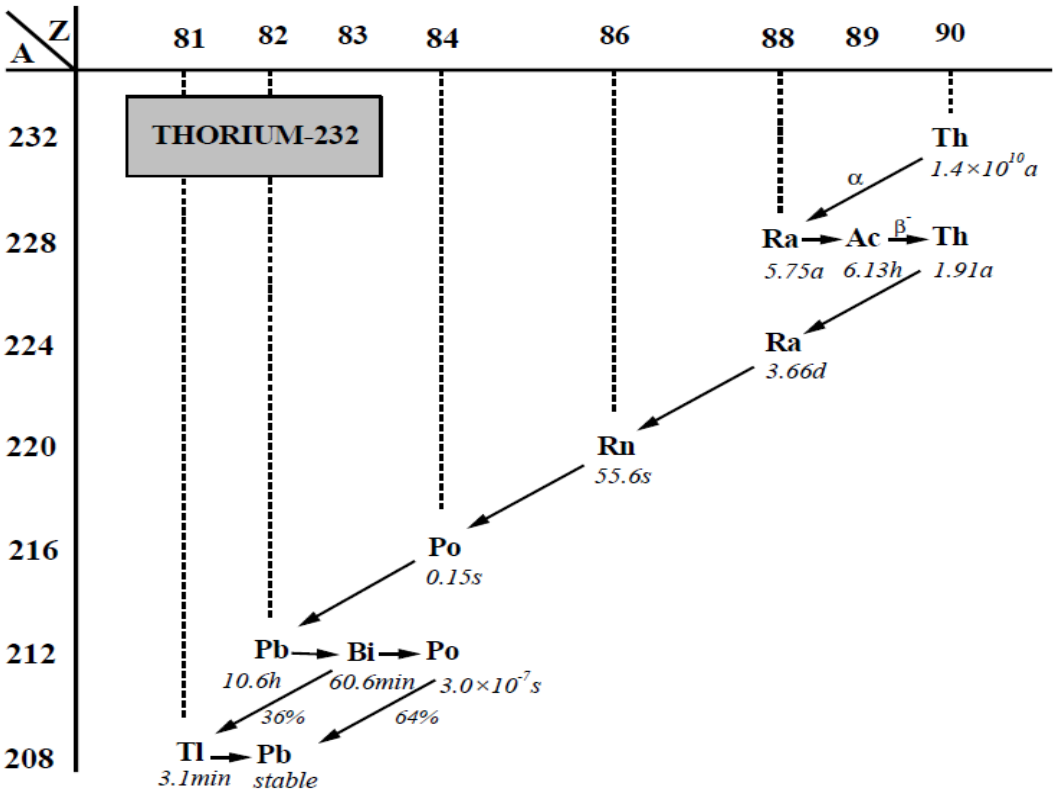

Fig.II.19: Decay chain of 232Th (branchings with a probability of less than 1% are omitted).

When ^{40}K nuclei with a natural atomic abundance of 0.0117% undergo radioactive decay, beta particles and a gamma ray with energy of 1460.8 keV are emitted.

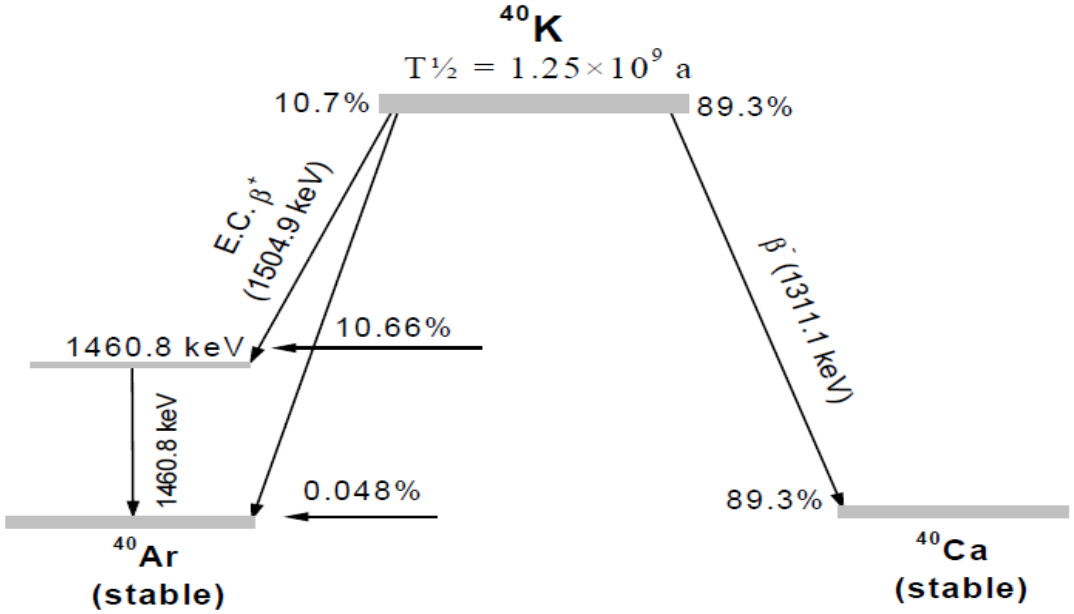

Fig.II.20: Decay scheme of ^{40}K.

Most of the alpha particles emitted by the uranium and thorium series have a relatively high energy, ranging from 3 to 8.8 MeV (for 212Pb, element of the 232Th series). The speed at which they pass through matter is the lowest of all common types of radiation. Alpha particles lose their energy quite quickly, so over a very short distance (point deposition). They can penetrate up to about 20 µm around the emitting nucleus (up to 50 µm for the most energetic particles).

Relativistic electrons, being 8000 times lighter than alpha particles, can go up to approximately 2 mm deep in matter. The effects caused by beta particles will therefore be visible over greater distances than those caused by alpha particles. In addition, electrons are easily deflected as they slow down in matter, and irradiation occurs more in volume than in a straight path.

Gamma radiations are very energetic photons with wavelengths less than 10^{-11} m and an energy ranging from a few keV to several MeV (for those from natural radioactive series), they are capable of penetrating materials over distances of several tens of centimeters for what corresponds to the most energetic gammas of the natural series (approx 3 MeV). This is more penetrating radiation than alpha and beta radiation.

Cosmic radiation is a significant component of natural ionizing radiation. It originates from stellar nuclear reactions or particles emitted into the universe which are accelerated by various astrophysical processes. The interaction of these high-energy particles with the atmosphere produces muons, which form the essential component of cosmic radiation at ground level, and pass entirely through the material. The presence of obstacles, in particular due to masonry which shields cosmic radiation, makes this component quite variable depending on the position of the sample (Fig.21). The cosmic dose rate depends on the burial depth, altitude and latitude [48-50]; formulas are available in the literature for the calculation of the cosmic dose rate [51].

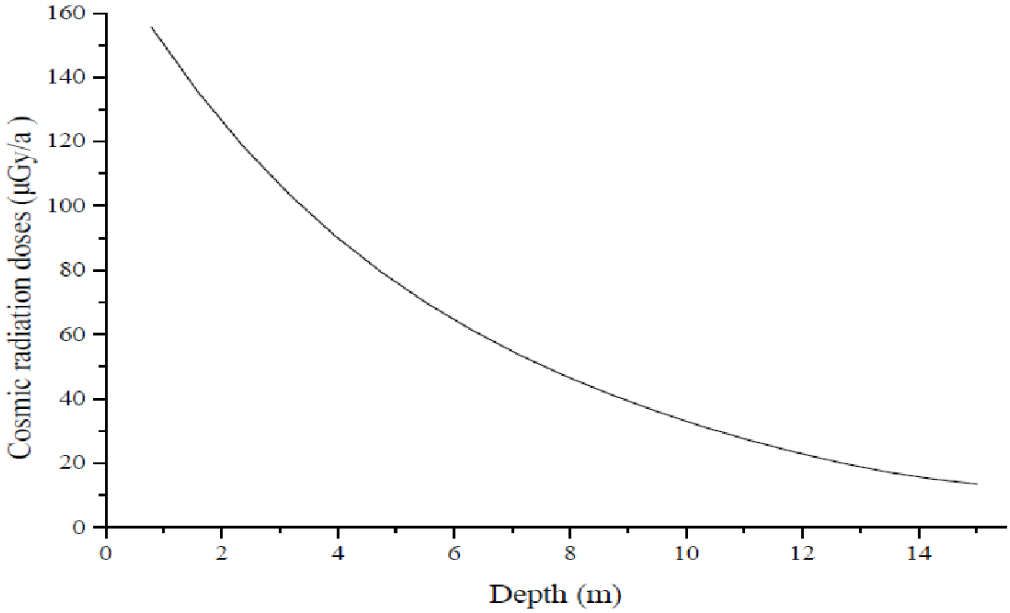

Fig.II.21: Cosmic radiation dose rate variation with depth below the earth's surface, for latitudes above 40°C, at sea level [52].

II.6.5.2 Radioactive system

An archaeological sample is exposed to radiation from naturally occurring radioisotopes that are present in the sample itself and also in its environment (Fig.II.22). The radioactive effects which come from the radioelements present in the sample itself will take place at different levels depending on their location. Radiation from radioisotopes outside the sample reaches different depths depending on its nature and therefore its penetrating power.

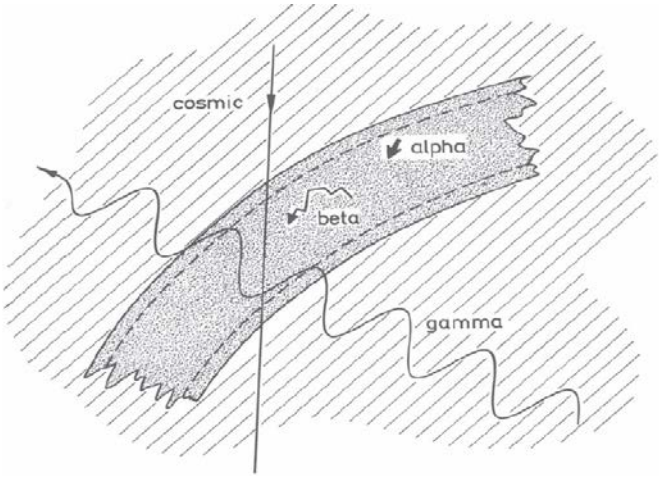

Fig.II.22: Illustration of the different ranges of the components of the radiation flux giving rise to TL [41].

A radioactive system is defined in relation to the minerals analyzed in TL (factors internal and external to the grains and to the sample) as follows:

$$Itot = Iint + Isam + Ienv \qquad \text{(II.11)}$$

Where *Iint* corresponds to the internal radioactivity to the grains analyzed in TL, *Isam* to the radioactivity specific to the sample and *Ienv* to the radioactivity of the environment in which the sample was located. The above equation can be developed into a more detailed formulation, where the different types of radiation are specified:

$$Itot = Iint + (kI\alpha + I\beta + I\gamma)\ sam + (kI\alpha + I\beta + I\gamma + Icosm)\ env \qquad \text{(II.12)}$$

Gamma photons, as mentioned earlier, can penetrate through the material under study. The gamma component from the sample depends on its dimensions and its radioactivity. In the case of terracotta fragments, it is not necessary to distinguish and measure them or determine them separately because the gamma contribution of the sample *(Iγ)sam* and that of the environment *(Iγ)env* can be integrated directly by the dosimetric measurement (i.e. *Iγ* the measurement of the global annual gamma dose) or separately.

As mentioned above, the path of alpha particles in the mineral matrix does not exceed 30 µm, and the penetrating power of beta particles approaches 3 mm. Since the 2-3 mm layer of the surface of the studied samples (maximum beta particle path) was removed during preparation, alpha *(kIα)env* and beta *(Iβ)env* contributions to the environment can be eliminated. Taking these aspects into account, the above equation is reduced to the following formulation:

$$Itot = Iint + (kI\alpha)sam + (I\beta)sam + I\gamma + Icosm \qquad \text{(II.13)}$$

This equation summarizes the various contributions that will be taken into account to estimate the annual dose rate received by the sample studied. For coarse grain sizes, beta and gamma contributions are predominant and their estimation is particularly important for the assessment of the annual dose. The determination of each of these parameters is described separately below.

II.6.5.3 Determination of the different contributions to the annual dose

The radioactivity of the material can be estimated by different methods. Their principle is based on measuring the concentrations or activities of radionuclides contained in the analyzed material [53]. These are very sensitive analytical methods used to determine trace elements of the order of ppm, such as inductively coupled plasma mass spectrometry (ICP-MS) [54,55],

low background gamma spectrometry which also makes it possible to determine the state of imbalance of the uranium series, or the XRF fluorescence [16]. The radiochemical data acquired are then converted into annual irradiation doses by applying the content/annual dose correspondence coefficients [56]. The attenuation effects of alpha and beta irradiation by the spherical grain are evaluated by applying the factors of attenuation depending on the particle size used [57, 58].

II.6.5.3.1 Internal grain contribution

The internal grain contribution of quartz (*Iint*) is often considered to be zero, since these minerals are believed to contain no radioelements. However, in recent years, several experiments have shown that this hypothesis is not always true [59]. More particularly, when the radioactivity external to the grains is rather low, it is more prudent to evaluate this contribution to avoid inaccuracies in the determination of the annual dose.

II.6.5.3.2 Alpha and beta irradiations of the sample

The alpha ($kI\alpha_{sam}$) and beta ($I\beta_{sam}$) contributions of the sample are measured by low background gamma spectrometry. The minerals of the matrix are at the base, composed of gravel and coarse sands; the latter have dimensions greater than the penetrating power of the beta particles (2 mm), approximately 10 grams of the rest of the sample (less than 2 mm) are taken, crushed and sieved, in order to have a homogeneous and thinner powder. Their elimination should be an essential step in determining the beta dose rate from the matrix and surrounding the quartz grains measured by TL. The powder obtained must be packaged in polyethylene tubes and the tubes must be hermetically sealed, in order to achieve the balance between radium-226 and radon-222 before being measured.

II.6.5.3.3 Contribution of the environment

The environmental gamma contribution and cosmic radiation can be assured by in situ dosimetry. The dosimeters are made up of three alumina pellets, a luminescent material that is extremely sensitive to radiation, inserted into a metal tube. The tube is 2 millimeters thick to ensure that only gamma and cosmic radiation will penetrate towards the pastilles.

The dosimeters are buried in the archaeological site for a period of several months [60] the annual dose will be determined subsequently by calculation.

II.7 Conclusion

Luminescence dating belongs to the category of so-called dosimetric radiation dating methods. Age determination by the luminescence dating method is based on measuring the luminescence of samples containing quartz or similar minerals. This is achieved by measuring, on the one hand, the paleodose, i.e. the energy stored since the last reset and, on the other hand, the dose received each year by the sample. The ratio of the paleodose to the annual dose provides the age of the object analyzed. Many types of techniques are used for sample preparation including thermoluminescence. Accurate determination of the luminescence signal is essential and closely related to sample preparation. Although the techniques are different, the sample preparation procedures for luminescence methods contain some common processes. To obtain the precise age of the sample, these processes must be applied in such a way as to avoid causing additional luminescence or loss of luminescence. Determining the most appropriate procedure and applying it correctly to samples provides reliable results.

References

[1] Yukihara E G, McKeever S W S (2011) Optically Stimulated Luminescence: Fundamentals and Applications. Wiley. 378 p.

[2] Boyle R (1664) Experiments and Considerations upon Colours with Observations on a Diamond that Shines in the Dark. London: Henry Herringham.

[3] Hunter M C W (2007) The Boyle Papers: Understanding the Manuscripts of Robert Boyle. 688 p.

[4] Mc Dougal D J (1968) Thermoluminescence of Geological Materials. New York: Academic Press.

[5] Daniels F, Boyd C A, Saunders D F (1953) Thermoluminescence As A Research Tool 343-349.

[6] Aitken M J, Tite M S, Reid J (1964) Thermoluminescence Dating Of Ancient Ceramics. Archeology 1032-1033

[7] Fleming S J (1966) study of thermoluminescence of crystalline extracts from pottery. Archeometry.

[8] Zimmerman D W (1967) thermoluminescence from fine grains from ancient pottery 26-28

[9] Fleming S J, Moss H M, Joseph A (1970) Thermoluminescence authenticity testing of some ‘six dynasties’ figures 57- 65

[10] Goksu H Y, Fremlin J H, Irwin H T, Fryxell R (1974) Age Determination of Burned Flint by a thermoluminescent method, science vol 183: 651-654

[11] Huntley D J, Godfrey-Smith D I (1985) Optically Optical Dating of Sediments. Nature 313: 105-107

[12] Aitken M J (1989) Luminescence dating: a guide for non-specialists. Archaeometry 31:147–159

[13] Murray A, Buylaert J P, Henriksen M, Svendsen, J I, Mangerud J (2008) Testing the reliability of quartz OSL ages beyond the Eemian. Radiation Measurements 43:776–780

[14] L Zoller, G A Wagner (2013) Luminescence Dating: History Encyclopedia Of Scientific Dating Methods: 1-10

[15] Preusser F, Degering D, Fuchs M, Hilgers A, Kadereit A (2008) luminescence dating: basics methods, and application. Quaternary science journal 57 1/2:95–149

[16] Aitken M J (1998) An Introduction to Optical Dating. Oxford University Press.

[17] Bos A J J (2001) High Sensitivity Thermoluminescence Dosimetry. Nuclear instruments and methods in research 184: 3-28

[18] Sunta C M (2015) Unraveling Thermoluminescence: Springer Series in Materials Science. Springer. New Delhi. India. Vol 202.

[19] Murraya A S, Wintle A G (1999) Isothermal Decay of Optically Stimulated Luminescence in Quartz. Radiation Measurements 30: 119-125

[20] Wintle A G (1973) Anomalous Fading of Thermoluminescence In Mineral Simples. Nature Vol 254: 143-144

[21] Richter D, Richter A, Dornich K (2011) Lexsyg – A new system for luminescence research. Geochronometria 20:220–228

[22] Bøtter-Jensen L (1997) Luminescence techniques: instrumentation and methods. Radiation Measurements 17:749–768

[23] Fuchs M, Owen L (2008) Luminescence dating of glacial and associated sediments: a review, recommendations and future directions. Boreas 37:636–659

[24] Stokes S (1999) Luminescence dating applications in geomorphological research. Geomorphology 59:153–171

[25] Wintle A G, Huntley D J (1982) Thermoluminescence Dating of Sediments. Quaternary Science Reviews Vol 1: 31-53

[26] Fleming S J (1970) Thermoluminescent Dating: Refinement of the Quartz Inclusion Method. Oxford University, England 133-145

[27] Franklin A D, Prescott J R, Scholefield R B (1995) the mechanism of thermoluminescence in an Australian sedimentary quartz. Journal of luminescence 63: 317-326.

[28] Hiitt G, Jaek I, Tchonka J (1988) Optical Dating: K-Feldspars Optical Response Stimulation Spectra. Quaternary Science Reviews Vol 7: 381-385

[29] Bøtter-Jensen L (2000) Development of Optically Stimulated Luminescence Techniques Using Natural Minerals and Ceramics, and Their Application to Retrospective Dosimetry. (RISO-R--1211(EN)). Denmark.

[30] Aitken M J (1985) Thermoluminescence Dating. London. Academic Press.

[31] McKeever S W S (1985) Thermoluminescence of Solids. Cambridge: Cambridge University Press. *123*(4), 471-472.

[32] Wintle A G (1997) Luminescence dating: laboratory procedures and protocols. Radiation Measurements 27:769–817

[33] Huntley D J, Godfrey-Smith D I, Thewalt M LW, Berger G W (1988) Thermoluminescence spectra of some mineral samples relevant to thermoluminescence dating. Journal of Luminescence 39:123–136

[34] Godfrey-Smith D I, Huntley D J, Chen W H (1988) Optical dating studies of quartz and feldspar sediment extracts. Quaternary Science Reviews 7:373–380

[35] Li S H, Tso M Y W (1997) Lifetime determination of OSL signals from potassium feldspar. Radiation Measurements 27:119–121

[36] Bøtter-Jensen L, Duller G A T, Poolton N R J (1994) Excitation and emission spectrometry of stimulated luminescence from quartz and feldspars. Radiation Measurement 23:613–616

[37] Ballarini M, Wallinga J, Murray A S, van Heteren S, Oost A P, Bos A J J (2003) Optical dating of young coastal dunes on a decadal time scale. Quaternary Science Reviews 22:1011–1017

[38] Wintle A G (2008) Fifty years of luminescence dating. Archaeometry 50:276–312

[39] Pawley S M, Bailey R M, Rose J, Moorlok B S P, Hamblin R J O, Booth S J (2008) Age limits on Middle Pleistocene glacial sediments from OSL dating, north Norfolk, UK. Quaternary Science Reviews 27:1363–1377

[40] Wintle A G (2008) Luminescence dating: where it has been and where it is going. Boreas 37:471–482

[41] Taylor R E, M J Aitken (1997) Chronometric Dating in Archaeology advances in archaeological and museum science Vol 2. Springer Science+ Business Media, LLC.lexy

[42] Botter-Jensen L, McKeever S W S, Wintle A G (2003) Optically Stimulated Luminescence Dosimetry. Elsevier science B.V.

[43] Wintle A G, Zhou L P (1994) Sensitivity change of thermoluminescence signals after laboratory optical bleaching: experiments with loess fine grains. Quaternary geochronology (quaternary science review) Vol 13: 457-463

[44] Rendell H M, Townsendt P D (1988) Thermoluminescence dating of a 10 m loess profile in pakistan. Quaternary Science Reviews Vol 7: 251-255

[45] Wintle A G (1985) Sensitization of TL signal by exposure to light 16-21

[46] Timar-Gabor A, Vasiliniuc Ş, Vandenberghe D A G, Constantin D, Cosma C (2011) luminescence dating of archaeological materials and sediments in romania using quartz, Romanian reports in physics, Vol. 63, No. 4: 929–939

[47] Mejdahl V, H H Christiansen (1994) Procedures used for luminescence dating of sediments quaternary geochronology, Quaternary Science Reviews Vol 13: 403-406

[48] J R. Prescott, J T Hutton (1988) Cosmic Ray and Gamma Ray Dosimetry for TL And ESR, Nucl Tracks Radiat Meas Vol 14: 223-227

[49] Guérin G (2011) Modélisation et Simulation Numériques Des Effets Dosimétriques Dans Les Sédiments Quaternaires : Application Aux Méthodes de Datation Par Luminescence, Thèse de Doctorat, Université Michel De Montaigne Bordeaux 3.

[50] Cinelli G, Gruber V, Felice D L, Bossew P, Ceballos M A H, Tollefsen T, Mundigl S (2017) European annual cosmic-ray dose: estimation of population exposure. Journal of Maps 13:2, 812-821.

[51] Prescott R, Hutton J (1994) Cosmic Ray Contributions to Dose Rates for Luminescence and ESR Dating: Large Depths and Long-Term Time Variations. Radiation Measurements Vol 23 Nos 2/3: 497-500

[52] Syed Mohammod H (2003) A critical comparison and evaluation of methods for the annual radiation dose determination in the luminescence dating of sediments. Thesis submitted in fulfillment of the requirements for the degree of Doctor (Ph.D.) in Science

[53] David Strebler (2013) Use of minerals other than quartz and feldspars for luminescence dating, university of oxford.

[54] Guérin G, (2016) The Complementarity of Luminescence Dating Methods Illustrated on The Mousterian Sequence of The Roc De Marsal: A Series of Reindeer-Dominated, Quina Mousterian Layers Dated to MIS 3, Quaternary International 1-14.

[55] Sánchez J S, Mato M P (2013) Delimiting the Urban Growth of Santiago De Compostela (Nw Spain) By OSL Dating of Medieval Anthropogenic Sediments. Mediterranean Archaeology and Archaeometry, Vol. 13, No 3: 163-173.

[56] Guérin G, Mercier N, Adamiec G (2011) Dose-Rate Conversion Factors: Update. Ancient TL Vol. 29 No1: 5-8

[57] Mejdahl V (1979) Thermoluminescence Dating: Beta-Dose Attenuation in Quartz Grains. Archeometry 21, 1: 61-72

[58] B J Brennan (2003) Beta Doses to Spherical Grains. Radiation Measurements 37:299- 303

[59] Guibert P, Lahaye C, Françoise B (2009) The importance of U-series disequilibrium of sediments in luminescence dating: A Case Study at The Roc De Marsal Cave (Dordogne, France). Radiation Measurements 44 : 223–231

[60] Gaillard-Lecanu E, Trompier F, Chau Q, Bottollier-Depois J F, Spurny F (2002) évaluation dosimétrique du rayonnement cosmique au Dôme C (Antarctique). Radioprotection Vol. 37: 173-180

CHAPTER III :

Cuicul-Djemila antic Roman City: Historical and urban development

III.1 Introduction

The Roman period in Algeria has left its mark on many sites housing the remains of ancient Roman cities. In eastern Algeria, the city of Djemila, located just 50 km from the city of Sétif, has one of the most beautiful archaeological heritage in the world. It offers an eminent example of a type of architectural ensemble illustrating a significant period in the Roman history of North Africa, from the 2nd to the 6th centuries. The site includes a very diverse typological and architectural repertory, with a defensive system and triumphal arch, municipal buildings and shows, craft and trade equipment, including the *Cosinii* brothers market that is a remarkable example of the economic prosperity of the region cited.

III.2 Presentation of Djemila-*Cuicul* archaeological site

The site of Djemila, whose name designates in arabic "the beautiful", shelters the remains of the ancient Roman city *Cuicul* (original name of the place, probably of Berber origin) [1]. It is located at 900 m above sea level, and 50 km northeast of the city of Sétif. It is today one of the most important Roman cities in the world and was classified in 1982 as World Heritage by the United Nations Educational, Scientific and Cultural Organization UNESCO [2]. The site is affiliated with the municipality of Djemila, which is administratively one of the 20 localities of the province of Sétif. It is limited:

- ✓ In the north by the locality of Maouia and the province of Mila.
- ✓ In east by the province of Mila.
- ✓ In the south by the localities of Belaa and Tachouda.
- ✓ In the west by the localitiesof Beni Fouda and Maouia.

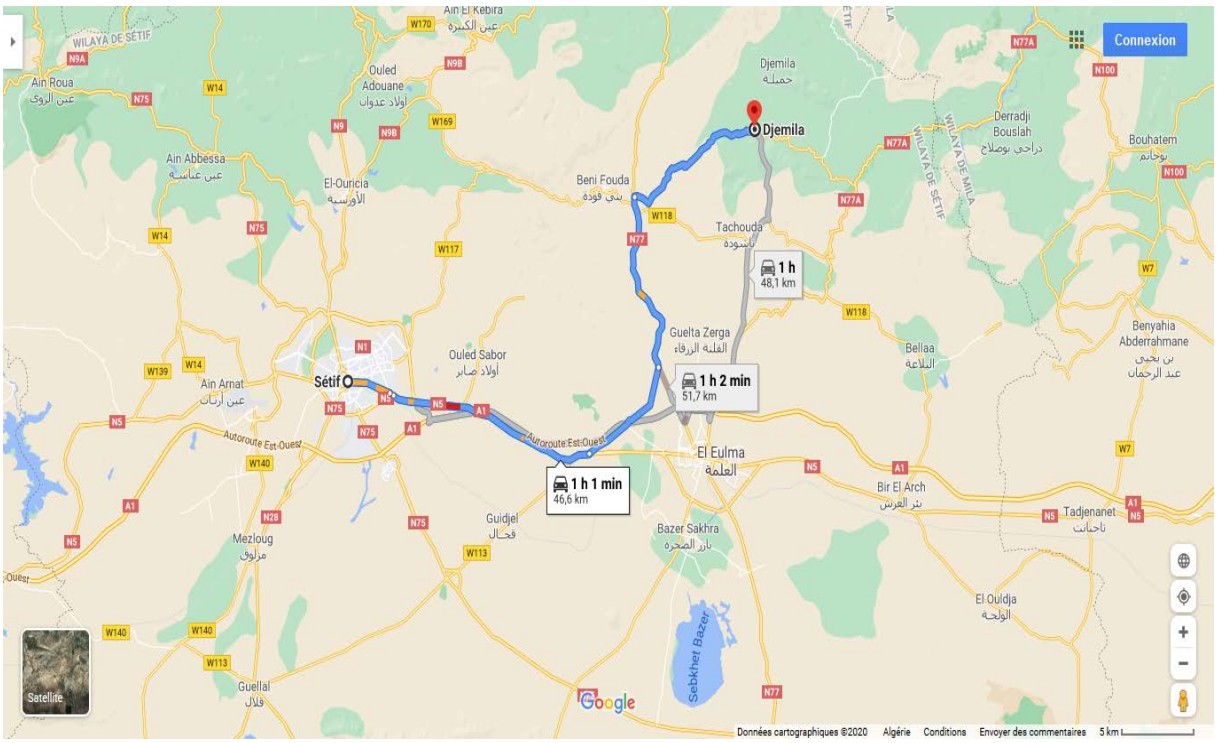

Fig III.1: Geographical location of Djemila [3].

The city of Djemila is structured by the CW117 that connects two national roads, in this case RN77 and RN77A in the East/ West direction of the state of Sétif. The main road of the city of Djemila November 1, 1954 leads directly to the archaeological site and is considered as structuring axis of the city.

The interest in the archaeological site began with the arrival of French colonization in the region from the end of 1838; the first excavations began in 1909 under the direction of the administrative director of the region [4].

III.3 History and development of *Cuicul*

Cuicul was founded by Emperor *Nerva* at the end of the 1st century [AD 96-98], on a spur, between two ravines. It was installed at the crossroads between *Cirta* (Constantine) and *Sitifis* (Sétif) on the one hand, and the north-south road from the port of *Igilgili* (Jijel) to *Lambèse* [1].

Cuicul was on the right bank of the wadi el Kebir (the *Ampsaga* of the ancients) which bounded *Mauretania* and *Numidia*, therefore in the extreme west of *Numidia*.

Due to the geographical difficulty of the place, it was built on a narrow plateau and stretched more from North to South than from East to West; it was surrounded by an enclosure that followed the triangular shape of the site [5].

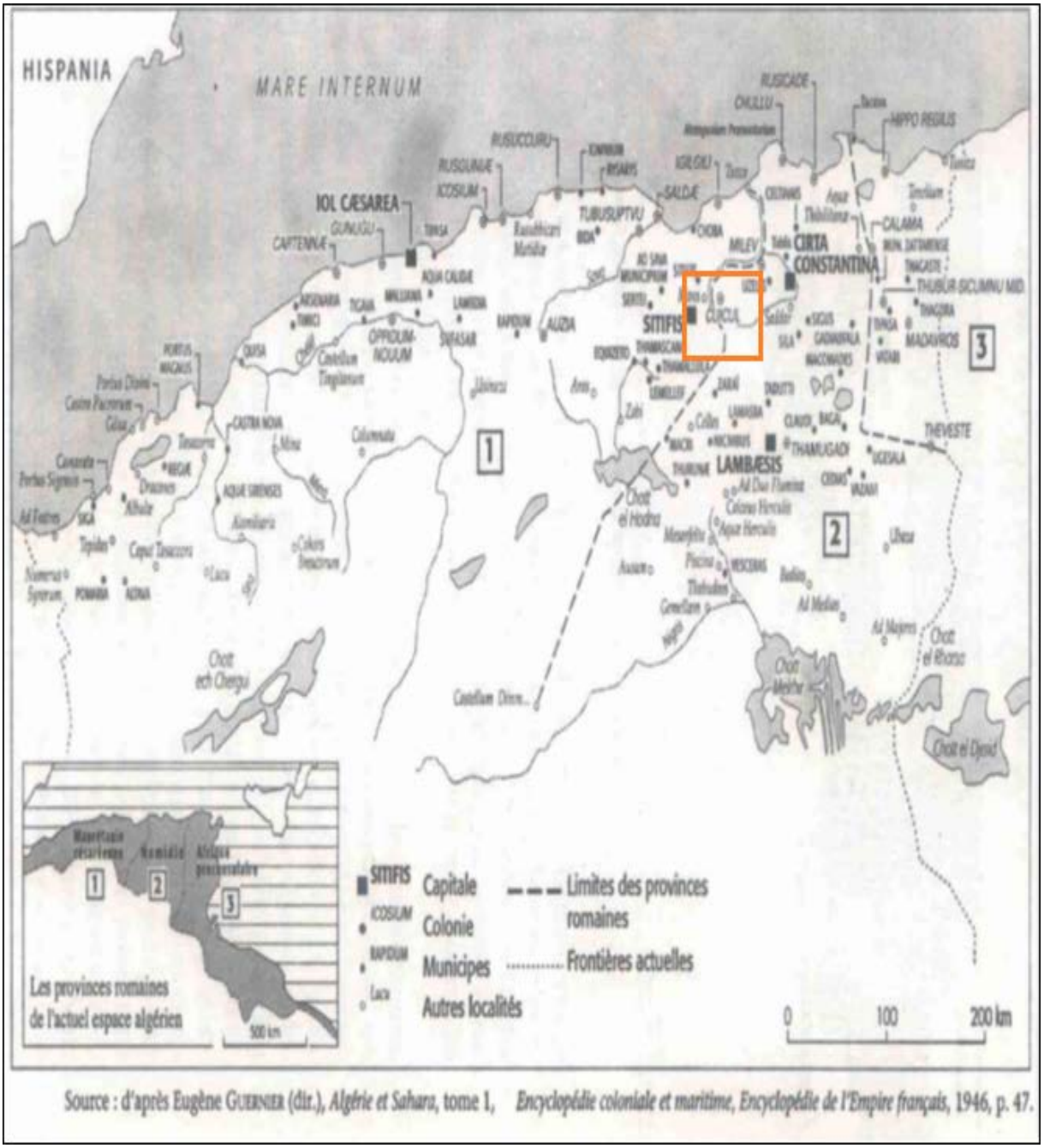

Fig III.2: Geographical location of *Cuicul.*

The Roman colony which was founded in *Cuicul* was first intended for veterans. Wealthy burghers subsequently came from older towns - *Carthage*, *Cirta* - to settle in *Cuicul* and brought their business experience to the new city. The urban population gradually increased to Berbers,

attracted by the material and legal advantages reserved for city dwellers [1]. Agriculture took an important place thanks to the presence of a humid climate and a clayey soil allowing the cultivation of olive trees and wheat. There were also small workshops making pottery, glassware, iron and bronze utensils necessary for domestic life. Trade developed thanks to the roads that linked *Cuicul* to regions of various productions and became an essential element in its prosperity [5].

Like any new town, *Cuicul* has grown over the years. One can still distinguish on the ground to the north of the spur the primitive nucleus, around an axial street.

The main religious and administrative buildings were built in the 2nd century during the reign of the *Antonines* (96 to 193 A.D.), around the forum: capitol, curia and judicial basilica. In the neighboring districts stood the market, thermal baths and other temples [6]. The city experienced a great extension, and in particular the extension of the cardo towards the south, which gave birth to the city theater around 160 A.D. [5]. Subsequently between 183 and 184, under the reign of the Emperor *Commodus*, the city acquired the great thermal baths of the south and at the end of the 2nd century many rich residences were created in this district [6].

At the beginning of the 3rd century, growth continued under the *Severus* period (193-235 AD.), the enclosure had become too narrow. Under the reign of *Caracalla*, the city then grew and there was an important transformation: the demolition of the southern rampart, new roads were built, it was equipped with the Severus's square on which was built, the arch of *Caracalla* [5]. The great temple of the *Severan* family was built, dedicated to the worship of the imperial family, the nearby baths were sealed, the development of a new forum in contact with the old city. For *Cuicul*, as for many African cities, the *Severus* period (193 to 235 A.D.) marks the apogee of a prosperity which declines around the middle of the century following a general crisis in the empire, economic crisis, social and political. A series of bad harvests ruins the small owners, frequent disturbances cut off communications, and insecurity paralyzes trade. The impoverishment of the city stops urban development: no new construction for about 50 years [5].

The 4th century brought about a renaissance as evidenced by public utility works: repair of the aqueduct supplying the city with drinking water, construction of fountains and restoration of various buildings [6]. Christianity came to *Cuicul* during the third century, but it’s during this period that Christianity triumphs and the city had developed what is known as the Christian

Quarter [5]. The Christians built a cluster of episcopal edifices at the top of the hill. Two basilicas were placed next to each other. Nearby were a round baptistery, as well as a bishop's house and a complicated group of annexes. This complex of buildings is the first which is seen when entering the archaeological site [7].

The luxurious houses of the notables are constantly being developed, reaching considerable surface areas, equipping themselves with private baths and providing considerable reception areas (private basilicas). The house of *Europe* or that of *Castorius* reveal this art of living of the rich local notables, and have preserved an important mosaic decoration [5].

The vandal army arrived in 431 and the city fell easily. The Vandals evolved in 442 and the area was taken over by the Byzantines in the first half of the 6th century. When the city was recaptured by the Byzantines, it regained some semblance of stability and activity. It was abandoned on the eve of the Arab invasion of North Africa, after which *Cuicul* - whom the Arabs later called Djemila (beautiful) - sank into obscurity. It disappeared around the second third of the 6th century [6].

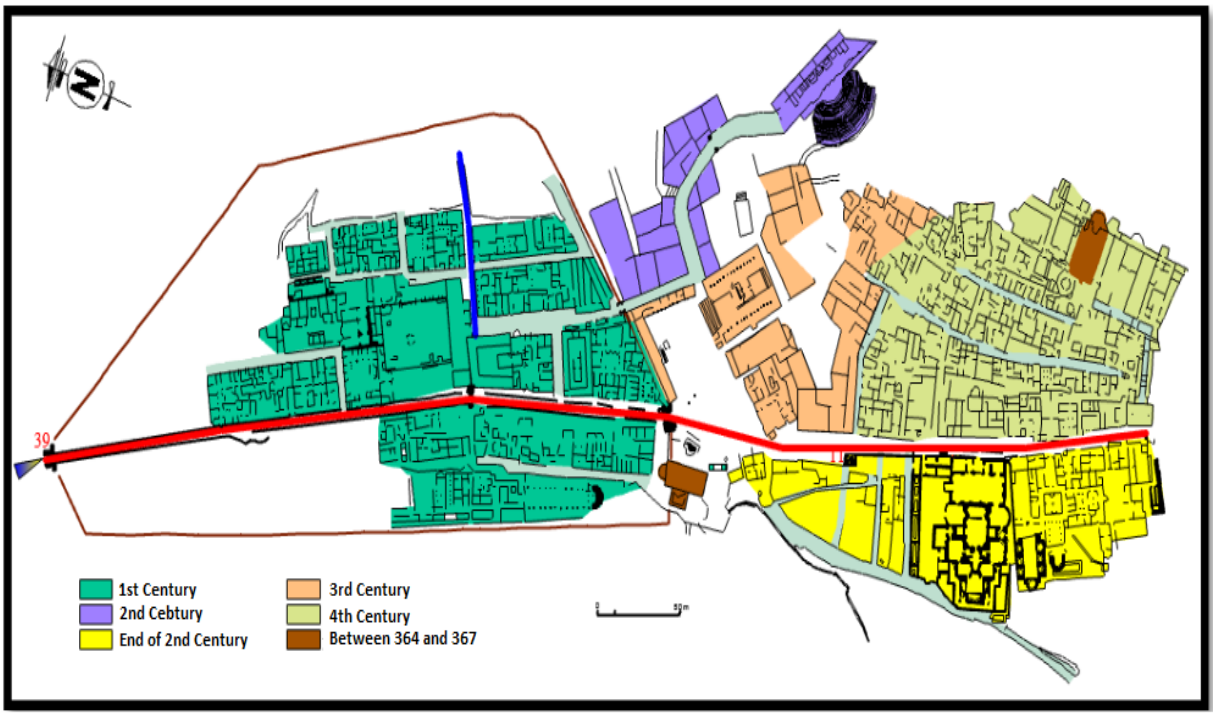

Fig III.3: Urban development of *Cuicul* according to Louis Leschi studies of 1950 [8-9].

III.4 Map of the city and its remains

Like any Roman colony, the plan of the town of *Cuicul* responded to the classic scheme of Roman town planning with some transformation due to the geographic difficulty of the ground [9]. One of the primary characteristics is the cardinal orientation, which seems to organize the cities around a crossroads, from which the main axes of the city depart.

The primitive city has a regular plan divided by two major axes the "*Decumanus maximus*" which represents the East/West axis and by the "*Cardo Maximus*" which, for its part, ran from the northwest gate to the southeast, up the slope of the land, instead of being oriented exactly north-south following the classical rule [10]. On these two avenues, the shops and the wealthy villas are concentrated. At their intersections are the forum, place of commerce, admiration and religious life. An organization of neighborhood is often set up according to trades.

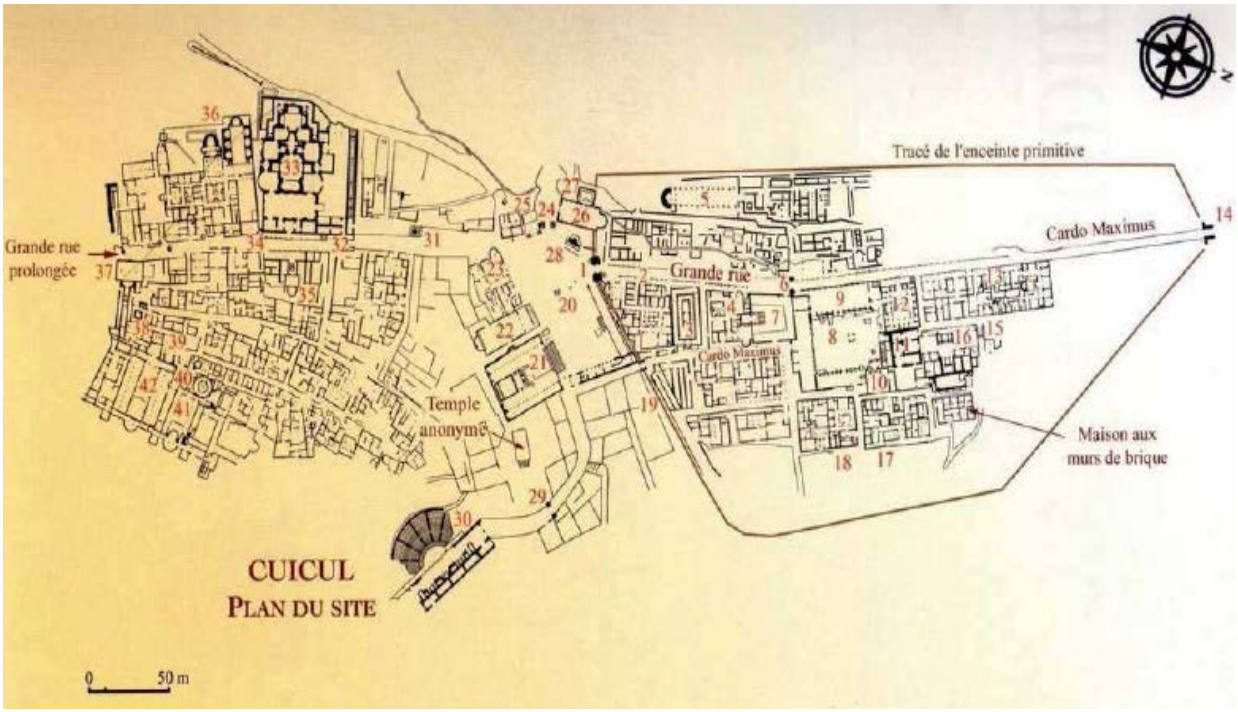

[1] Porte méridionale et enceinte
[2] Maison de Castorius
[3] Temple anonyme
[4] Maison de l'âne
[5] Quartier Ouest et basilique
[6] Arc
[7] Temple de Vénus Genetrix
[8] Forum
[9] Basilique Julia
[10] Curie
[11] Capitole
[12] Marché de Cosinius
[13] Maison d'Europe
[14] Porte septentrionale
[15] Latrines publiques
[16] Thermes
[17] Thermes de Terentius
[18] Maison d'Amphitrite
[19] Greniers publics
[20] Place des Sévères
[21] Temple de la famille Septimienne
[22] Basilique civile du IV° siècle
[23] Maison de la mosaïque d'Hylas
[24] Arc de Caracalla
[25] Petit temple
[26] Marché aux étoffes
[27] Latrines publiques
[28] Nymphée
[29] Arc de Julius Crescens
[30] Théâtre
[31] Fontaine
[32] Porte de basse époque
[33] Grands thermes
[34] Fontaine de la Tétrarchie
[35] Petite salle à abside
[36] Maison de Bacchus
[37] Entrée du quartier chrétien
[38] Maison de l'évêque et du clergé
[39] Chapelle chrétienne
[40] Baptistère et thermes annexes
[41] Basilique Nord
[42] Arc de Cresconius

Fig III.4: Site map, and main buildings and monuments of *Cuicul* [11].

III.4.1 Main monuments and buildings of *Cuicul*

- **The old Forum:**

The heart of the original city is a paved square 48 m long by 44 wide, decorated with porticoes on two of its sides; one entered it, on the south side, by a monumental arch of which only the base remains [5]. This later served as a support for the eastern wall of the temple of *Venus Genetrix*. The north forum (Fig III.5) gathered around its perimeter the main symbols of

Romanization: a Capitol that was a temple dedicated to Jupiter, Juno and Minerva, which symbolized the link with Rome where the three gods were worshipped on the Capitol Hill, a curia where the municipal council met. Some vestiges of the decoration of the room testify to the luxury of this town hall [12].

Fig III.5: The north forum (Source: https://www.photosetbalades.fr/galerie-d-hier/afrique-du-nord/numidie-djemila/**).**

- **The altar of Jupiter:**

Jupiter had a pre-eminent role in the Roman pantheon and more and larger altars and statues were dedicated to him in comparison with those to *Juno* and *Minerva* [7]. The temple itself is destroyed; fragments of its enormous columns (14 m high) rolled over the forum and into a courtyard below [5]. Some remains of Jupiter statue are shown in Figure III.6.

Fig III.6: Remains of the status of *Jupiter* (Source: https://www.photosetbalades.fr/galerie-d-hier/afrique-du-nord/numidie-djemila/**).**

- ***Venus Genetrix* temple :**

Another temple (Fig III.7) near the old forum enhanced the link of *Cuicul* with Rome. It is small, but its design is very elegant and it is one of the finest sights of the old town. It was dedicated to *Venus Genetrix*, similar to that built by *Julius Caesar* in his Roman Forum. An inscription near the temple celebrates the construction of public granaries, an indication that *Cuicul* flourished because of its role in the trade of grain between the inland plains and the ports on the coast from where it was shipped to *Porto*, the artificial harbor of Rome [7].

Fig III.7: *Venus Genetrix* temple. Source: https://www.photosetbalades.fr/galerie-d-hier/afrique-du-nord/numidie-djemila/).

- **The great thermal baths:**

The great thermal baths (Fig III.8) are located 100m south of the new forum and at the same distance northwest of the Christian basilica and cover an area of 2,600 square meters. This monument, very well preserved, is particularly interesting for the clarity of its palestra plan, changing rooms, stoves, hot and cold bathrooms separated by temperate rooms, follow one another in a perfectly symmetrical distribution [5].

Fig III.8: Great thermal baths (Source: **https://www.photosetbalades.fr/galerie-d-hier/afrique-du-nord/numidie-djemila/).**

- **The Septimian temple:**

This temple (Fig III.9) was built around the beginning of the 3rd century. It is located on the southeast corner of the new forum. An inscription found during excavations in 1912 indicates that the temple was probably dedicated in AD 229. J.C to *Gens Septimia* by the *Cuiculitaine Republic* [13].

Fig III.9: The Septimian temple [7].

- **Theater:**

It dates from the 2nd century. An inscription says that the theatre was built in 161AD. at the initiative of *Caius Julius Crescens* and *Caius Julius Didius Crescentianus*, who decorated it with statues of *Fortuna* and *Mars*, patrons of *Cuicul* [7]. It could hold around 3,000 spectators. It leans against a slope of land allowing the bleachers to sit. The circular wall was redone; the scene took place in the front semicircle and on the floor. Two galleries on either side that allow artists to enter behind to prepare their spectacle (Fig III.10) [5].

The back wall of the stage remains largely, with the two doors through which the actors entered; the low wall, which supported the stage, has retained its elegant decoration [7].

Fig III.10: The theater (source: https://www.photosetbalades.fr/galerie-d-hier/afrique-du-nord/numidie-djemila/)

- **The Arch of *Caracalla*:**

The community of *Cuicul* erected a triumphal arch (Fig III.11) at the beginning of the 3rd century in honor to the emperor *Caracall*a, his living mother *Julia Domna* and his deceased father *Septimius Severus*. The arch retains the bases of the three statues which stood at its top. It is located west of the new forum, at the top of the slope [7].

Fig III.11: Arch of *Caracalla* [7].

- **The new forum:**

The southern forum (Fig III.12) covers an area of 3200 meters, the side is in a straight line, the other three are made-up of broken lines, which constitute an irregular polygonal contour for surface, rather than a quadrilateral shape area of the forum is very irregularly paved. Five streets leave from the new forum, two serving the old town; a third passed under the arch of *Caracalla* and probably continued west by the road to Sétif; another leaves the square to the south-east to lead to the theater; the widest, which extended the cardo to the south, leads to the large thermal baths and to the Christian quarter [5].

Fig III.12: The southern forum (source: https://www.photosetbalades.fr/galerie-d-hier/afrique-du-nord/numidie-djemila/).

- **The baptistery:**

It was built at the same time as the civil basilica (Fig III.13) that is to say around the middle of the 4th century. It is a circular building with very thick walls. It is made of an annular corridor in these two sides of small semi-circular niches covered with stucco, traces of which remain today [13].

Fig III.13: The Baptistery (source: https://www.photosetbalades.fr/galerie-d-hier/afrique-du-nord/numidie-djemila/) for the picture in right and [7] for picture in the left.

- **The civil basilica of new forum:**

This new basilica was built towards the end of the 4th century, in 364-367 [14], on the edge of the *Severian* forum in place of the temple of *Saturn Frugifère*, god of vegetation and fertility of Roman Africa, its location and its materials were then used in the construction of the civil basilica [13]. (Fig III.14).

Fig III.14: The civil basilica [7].

- **House of Europe:**

The house of Europe was built around the 2nd century (Figure III.15). It has 1,250 m2 of massive buildings in several levels, its basements, its monumental facade, its vast thermal baths, its shops, its varied premises and its winding corridors [15]. It seems to be the result of the reunification of two dwellings forming part of the buildings of the primitive city [13]. The largest, nicknamed the House of Europe because a mosaic depicting the kidnapping of Europe was found there. The monumental entrance, the freestone facade, the large number of rooms (about twenty), the luxurious decoration, everything indicates the home of an important figure [5].

Fig III.15: The House of Europe [14].

- ***Cosinius* market:**

It was built in the 2nd century by the *Cosinius* brothers [16], monument whose condition of its conservation is remarkable (Fig III.16) [12]. On the occasion of his elevation to the perpetual flame, *L. Cosinius* Primus offered a market to *Cuicul*; he commissioned his brother, *C. Cosinius Maximus*, an important figure in *Cuicul*, to supervise its construction. A gray marble colonnade of *Filfila* frames an almost square courtyard; on the four sides were distributed sixteen shops; at the entrance to each, a massive stone table with carved supports served as a stall. Next to a measuring table are three cavities for measuring wheat, barley and liquids [5].

Fig III.16: *Cosinius* market [7].

- **Donkey house:**

The Donkey House, so called because the image of this animal appears twice, accompanied by the inscription *Asinus Nica* on the pavements decorating it. It opens onto the two main cardines which, not parallel, impose the shape of a trapezoid on it. It is a complete and harmonious residence, with its peristyle with vast basins, its small baths, its reception rooms adorned with mosaics that are particularly interesting in terms of their size, style and iconography, which has given rise to numerous comments (Fig III.17) [15].

Fig III.17: Donkey house [15].

- **House of *Bacchus* :**

From the name of a mosaic, it is a complex set of rooms that belong to two dwellings, originally distinct, which until very early times were reworked and considerably transformed [17]. The group of buildings known as " house of *Bacchus*" has three gardens, very diverse nature and dimensions, which preserve, better than buildings, the trace of the transformations of town planning in this district, originally suburban, of the *Cuicul* colony (Fig III.18) [18]. The house of *Bacchus* was very large and it is thought that its halls could house meetings, maybe banquets, of worshippers of the god [7].

Fig III.18: House of Bacchus [18].

- ***Castorius* house :**

The so-called *Castorius* house leans to the south on the surrounding wall transformed and embellished by niches and a portico on the side of the *Severan* Forum. It overlooks the primitive Cardo Maximus to the north. With its 1,500 m2, its two courtyards including a monumental peristyle with basins, its vast thermal baths, it is the most imposing residence in the city (Fig III.19) [15].

Fig III.19: *Castorius* house [15].

- ***Cresconius* cathedral :**

In 411 A.D., Donatism was declared a heresy by Emperor *Honorius* who endorsed the outcome of a council held at *Carthage*. In this context *Cresconius*, Bishop of *Cuicul*, decided to build a very large church where all the Christians of the town could gather (Fig III.10) [7].

Fig III.20: *Cresconius* cathedral [7].

- **Christian basilica :**

It is located at the start of the site; it consists of a main nave and two aisles from which it is separated by five columns with six bays [12]. It occupies the entire south-western part of the district, between the west cardo and the rampart; it was probably founded in the last years of the 4th century or at the beginning of the 5th. At first a simple memorial built on the tomb of a martyr, it grew later, probably during the Byzantine period, and filled with tombs which gradually invaded the entire area between its facade and the north. The site of the church had previously been occupied by private houses of which some vestiges remain [10].

Fig III.21: Christian Basilica of the 4th century
(Source: https://jeanyvesthorrignac.fr/wa_files/info_414_20Djemila.pdf).

III.5 Conclusion

Djemila or *Cuicul* is one of the most important Roman remains in Algeria both for its beauty and for the treasures, it contains. If some monuments could be placed at a certain time or date because of the discovery of some inscriptions; many remain unknown and elude absolute chronology. Indeed, archaeologists and historians are continually faced with the difficulty of dating remains in order to be able to put the facts into real context and therefore reconstruct right history. The problematic of our work fits with this context of accurate dating and scientific reconstitution of the historical development of the city. The main findings of our work will be presented in Chapter IV.

References

[1] D René, L Leschi (1954) Djemila, antique Cuicul. In Syria Tome 31: 338-339.

[2] https://whc.unesco.org/fr/list/191/ . Accessed 19 March 2018.

[3]https://www.google.com/maps/dir/S%C3%A9tif/Djemila/@36.1943465,5.6125381,11z/data=!4m13!4m12!1m5!1m1!1s0x12f3159c5fcafc4b:0xb063cfbbd3cadcd5!2m2!1d5.4107984!2d36.1897593!1m5!1m1!1s0x12f307f12726440f:0x93d5bf4b11ab2fe0!2m2!1d5.7255242!2d36.3142408. Accessed 5 September 2020.

[4] N. Duval (1995) Djemila. Peeters Publishers. Vol.16.

http://journals.openedition.org/encyclopedieberbere/2185. Accessed 19 March 2018.

[5] http://alger-roi.fr/Alger/documents_algeriens/culturel/pages/34_djemila_cuicul.htm. Accessed 28 August 2020.

[6] http://christocentrix.over-blog.fr/article-djemila-antique-cuicul-suite-et-fin71945622.html. Accessed 19 March 2018.

[7] https://www.romeartlover.it/Djemila.html. Accessed 30 September 2020. Accessed 5 September 2020.

[8] Leschi L (1950), Djemila Antique CVICVL, OFALAC, France

[9] Khalafa D, Labiod L, Loaouar S(2019) La valorisation du patrimoine culturel en Algérie : cas de Djemila antique, Cuicul. Mémoire Master, Université Mohamed Seddik BENYAHIA – Jijel

[10] Allais Y (1971) Le quartier occidental de Djemila (Cuicul). In: Antiquités africaines 95-120.

[11] Blas de Roblès J M, Sintes C (2003) Sites et monuments antiques de l'Algérie. Edisud, Saint-Rémy-de-Provence; France

[12] Ballu A (1921) Ruines de Djemila (antique Cuicul). Revue africaine, 62: 201-274.

[13] Boukhenouf A (2006) Caractérisation des mortiers archéologique, le cas des sites de Djemila et la citadelle d'Alger. Thèse de Magister, Université Mohamed Bougara, Boumerdes.

[14] Albertini E (1943) Une nouvelle basilique civile à Cuicul (Djemila). In: Comptes rendus des séances de l'Académie des Inscriptions et Belles-Lettres, 87e année, 3 : 376-386.

[15] Blanchard-Lemée M (1975) Maisons à mosaïques du quartier central de Djemila (Cuicul). Études d'Antiquités africaines N°3.

[16] Cagnat R (1915) Le marché des Cosinius à Djemila. In: Comptes rendus des séances de l'Académie des Inscriptions et Belles-Lettres, 59e année, 5 :316-323.

[17] Février P-A (1996) Notes sur le développement urbain en Afrique du Nord : les exemples comparés de Djemila et de Sétif. Publications de l'École Française de Rome, 225 : 651-697.

[18] Blanchard-Lemée M (1998) Dans les jardins de Djemila. In: Antiquités africaines, 34 : 185-197.

CHAPTER IV :

Thermoluminescence dating of Cuicul Roman city and study of the construction terra-cotta material provenance

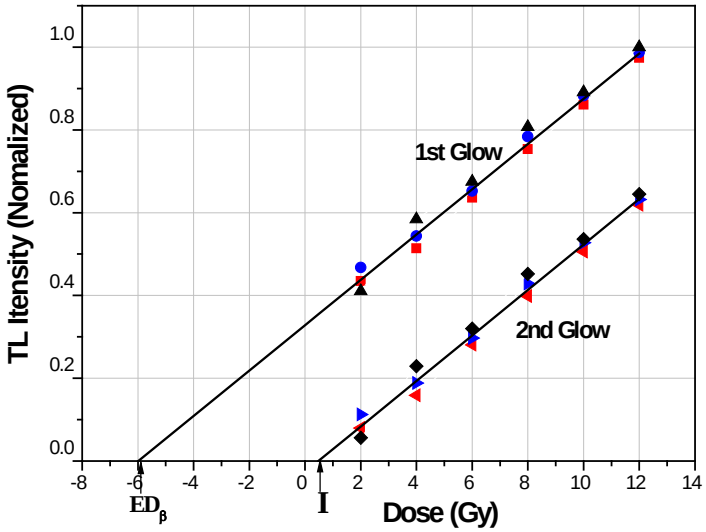

IV.1 Introduction

Nowadays, the impressive scientific development allows archaeological dating to use scientific high precision methods for dating with an absolute chronology. The material being of various natures and compositions prompted the scientists to develop numerous methods of dating such as TL and OSL techniques that are widely used on construction material and objects made from terra-cotta. They are based on the property of certain minerals (quartz and feldspars) to behave like natural dosimeters. Thus, the measurement and the calibration of their luminescence signal using a laboratory radioactive source lead to an assessment of the accumulated dose in the dated sample (paleodose) by OSL or TL techniques. The estimate of this paleodose and that of the annual dose rate at which the minerals were submitted allows the calculation of the time since resetting the OSL or the TL signal which occurs when the minerals were heated to a high temperature (> 450°C). A precise age can be obtained by determining the most appropriate procedure and applying it correctly to samples.

The historical development of *Cuicul* has been described by several authors, but no scientific study has been conducted on the site. Spectrometric analysis and archaeological dating using scientific methods are very powerful and more than necessary tools to place all cultural and archaeological vestiges and objects in their real historical context and to avoid any controversy regarding their origin. This work is a contribution aiming the scientific reconstruction of *Cuicul* history by dating a terra-cotta brick and the study of its fabrication material origin.

The actual thesis considering all the experimental and practical works undertaken has a common objective that was achieved in three main phases that are the following:

1. Implementation of quartz separation procedure and TL&OSL signals collection for accurate archaeological terra cotta dating;

2. Thermoluminescence dating and X-ray fluorescence clay provenance analysis of an ancient brick taken from *Cuicul* roman city;

3. Establishment of a construction timeline map of *Cuicul* roman city by thermoluminescence dating.

In addition to thermoluminescence technique, many other scientific techniques were used, such as XRD, XRF and γ-spectrometry, for the collection of requested dating data.

IV.2 Quartz separation procedure and TL&OSL signals collection

In this part of the study, we are interested in the preliminary works and steps that are necessary for accurate TL and OSL dating. Particularly, we have investigated the quartz separation procedure, the photomultiplier tube (PMT) suitable high voltage supply, and the TL and OSL signals collection conditions that must be optimized for accurate dating.

IV.2.1 Material and Methods

IV.2.1.1 Sample selection

In this work, a terra-cotta brick fragment taken from the *Cuicul* roman archaeological city is used. A Rigaku ZSX primus wave dispersive X-ray fluorescence spectrometer was used for the elemental analysis of the sample and thus the determination of the mass fraction of the main oxides (Table IV.1).

Table IV.1: Terra-cotta composition of studied brick by X-ray fluorescence

Element	SiO_2	Al_2O_3	Fe_2O_3	CaO	MgO	Na_2O	K_2O	P_2O_5	TiO_2	MnO	H_2O
Mass fraction (%)	54.30 ±0.03	14.07 ±0.02	6.16 ±0.01	5.97 ±0.01	3.18 ±0.02	1.44 ±0.02	1.85 ±0.005	0.28 ±0.004	0.74 ±0.02	0.05 ±0.005	11.96 ±0.02

IV.2.1.2 Quartz separation and exposure to additional Beta dose

In the dating thermoluminescence procedure, quartz must be well separated for the establishment of accurate growth curves to be used for equivalent and therefore archeological dose determination. The used quartz procedure in this work includes the following steps:

1. Outer layers removing by two millimeters. The scraping is done using a micro-drill with a slight pressure on the head of the mesh to avoid heating the sample and loss of the thermoluminescence signal.

2. The sample crushing and sieving, for the grains fraction selection below 40µm. Small size mesh must be used (0.0475 mm). Sieving operation must be done slowly in a well equipped laboratory under inactinic red light.

3. The selected grains fraction is subject to etching procedure which consists of: 10% (v/v) HCl for 1 hour to remove the carbonate, 10% (v/v) H_2O_2 for 48 hours to remove the organic

component, 1% (v/v) HF for 1 hour to remove clay and 10% (v/v) HCl for 30 minutes to eliminate fluorosilicates that had possibly formed.

4. Polymineral fine grains fraction in the range of 1-8 μm separation through a time controlling grain sedimentation procedure in acetone (~0.8g/cm^3).

5. Separated grains deposition onto stainless steel disks and acetone evaporation in a suitable oven at 40°C for 24 hours.

The purity of the separated phase was checked by X-ray diffraction (XRD) using X'pert pro diffractometer with the main characteristics indicated in Table IV.2.

Table IV.2: X'pert pro X-ray diffractometer characteristics

Detector	PIXcel
X-ray source	CuKα, Ni-filter
Collimator	Soller Slits: 0.04 rad
Divergent slit	fix, 0.5°

After quartz separation, the necessary natural and artificial TL and OSL signals were collected. Additional artificial doses were induced by a suitable ^{90}Sr-^{90}Y calibrated beta source, which is integrated into the Risø system reader used, and delivering 0.1Gy/s. In this work, two aliquots of the quartz grains are used, one after additional exposure to beta dose and the other one without additional exposure. The obtained TL and OSL signals are used for the establishment of TL and OSL growth curves that are necessary for the determination of the equivalent dose and therefore the archaeological dose (paleodose). The TL and OSL signals will be prepared for the TL multi-aliquots additive dose standard protocol (MAAD) and fine grains technique [1-2]. With these protocol and technique, the paleodose is determined by measuring on several identical treated aliquots in terms of mineral phase separation (quartz), separated grains size and deposited quantity on each disk, the TL and OSL signals of natural plus artificial beta doses (1st glows) and the TL and OSL signals for different only additive beta doses after natural TL and OSL removing (2nd glows).

IV.2.1.3 OSL and TL signals reading

For our measurements, the Risø National Laboratory TL/OSL-DA-20 luminescence reader was used (Fig.IV.1). All necessary Beta-dose exposures used for its characterization and response established are performed with its embarked Beta-source.

This reader includes three main modules:

1. Light detection system (Photomultiplier PM);

2. Stimulation system for optical and thermal light emission;

3. Additional irradiation sources: alpha, beta and X-rays.

Fig.IV.1: Used RISØ TL/OSL-DA20 Reader, a) The Reader, b) The Controller, c) The X-ray generator controller.

The light detection system comprises a photomultiplier combined with a plurality of light filters. The light stimulation system includes a light emitting and heating plate source, which can be used separately to make optically stimulated luminescence (OSL) or thermoluminescence (TL). Additional in-situ irradiations can be provided by a beta source, an alpha source and an X-ray generator. The reader is able to analyze in a single pass 48 samples each with its own programming sequence in terms of luminescence reading mode, thermoluminescence heating interval, irradiation supplementations, type of light filter, etc. The main characteristics of the used reader are summarized in Table IV.3. Separated quartz is placed on stainless-steel disks

and exposed to beta dose. TL signal reading is performed in the same manner by just moving the disk to the reading position under the photomultiplier tube.

Table IV.3: Main characteristics of the RISØ TL/OSL reader

Photomultiplier	CsSbcrystal with maximum detection efficiency between 200 and 400nm and 0.4sr as solid detection angle (CsSb, EMI 9235QBPMT)
Heater material	Khantal with maximal temperature of 700°C and heating rate varying from 0.1 to 10°C/s
Beta source	$^{90}Sr/^{90}Y$, E_{max}: 2.27 MeV, Strength: 1.48GBq, Dose rate 0.1Gy/s in the quartz
X-ray Generator	Tungsten, 50 kV, 1 mA, 50 W, Dose rate in the quartz 2Gy/s

The plateau characteristics of the reader photomultiplier tube PMT is checked to determine the suitable PMT voltage to be used for TL and OSL signals collection [3]. This task was done by the collection of TL signals induced on commercially standard quartz powder, generally used for the calibration of the reader. Thus, 2 mg of quartz was each time exposed to 2 Gy beta dose and TL and OSL signals were collected for many PMT high tension voltages varying from 800 volts to 1400 volts. After optimal PM high voltage setting, the TL and OSL signals of the dated bricks were checked for different experimental conditions according to the literature [1,4-9]. The optimal found conditions that ensure the optimal TL and OSL growth curves are reported in this work. It is important to mention that two criteria were used for the growth curves evaluation: 1. the linearity of the 1st and the 2nd glow curves particularly for TL and OSL, and 2. 1st and 2nd glow curves glows slopes must almost be parallel for TL and OSL [2,10-13]. This is because the paleodose is determined by the measurement of the dose distance between the two growth curves on the dose axis of the TL and OSL growth curves.

IV.2.2 Results and discussion

The analysis of the obtained XRD show peaks of the quartz (SiO_2) with a total concentration of 93.6 % in weight (Fig.IV.2). The analysis and the comparison of the obtained XRD spectra allow us to conclude that the mineral phase of the quartz is identified but mixed to a small amount of other minerals in the terra-cotta which have no interest in our work.

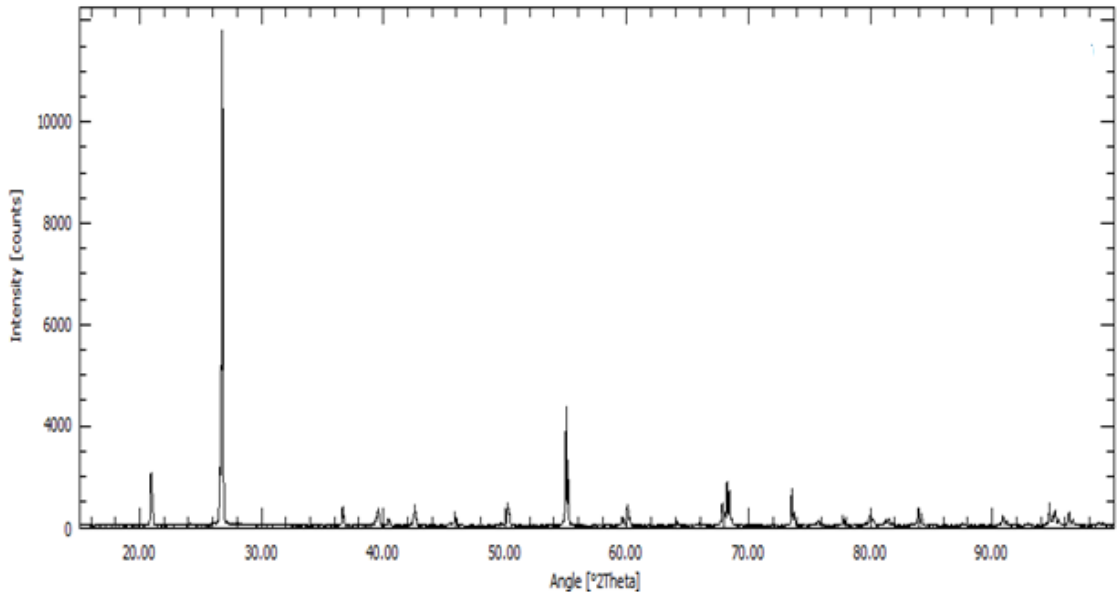

Fig.IV.2: XRD spectrum of separated quartz showing main diffraction peaks of the quartz SiO_2 ($p3_221$)

Figure IV.3 shows the obtained plateau characteristics curve of the CsSb-EMI 9235QB PMT. In this plateau, characteristics checking the pulse high are kept constant. As we can observe, the obtained curve is divided into three regions. Only the region referring to the plateau is of interest and the high voltage must be selected within this region. Thus, the value of the PMT supply high voltage of 1100V is used for all TL and OSL signals collection.

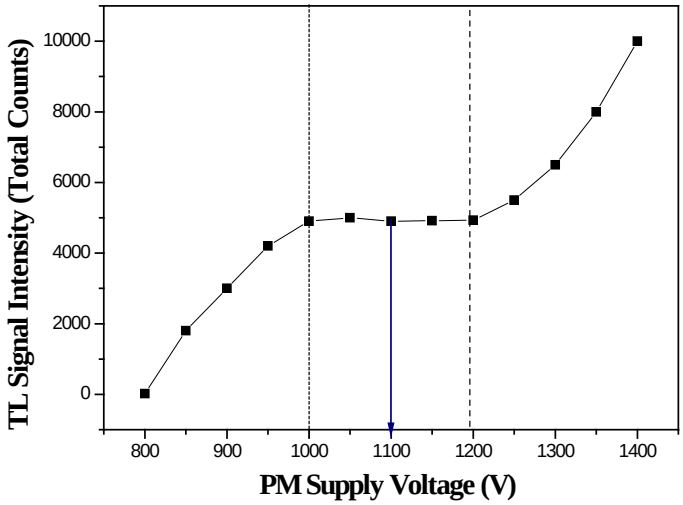

Fig.IV.3: Plateau characteristics of the PMT (CsSb, EMI 9235QBPMT) of Riso DA-20 reader.

After several tests and checks on the TL and OSL signals under deferential reading conditions, the optimal experimental conditions presented on Tables IV.4 and IV.5 were selected.

Table IV.4: Optimized conditions for OSL signal reading.

Readingtemperature	125 °C
Heating rate	5 ° C/s
OSL signal sampling	250
Lighting time	40 s
Stimulation light	Blue LED (470 nm±20 nm of FWHM, 80 mW/cm^2)
Light filter type	Hoya U-340 filter
Nitrogen volumetric flow rate	~30 l/min
Analyzed sample weight	~2 mg

Table IV.5: Optimized conditions for TL signal reading

Maximum reading temperature	450 °C
Heating rate	5 ° C/s
TL signal sampling	250 points over the range 0 °C to 450 °C
Analyzed sample weight	~2 mg

These conditions allowed us to collect the suitable TL and OSL signals (Figs IV.4 and IV.5) needed to establish growth curves (Figs IV.6 and IV.7) and therefore the determination of paleodose necessary for the age calculation of the different studied bricks. The paleodose to be determined from the TL growth curves (Fig.IV.7) will be certainly more relevant than that from OSL growth curves (Fig.IV.6). This is because the 1st and the 2nd growth curves are linear and quiet parallel in TL while this is not the case with OSL.

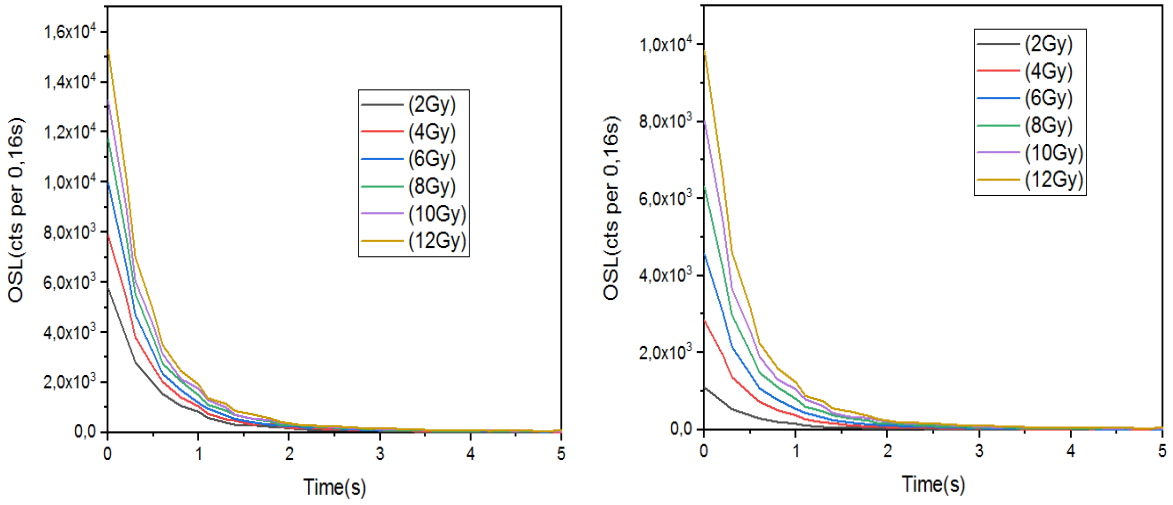

Fig.IV.4: OSL signals collected for the different beta dose of the separated quartz with (left) and without (right) the natural dose.

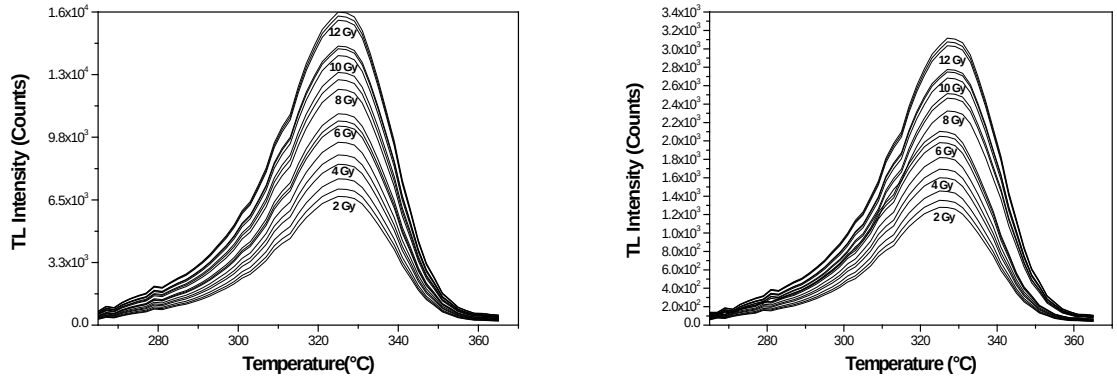

Fig.IV.5: TL signals collected for the different beta dose of the separated quartz with (left) and without (right) the natural dose.

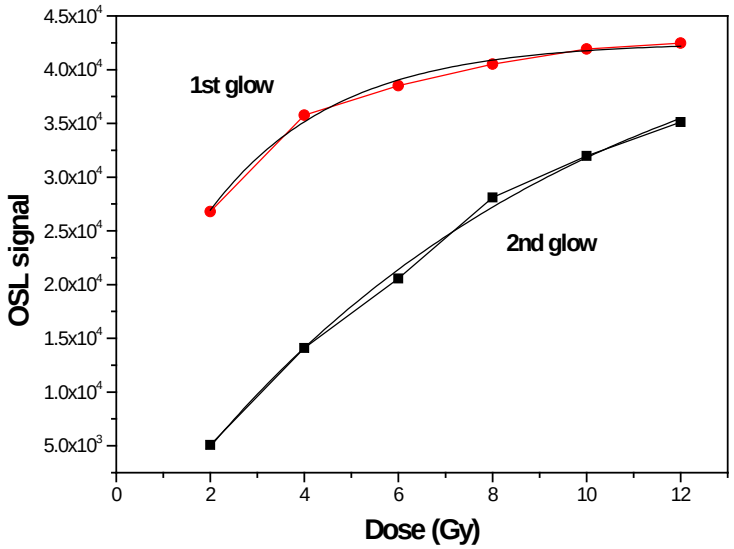

Fig.IV.6: OSL growth curves as a function of dose allowing the determination of the equivalent dose (ED_β) and the intercept dose (I) and therefore the paleodose ($ED_\beta+I$)

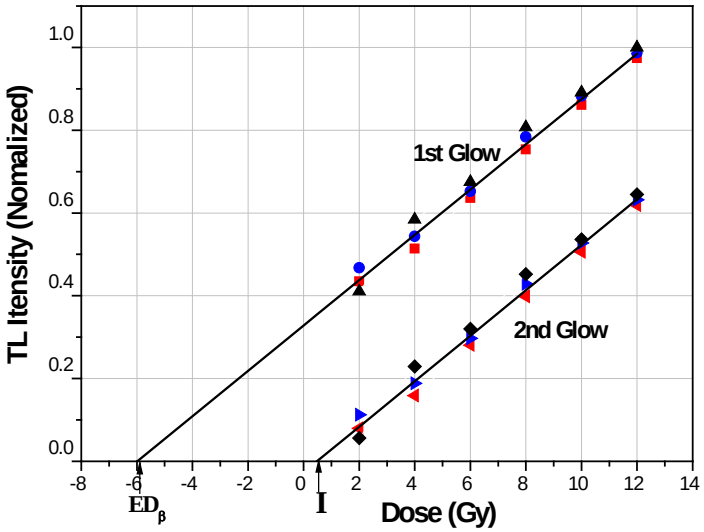

Fig.IV.7: TL growth curves as a function of dose allowing the determination of the equivalent dose (ED_β) and the intercept dose (I) and therefore the paleodose ($ED_\beta+I$)

The obtained results demonstrated well, through X-ray diffraction (XRD), that the good execution of the quartz separation procedure is able to produce suitable and pure mineral phase of quartz from the dated terra-cotta samples. Indeed, the used procedure was found very suitable and efficient for that purpose. The established plateau characteristics curve of the used photomultiplier (CsSb, EMI 9235QBPMT) of the Riso DA-20 reader shows that the supply high voltage of 1100V is the most suitable for TL and OSL signal reading. After TL and OSL reading conditions optimization, appropriate TL and OSL signals were obtained. These TL and OSL response tests were necessary to get the suitable OSL and TL signals that can be used for the determination of accurate paleodose which is necessary for the determination of the age of the dated terra-cotta brick. For such dated brick (~19 centuries old), the TL growth curves were found to be more suitable for the determination of the paleodose than OSL ones. This is because the 1st and the 2nd growth curves were found linear and well parallel in TL than in OSL. This is not due to the preparation and the good collection of the OSL signals but it is essentially due to the used protocol. Indeed, OSL method is recommended for the determination of age of older objects and sediments by using the single aliquot additive dose (SAAD) protocol instead MAAD or by using the widely used single aliquot regeneration (SAR) method [14].

IV.2.3 Conclusion

In conclusion, the study shows that the necessary conditions in quartz separation procedure must be fulfilled in order to get suitable amount of quartz in terms of purity and grain sizes for the used dating method. OSL and TL signals reading must also be performed under specific reading conditions in terms of heating, lighting and controlling atmosphere. The adjustment of the photo-multiplier is also primordial to get suitable TL and OSL signals. Accurate determination of the luminescence signals is essential and closely related to the sample preparation. According to results, the best sample preparation technique, and TL and OSL signals reading were determined. In conclusion, we propose a specific sample preparation technique for OSL and TL dating methods and particularly for the determination of an accurate paleodose.

IV.3 Thermoluminescence dating and clay provenance study of an ancient brick taken from *Cuicul*

In this part of our study, we aim to give a scientific reconstitution of Cuicul history in two steps: the first consist of dating a terra-cotta brick by thermoluminescence technique, and the second is to study the material origin of this brick by using XRF for clay provenance identification.

IV.3.1 Theory

IV.3.1.1 Thermoluminescence dating

As it was mentioned in chapter II, in archaeological dating, TL is used for the determination of the paleodose (D) stocked in the dated artefact through the determination of the equivalent beta dose (ED_β) by additional and artificial exposure to β doses. Indeed, by TL dating, the age of a dated artefact is given by the following formula Eq. (IV.1).

$$Age(y) = \frac{D(Gy)}{D_a(Gy\ /\ y)}, \qquad \text{(IV.1)}$$

where D is the archaeological dose (Paleodose) and D_a is the total annual dose.

The main steps of the dating experimental procedure are the following:

1. Identification of the suitable protocol for measuring the archaeological dose by thermoluminescence,

2. Preparation of the samples,

3. Plateau dose test,

4. TL signals acquisition,

5. Archaeological dose determination,

6. Determination of the effective alpha contribution k_α,

7. Measurement of the main radionuclides (U, Th, K) mass fractions in terra-cotta,

8. Study of the radiochemical homogeneity of terra-cotta: microdosimetry considerations,

9. Determination of the annual irradiation dose.

IV.3.1.2 Clay provenance study

Because of the spread availability of clays in nature around cities, it is acceptable to consider that the chemical composition of the brick (terra-cotta) is a good indicator of their provenance. Thus, the comparison between the chemical composition of the terra-cotta of the dated brick and those of certain clay deposits allows the determination of which site is the most probable of the clay provenance. In this work, XRF analysis was conducted to compare the chemical oxides compositions of the clay samples collected around the archaeological site with the dated brick's terra-cotta in order to identify the provenance of the construction material. In the followed comparison procedure, oxydes like Na_2O, P_2O_5, and CaO were excluded from the comparison to avoid considering the contamination and some components elimination due to the fabrication and the archealogical preservation of the brick such as firing conditions, moisture and organic material contents. Thus, the average relative difference in oxides (Δ) and the independent samples student t-test (*t*) for bilateral distribution were considered for this comparison. Δ *and t* were calculated by the following formulas:

$$\Delta = \frac{\sum_{i=1}^{n} \frac{C_{ox\,(i)}(brick) - C_{ox\,(i)}(clay)}{C_{ox\,(i)}(brick)}}{n}, \quad \text{(IV.2)}$$

$$t = \frac{\bar{C}_{clay} - \bar{C}_{brick}}{\sqrt{\frac{S^2}{n}}}, \quad \text{(IV.3)}$$

$$S^2 = \frac{\sum_{i=1}^{n} (C_{ox\,(i)}(clay) - \bar{C}_{clay})^2 - (C_{ox\,(i)}(brick) - \bar{C}_{brick})^2}{2n-2}, \quad \text{(IV.4)}$$

where $C_{ox(i)}(brick)$ is the content of the oxyde *i* in the brick's terra-cotta, $C_{ox(i)}(clay)$ is the content of the oxyde *i* in any given clay, $\bar{C}_{clay}$ is the average oxide content in the clay, $\bar{C}_{brick}$ is the average oxide content in the brick, and *n* is the number of considered oxides. The collected clays came from three (3) different deposits around the archaeological city of *Cuicul*.

IV.3.2 Experimental

IV.3.2.1 Dated brick collection

In this work, a terra-cotta brick fragment taken from a separation wall located at approximately 25m (east) from the *Caracalla* arch of *Cuicul* Roman archaeological city was dated by TL technique (Fig. IV.8).

Fig.IV.8: The *Caracalla* arch and the separation wall of the dated brick

The local clay materials used for the fabrication of the dated brick were possibly collected from the neighbourhood of *Cuicul* archaeological city. In order to confirm if local construction material was used and from which deposit site it was probably collected, we have first identified all the old clay deposits around the city (Fig.IV.9), and then we have analyzed the clays composition by XRF. The different clays compositions were then compared to the terra-cotta composition of the dated brick.

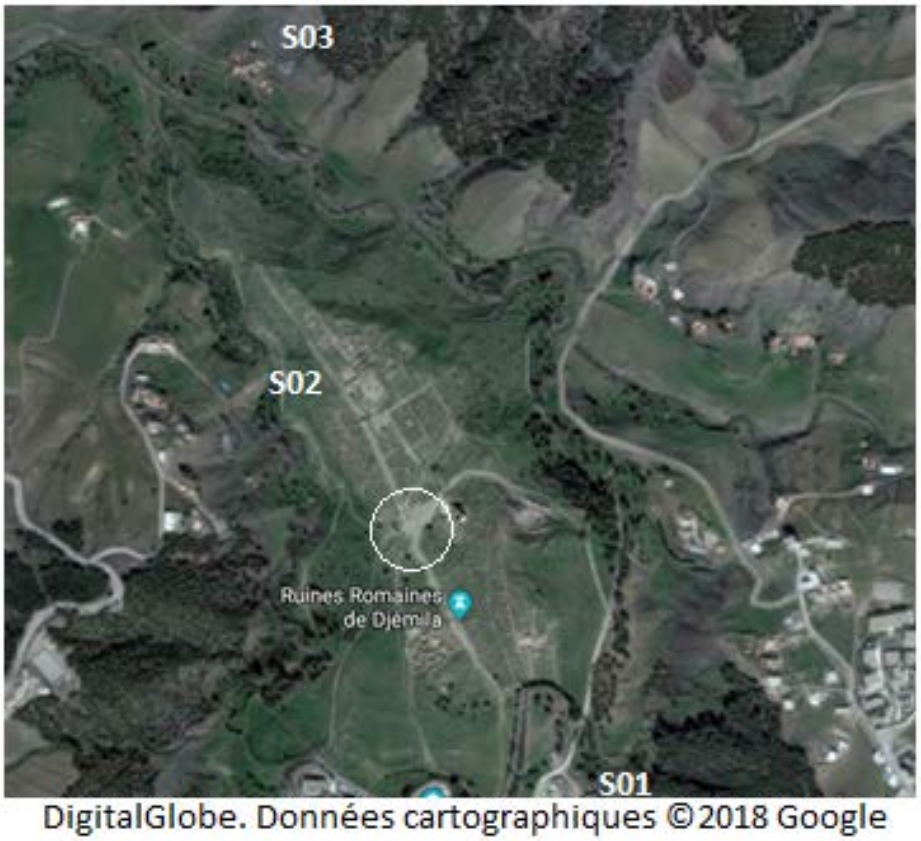

Fig.IV.9: Google map photo showing the dated site (white circle) and the localizations of the identified clay provenance deposits (S01, S02 and S03)

The necessary geographic coordinates of the archaeological site and the burial depth of the dated brick requested for cosmic dose determination are presented in Table IV.6.

Table IV.6: Necessary geographic and burial data for cosmic dose

Site	**Geographic Coordinates and burial depth of the brick**	
***Cuicul* (Djémila), Setif, Algeria**	Latitude	36.3°
	Longitude	5.7°
	Altitude	900 m
	Burial depth	0 m

IV.3.2.2 Determination of the Paleodose

In this study, a mixed additive and regeneration method similar to that described by Sanzelle et al. (1996) is used [15]. This method is based on TL multi-aliquots additive dose standard protocol (MAAD) and fine grains technique [16-17]. The Paleodose was determined by measuring several identical treated aliquots in terms of mineral phase separation (quartz),

separated grains size and deposited quantity on each disk, the TL signals of natural plus artificial beta doses (1st glows) and the TL signals for only additive beta doses after natural TL removing (2nd glows). To ensure that all aliquots are identical, the normalization procedures described by Jain et al. (2003) and Richter D (2007) were followed [18-19]. The considered normalization procedures were the weight normalization (WN) and the glow growth curves matching by the observation if the two curves match well when one of the two curves is shifted towards the other. The measurement protocol was also optimized in terms of errors and checked in terms of extrapolation procedures according to Felix and Singhvi review (1997) [20]. Thus, on the obtained line going back to the abscissa axis representing dose, we obtain the equivalent beta dose (ED_β). The natural TL growth curve was also measured from the origin using the same samples (2nd glows) and the supralinearity intercept, *I*, is then determined. The Paleodose is then taken to be equal to the sum of the absolute values of ED_β and *I* by assuming that the measured 2nd glow growth curve is identical to the natural glow growth curve. This assumption was experimentally checked in many thermoluminescence dating works. Indeed, many dating experiences showed that the intercept, *I*, does not generally change between 1st and 2nd glows, particularly if the 1st and the 2nd glows slopes are parallel in the linear region (above the supralinear knee) as in our case [17-21]. In the used method, TL measurements were made on a number of separated quartz grains deposited on many TL reading stainless steel disks. Two sets of disks were necessary: the first set is used for the natural plus additive β doses TL signal reading (1st glow) and the second set for TL signal reading due to different β doses after natural signal removing (2nd glow). The difference between the two obtained TL growth curves must be uniform and gives the paleodose. In this method, it is assumed that the dating clock was set to zero at the time of the brick's baking.

The sample preparation is already described in paragraph IV.2.2.2.

The necessary artificial thermoluminescence signals were induced by the ^{90}Sr-^{90}Y calibrated beta source integrated in the Risø system delivering 0.1Gy/s. A plateau test was also performed in order to determine the temperature interval where the TL signal must be considered. In this test two aliquots of the quartz grains are TL tested, one after additional exposure to beta dose and the other one without additional exposure. Ratio of the two TL curves obtained should provide a plateau in the TL range.

The TL signals were all collected under the same experimental conditions presented in Table IV.7.

Table IV.7: Conditions of TL signals reading

Luminescence reading mode	Thermoluminescence
Maximum reading temperature	450 °C
Heating rate	5 °C/s
Preheating	230°/10s
TL signal sampling	250 points over the range 0°C to 450°C
Analyzed sample weight	2 mg
Regeneration	2 hour at 450°C

IV.3.2.3 Determination of the annual dose

The annual dose, D_a, is the natural radioactivity contribution in TL essentially by the nuclear radiation from Potassium ^{40}K(β and γ emitter) ,Thorium(α-emitter), and Uranium (α-emitter) plus its additional β and γ radiation which is emitted along the decay chains. Minor contributions yield from rubidium contamination (β-emitter) and cosmic radiation. It is expressed according to the relation: $D_a = k_\alpha D_\alpha + D_\beta + D_\gamma + I_{cosmic}$. Thus, the annual dose rate was calculated from the activity and the mass fractions of the relevant α, β, and γ emitting radionuclides which have been determined by γ-spectrometry. The natural radionuclides providing the annual dose have very long half-lives and therefore the annual dose rate is assumed to be constant. Generally, when considering the fine grain protocol of Zimmerman, such as our case, the alpha particles do not have the same efficiency to contribute to the annual dose. This is why some studied aliquots were also exposed to different alpha doses (3, 6, and 12 Gy) delivered by a calibrated ^{241}Am alpha source (45mGy/s) for the determination of the effective alpha contribution k_α. k_α is determined as a ratio of the equivalent beta dose (ED_β) to the equivalent alpha dose (ED_α). The equivalent alpha dose was determined by the same manner as the equivalent beta dose. The annual α, β, and γ-corrected doses were calculated by the following expressions [17, 22-26].

$$D_\beta = q(1-h)\left[0.146\times 0.940\times \mu_U \times C(U) + 0.273\times 0.915\times \mu_{Th}\times C(Th) + 0.649\times \mu_{K_2O}\times C(K_2O)\right], \quad \text{(IV. 5)}$$

$$D_\gamma = q(1-h)\left[0.113\times C(U) + 0.0476\times C(Th) + 0.202\times C(K_2O)\right], \quad \text{(IV. 6)}$$

$$D_\alpha = k_\alpha \left[2.78 \times C\left(U\right) + 0.732 \times C\left(Th\right) \right], \qquad \text{(IV.7)}$$

where: *C(x)* are the mass fraction expressed in mg kg^{-1} for Uranium (U) and Thorium (Th) and in % for K_2O, *h* is the relative water content, k_α is the effective alpha contribution obtained by comparing TL produced per unit of beta and alpha doses.The used attenuation factors μ_x of the β outer dose corresponding to the grain size interval of the dated brick varying, by microscopy observation, from 200µm-315µm are given in Table IV.8 [25].

Table IV.8: The attenuation factors μ_i of the β outer dose

μ_U	μ_{Th}	μ_{K2O}
0.83	0.77	0.91

q is a correction factor that takes into account the fact that requested doses for age calculation are those delivered to the quartz and not to whole sample matrix and is given by:

$$q = \frac{LET_{av}\left(Quartz\right)}{LET_{av}\left(Humid\ \ matrix\right)} = \frac{LET_{av}\left(SiO_2\right)}{\sum_i \rho_i LET_{av}\left(i\right)}, \qquad \text{(IV.8)}$$

Where: LET_{av} is the average linear energy transfer, ρ_i is the mass fraction of any given oxide *i* in the matrix.

The experimental procedure for determining the relative water content *h* of the sample is as follows: a portion of the raw sample is weighed, and then it is put in the oven at 110°C until full dry. This portion is then weighted again. By convention, water that is removed at 110°C is called free water. *h* is then obtained by taking the weight ratio of the free water and the same sample before drying.

The determination of the annual dose rate requests the determination of the Uranium-238 (^{238}U), the Thorium-232 (^{232}U) and Potassium-40 (^{40}K) mass fractions in the matrix (terra-cotta) and the main oxides weight fractions in the sample. High resolution gamma spectrometry was used to determine the radionuclides mass fractions in the matrix in which the quartz grains were separated. A brick sample (powder) of 10g of weight was dried at 110°C for 20 hours and crushed to less than 100µm and then packaged in an airtight PETP (Polyethylene Terephthalate) tube. This material prevents losses of Radon (^{222}Rn), element of short half life (3.8 days), and thus guarantees γ spectrometric measurements under secular equilibrium conditions. A delay

of fifteen days is respected between the setting in tube and the measurement in order to ensure the radioactive equilibrium between this gas and its descendants. The detector containing the sample was placed in a lead enclosure with low activity to reduce the count of γ-rays in the environment. The γ-photons produced during the decay of the U, Th and K elements are detected by a Canberra High-Purity Germanium (HPGe) well detector with a relative efficiency of 40%. The determination of the mass fractions of the different radionuclides is carried out by comparing the intensities of the lines with those obtained for standards. The gamma spectrometer thus makes it possible to separately obtain the uranium, thorium and potassium contents of our brick sample.

Cosmic dose varies with longitude, latitude, altitude and burial depth and was calculated using the equations given by Prescott and Hutton (1994) [27]. In-situ annual dose rate was also determinate by the use of three TLD-200 (CaF_2: Dy) dosimeters positioned inside the wall for six month and at the exact position from where the dated brick was taken. The TLDs were covered by the remaining brick fragments not used for TL signal reading in order to reproduce the same exposure conditions.

IV.3.2.4 Determination of clay and terra-cotta chemical composition

The Rigaku ZSX primus wave dispersive X-ray Fluorescence spectrometer was used for the elemental analysis of the sample and thus the determination of the mass fraction of the main oxides. Thus, after a drying phase at 100°C for 24h, the samples were ground and screened at ~50µm. To analyze powder samples, the briquette method was used, in which the obtained powder is pressed at 200 kilonewtons to make a disk which is suitable for the undertaken XRF analysis (Fig.IV.10).

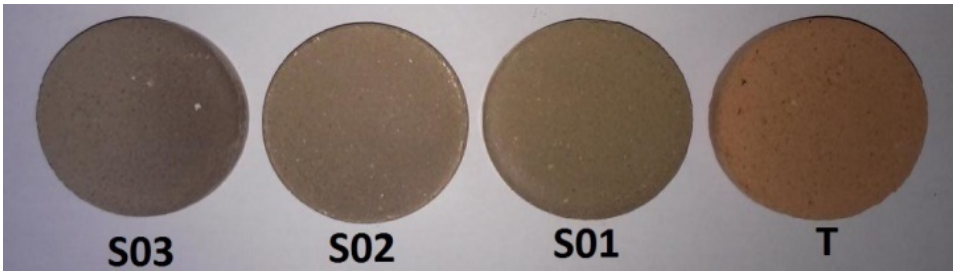

Fig.IV.10:Prepared XRF samples of the brick's terra-cotta (T) and collected clays (S01, S02 and S03)

IV.3.3 Results and discussion

The ED_α and I values of the dated brick were determined using TL measurements. Three fragments of the same brick were separately used for the separation of quartz grains and the establishment of the necessary glow growth curves for the determination of the paleodose. From each fragment, 18 aliquots were prepared and grouped into six groups for measuring the necessary TL signals. Two (2) additional aliquots were used for the plateau test. Established glow growth curves of the first fragment (Frag.1) were found as the most suitable for the paleodose determination in terms of minimum error, supralinearity and parallel growth of the two glow curves. The necessary collected TL signals of Frag.1 corresponding to natural plus beta doses (1st glow) and corresponding to only beta doses (2nd glow) with additive beta doses varying from 2 to 12 Gy are given in triplicate aliquots in Figs. IV.11 and IV.12. The plateau dose was also checked by the comparison of TL curves due the paleodose and to an additive beta dose of 6 Gy and shows that TL signals must be considered within the interval 265°C-365°C.

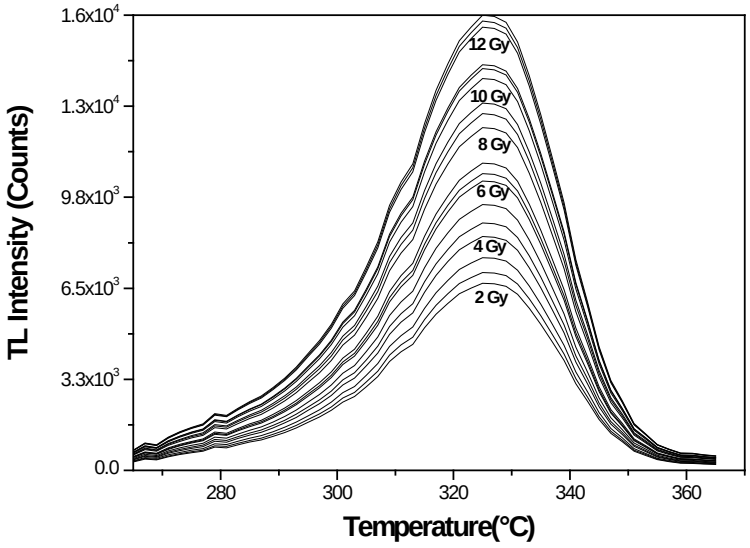

Fig.IV.11: TL signals induced by natural plus additive beta doses (1st glow)

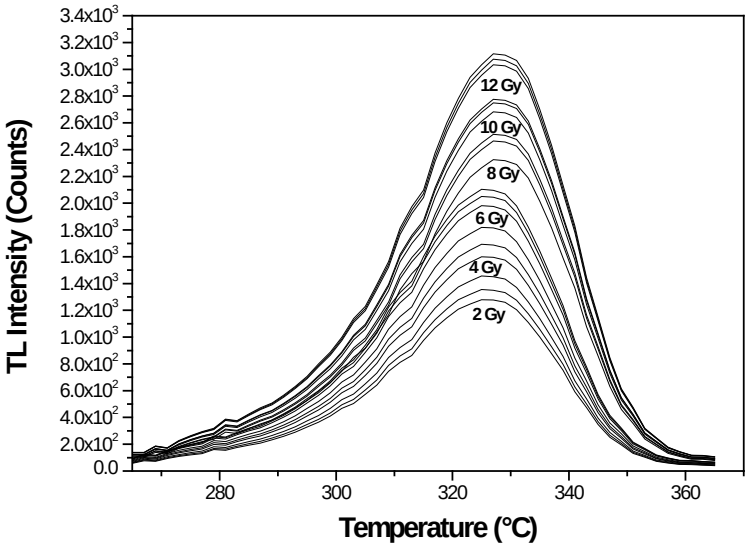

Fig.IV.12: TL Signals induced by additive beta doses only (2nd glow)

On the basis of the TL signals obtained, the dose response curves were then established allowing the determination of the equivalent dose (ED_β) and the dose intercept (I) (Fig.IV.13).

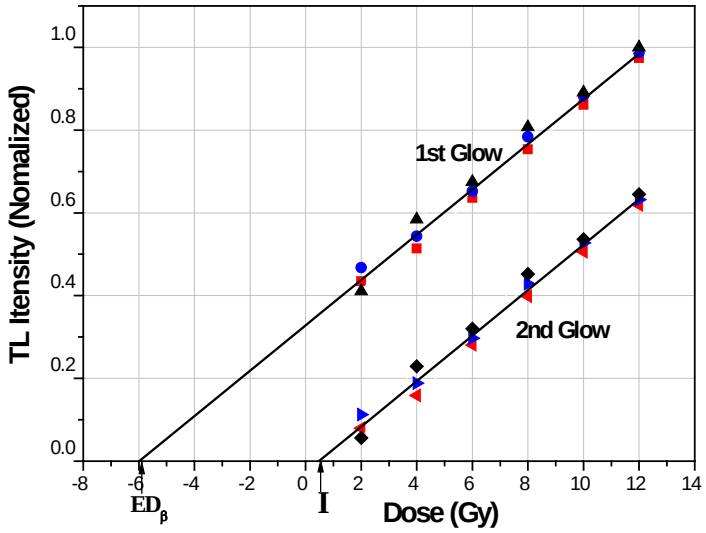

Fig.IV.13: Requested TL growth curves as a function of dose allowing the determination of the equivalent dose (ED_β) and the intercept dose (I) and therefore the paleodose ($ED_\beta+I$)

From results presented in Fig.IV.13, the paleodose was determined as 6.48±0.20 Gy. The X-ray fluorescence analysis data requested for the determination of the annual dose are presented in Table IV.9. *LET* data are taken from reference [28].

Table IV.9: X-ray fluorescence analysis results and used *LET*s for *q* factor calculation

Element	SiO_2	Al_2O_3	Fe_2O_3	CaO	MgO	Na_2O	K_2O	P_2O_5	TiO_2	MnO	H_2O^*
Mass fraction (%)	54.30 ±0.03	14.07 ±0.02	6.16 ±0.01	5.97 ±0.01	3.18 ±0.02	1.44 ±0.02	1.85 ±0.005	0.28 ±0.004	0.74 ±0.02	0.05 ±0.005	11.96 ±0.02
$LET_{av}(i)$ ($MeV.g^{-1}.cm^{-2}$)	1.71	1.67	1.54	1.66	1.70	1.65	1.61	1.69	1.58	1.50	2.03

*Calculated mass fraction.

The determined equivalent alpha dose (ED_α) is 58.72 Gy. Thus, k_α-value, which is the ratio between the ED_β (5.99±0.20 Gy) and the ED_α (58.72±6.80 Gy), was calculated as 0.102±0.015 (~0.1). Because the brick fragment is found on the ground (burial depth equal to 0 m) and because some radioisotopes mass fractions are very low, the contributions of ^{226}Ra, ^{222}Rn and ^{87}Rb in the annual dose were considered as negligible. The mass fractions of ^{238}U and ^{232}Th measured by γ spectrometry are presented in Table IV.10 with the main used factors and the corresponding specific and total annual doses.

Table IV.10: γ-spectrometry analysis results, correction factors and annual doses

	U	**Th**	**$K_2O^{\#}$**
Mass fraction and concentration	2.24±0.08 mg kg^{-1}	8.00±0.20 mg kg^{-1}	1.85±0.05%
H	0.12		
Q	1		
q(1-h)	0.88		
Specific annual Dose (mGy/y)	1.07±0.02	2.49±0.02	0.013±0.001
Total annual dose (mGy/y)	3.57±0.05		

the concentration of ^{40}K is 0.01167% in natural Potassium K.

From the above obtained data on paleodose and annual dose resumed in Table IV.11, the age and thus the fabrication date of the studied brick were estimated. A value of the age of 1820±127 years was found dating back the fabrication of the brick to the year 198 A.D.

Table IV.11: Measured paleodose, annual dose and the corresponding age

Sample	Frag.1[§]	Frag.2	Frag.3
Paleodose (Gy)	6.48±0.20	6.57±0.75	6.42±0.87
Cosmic dose rate (calculated)	0.34±0.02 mGy/y		
Annual α, β and γdose	3.57±0.05 mGy/y		
Total environmental annual dose	3.91±0.07 mGy/y		
In-situ average annual dose measured by TLD-200	3.21±0.20 mGy/y		
Average annual dose	3.56±0.14 mGy/y		
Age (y)	1820±127	1822±21(SD[δ])	

[§] the best in terms of minimum error glow growth curves quality (parallel growth and supralinearity). [δ] Standard deviation.

The dated brick was taken from a separation double-walled brick wall. The wall location is almost 25 meters at the east of the *Caracalla* arch overlooking the southern forum. The construction period of the *Caracalla* arch is known by the emperor *Caracalla* titulature: 211-217 A.D.. Given the proximity of the wall to the arch of *Caracalla*, it is possible to assume that the wall was built during the same period as the arch. According to the epigraphic table (Fig.IV.14), the arch was erected probably in 216 in honour of the emperor *Caracalla*, his mother *Julia Domna* and his deceased father *Septimius Severus* [29]. Thus, the determined date by TL method gives satisfaction because it fits well in the historical context of the construction period and is conform to the development of the city. As the text is very discreet about the event which is at the origin of the construction, it remains to suppose an intervention of the municipality in relation with the great works undertaken during this period for the development of the southern forum and on the juxtaposing constructions like the wall from which the brick's fragment is taken.

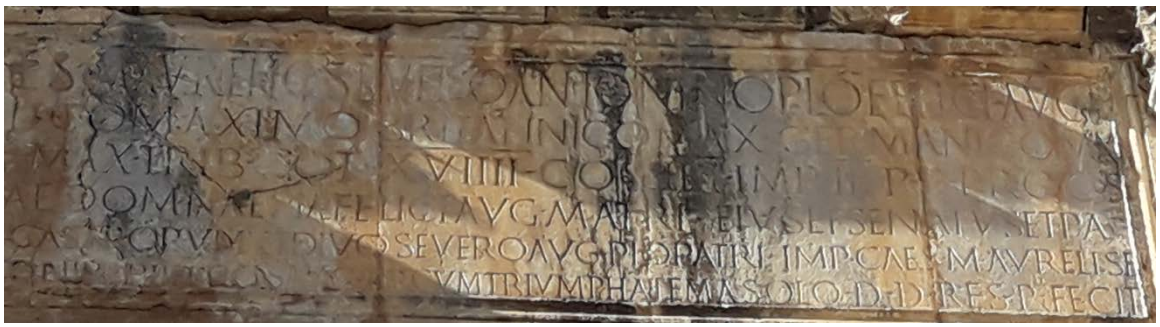

Fig.IV.14: The epigraphic table of the Caracala arch of *Cuicul* Roman city

The XRF analysis results and the comparison results of the clay materials taken from the three considered deposits around the city are presented in Table IV.12.

Table IV.12: XRF analysis and comparison between clays of the studied three deposits and the brick terra-cotta

Oxyde		**SiO_2**	**Al_2O_3**	**Fe_2O_3**	**CaO**	**MgO**	**Na_2O**	**K_2O**	**P_2O_5**	**TiO_2**	**MnO**
Mass Fraction (%)		**Terra-Cotta of the dated brick**									
		54.30	14.07	6.16	5.97	3.18	1.44	1.85	0.28	0.74	0.05
		Clays from deposit sites									
	S01	55.50	16.90	7.67	12.10	1.79	0.18	1.15	0.37	1.02	0.04
	Δ	0.26±0.14					t-test	0.36			
	S02	47.90	19.10	8.72	19.90	1.58	0.47	1.71	0.26	0.99	0.04
	Δ	0.29±0.16					t-test	0.97			
	S03	46.40	19.10	8.96	20.60	1.31	0.36	1.50	0.33	0.99	0.04
	Δ	0.32±0.16					t-test	0.85			

From the obtained XRF results, it is obvious that S01 is close in composition to the terra-cotta of the dated brick. Thus, the dated brick material comes from S01 although it is relatively difficult to access. The S01 clay is essentially a silicon-aluminous one with lower carbonates contents. The brick fabricated from this clay sintered generally at 900°C and is of good quality regarding the technical properties actually required in the manufacture of terra-cotta products [30]. Thus, it is possible that Roman builders did some simple tests on the brick in order to select the most suitable clay to be used. Thus, we can assume that the Roman construction knowledge was not limited in the architecture aspect but it was possibly extended to some construction material selection mastering. These assumptions have to be confirmed by further investigations and multidisciplinary studies.

IV.3.4 Conclusions

In this work, a first scientific study was conducted on the famous archaeological site of *Cuicul* (Djémila) for dating and construction materials origin detemination purposes. The results presented in this work indicate that the used TL technique is a suitable dating method, particularly, when samples are well prepared, the supralinearity TL growth is achieved and all corrections on dose and TL signal are considered. The fabrication date of studied brick is in good agreement with the known construction phases and the history of *Cuicul* and the *Caracalla* arch reported by many archaeologists and historians [29,31-34]. The XRF analysis of the

construction materials taken from different clay's deposits demonstrates that only S01 clay is close in composition to the terra-cotta of the dated brick and is suitable for its fabrication regarding its characteristics. Indeed, the composition of the used clay was found very suitable for the fabrication of a good quality brick in terms of mechanical properties. This result allows us to suppose that Roman builders did some simple tests on the construction materials for the selection of the most suitable one. In conclusion, the results obtained in the framework of this work are very promising and will certainly contribute to put some of the *Cuicul* remains in their real chronological context. These results have, in fact, served to formulate some hypotheses on the manufacture technique as well as the provenance of the construction materials.

IV.4 Thermoluminescence establishing of the construction timeline map of *Cuicul*

IV.4 .1 Introduction

In this work and after a successful thermoluminescence dating of a brick's wall near the Caracalla arch [35], a big project was conducted, just after this first achievement, aiming the reconstruction of an accurate timeline map of the whole city by the same dating technique. This project was conducted in four (4) major phases: 1. Historical study on the site, 2. site subdivision and dated terra-cotta bricks collection, 3. Thermoluminescence dating, 4. data analysis and timeline map establishment.

IV.4.2 Theory

IV.4.2.1 Brick fabrication and construction technique

Cuicul has known during the ancient period several construction phases. At the beginning the choice and the construction of the site were based on military considerations and then the city starting to be populated by the veteran soldiers and the civilians coming from different regions. Thus, the city lived an exemplary stability and was developed to become a small city with all the roman conveniences of the time. During the next Byzantine period many maintenance and restitution works were carried out. Several construction techniques were used in the construction of this city. Brick's samples dated in the framework of this work were collected from walls constructed by two different techniques. The first technique is the so-called *Opus Testaceum* and the second one is the *Opus mixtum* technique. In *Opus Testaceum* technique only terra-cotta bricks are used with a lime mortar. This technique has been used since the

beginning of the 1st century and has gradually replaced other techniques, due to its strength and ease of use [36,37]. The *Opus mixtum* is a technique of wall constrcution with both brick and stone facing. This techique became common in the 1st and 2nd centuries AC. In the *opus mixtum* technique, panels of shaped stones were separated by bands of brick facing. This technique saved on manpower and on bricks which were relatively expensive at the time. Finally, it is important to mention that brick is a reused construction material and therefore erroneous dating may come from the reutilization of bricks from older destroyed walls voluntary or because of earthquake [38-40].

IV.4.2.2 Site subdivision and sampling strategy

By taking into consideration the possible modifications on the site due to restauration works as well as lootings by vandals and other invaders, an adequate city subdivision in urban area (zones) was carried out by targeting the existence of at least one building constructed with the *Opus Testaceum* or *Opus mixtum* techniques and not seeming to undergo any modification. The city has been divided into 10 separated urban zones that have some similarities. The city subdivision was performed from the south to the north according to the observable architecture harmony and by making cross-checks with the historical texts although little information on the exact period of construction (Fig.IV.15). The operation of brick's samples collection (Table IV.13) was conducted with the assistance of experienced archaeologists and museum's technicians to avoid samples selection from recent restored places.

Fig. IV.15: Google map photo showing the dated site, subdivision zones and examples of walls from where dated bricks were taken

Table IV.13: Site subdivision into main urban zones and collected brick samples with construction technique

Zone N°	Name	Sample N°	Origin of the sample	Construction Technique
1	Christian Street: Bishop house.	1A	Wall of the house of Bishop	*Opus Testaceum*
		1B	Wall of the house of Bishop	*Opus Testaceum*
		1C	Wall of the house of Bishop	*Opus Testaceum*
2	Christian Street: Church, Cathedral and Baptistery	2A	Wall of the Cresconius cathedral	*Opus Testaceum*
		2B	Crypt of the Cresconius cathedral	*Opus Testaceum*
		2C	Wall of the Church	*Opus Testaceum*
		2D	Foundation of Church	*Opus Testaceum*
		2F	Wall of the Church underground chamber	*Opus Testaceum*
		2G	Walls of the Baptistery: east, south and west sides	*Opus Testaceum*
3	Christian Street: Houses	3A	Walls of a Christian neighbourhood house	*Opus Testaceum*
4	Bacchus House	4A	Walls of the house of Bacchus	*Opus Testaceum*
5	Great baths	5A	Walls of the baths	*Opus Testaceum*
6	Severian place	6A	Wall of civil basilica	*Opus Testaceum*
		6B	Wall near the Septum temple	*Opus Testaceum*
7	Eastern street	7A	Wall of the house with bath	*Opus Testaceum*
8	Top of the Cardo Maxium	8A	Wall of the house of Castorius	*Opus mixtum*
		8B	Wall of the house of the Donkey	*Opus mixtum*
		8C	Venus Genetrix Temple	*Opus mixtum*
9	Western street	9A	Christian basilica	*Opus mixtum*
10	Down of the Cardo Maximus:	10A	Cosinius market: east wall	*Opus mixtum*
		10B	Walls of the house of Europe	*Opus mixtum*

IV.4.2.3 Brick identification and comparison

The chemical composition of the brick (terra-cotta), particularly the oxides fraction (%) is a good indicator for their identification and comparison. Thus, the comparison between the chemical composition of the terra-cotta of the dated brick allows the determination the origin of the brick and if it was taken from another place and resued or not . In this work, XRF analysis was conducted to compare the chemical oxides compositions of the dated brick's terra-cotta collected from different places of the archaeological site for their classification. In the followed comparison procedure, oxides mass fraction was considered. Oxides mass fraction will be also

used for the determination of *q* correction factor that takes into account the fact that requested doses for age calculation are those delivered to the quartz and not to whole sample matrix.

IV.4.2.4 Thermoluminescence dating

The theory and practice of the used dating procedure was the same that was described in part IV.3 of this chapter.

IV.4.3 Experimental

IV.4.3.1 Samples collection and dating by thermoluminescence

In this work, a terra-cotta brick fragment taken from different areas from *Cuicul* Roman archaeological city was dated by TL technique. The necessary geographic coordinates of the archaeological site and the burial depth of the dated brick requested for cosmic dose determination are presented in Table IV.6. For the samples preparation, the same experimental procedure based on the use of HCl, H_2O_2 and HF, described in our previous work, is used [41]. Time controlling grain sedimentation procedure in acetone (~0.8g/cm^3) allow separation of polymineral fine grains fraction in the range of 1-8 μm which were deposited onto stainless steel disks. The necessary artificial thermoluminescence signals were induced by the ^{90}Sr-^{90}Y calibrated beta source integrated in the Risø system delivering 0.1Gy/s. In this work, the RisøTL/OSL-DA-20 luminescence reader was used [42]. The TL signals were all collected under the same experimental conditions presented in Table IV.7.

The experimental procedure for determining the relative water content *h* was also described in kharfi el al. [35]. For the determination of the effective alpha contribution k_α the used grain disks for beta equivalent dose determination (ED_β) are exposed to 3, 6, and 12 Gy alpha dose delivered by a calibrated ^{241}Am alpha source (45mGy/s). Thus k_α is determined as a ration of the equivalent beta dose (ED_β) to the equivalent alpha dose (ED_α). However, the determination of the Uranium-238 (^{238}U), the Thorium-232 (^{232}U) and Potassium-40 (^{40}K) mass fractions in the matrix (terra-cotta) was performed by high resolution gamma spectrometry following the same procedure described in [41]. Indeed, a Canberra High-Purity Germanium (HPGe) well detector with a relative efficiency of 40% was used for γ-photon detection.

Finally, in-situ annual dose rate was also determinate by the use of TLD-200 (CaF_2: Dy) dosimeters positioned inside the wall for six month and at the exact position from where the

dated bricks were taken. The TLDs were covered by the remaining brick fragments not used for TL signal reading in order to reproduce the same exposure conditions.

IV.4.3.2 Brick's terra-cotta chemical composition determination:

This part of work is the same as described in part IV.3.2.4, using a Rigaku ZSX primus wave diffractive X-ray fluorescence spectrometer for the elemental analysis of the samples.

IV.4.4 Results and discussion

The checked plateau for an additive Beta dose of 6 Gy demonstrates well that it is necessary to consider the TL glows in the temperature interval of 260°C-370°C and this for the growth curves establishment and therefore for the determination of the paleodose. The X-ray fluorescence analysis data requested for the determination of the annual dose are presented in Table IV.14. *LET* data are taken from reference [43].

Table IV.14:X-ray fluorescence analysis results and used *LET*s for *q* factor calculation

Sample	Oxide mass fraction (%)										
	SiO_2	Al_2O_3	Fe_2O_3	CaO	MgO	Na_2O	K_2O	P_2O_5	TiO_2	MnO	H_2O^*
1A	53.50 ±0.03	11.80 ±0.02	13.67 ±0.01	7.10 ±0.01	2.89 ±0.02	0.25 ±0.02	1.08 ±0.005	0.39 ±0.004	1.00 ±0.02	0.04 ±0.005	8.28 ±0.02
1B	53.50 ±0.03	11.80 ±0.02	13.67 ±0.01	7.10 ±0.01	2.89 ±0.02	0.25 ±0.02	1.08 ±0.005	0.39 ±0.004	1.00 ±0.02	0.04 ±0.005	8.28 ±0.02
1C	53.50 ±0.03	11.80 ±0.02	13.67 ±0.01	7.10 ±0.01	2.89 ±0.02	0.25 ±0.02	1.08 ±0.005	0.39 ±0.004	1.00 ±0.02	0.04 ±0.005	8.28 ±0.02
2A	49.50 ±0.03	17.50 ±0.02	8.72 ±0.01	10.10 ±0.01	1.38 ±0.02	0.45 ±0.02	1.73 ±0.005	0.25 ±0.004	1.00 ±0.02	0.04 ±0.005	9.33 ±0.02
2B	49.50 ±0.03	17.50 ±0.02	8.72 ±0.01	10.10 ±0.01	1.38 ±0.02	0.45 ±0.02	1.73 ±0.005	0.25 ±0.004	1.00 ±0.02	0.04 ±0.005	9.33 ±0.02
2C	47.20 ±0.03	12.90 ±0.02	15.96 ±0.01	9.60 0.01	2.30 ±0.02	0.35 ±0.02	1.50 ±0.005	0.35 ±0.004	0.99 ±0.02	0.04 ±0.005	8.81 ±0.02
2D	47.20 ±0.03	12.90 ±0.02	15.96 ±0.01	9.60 ±0.01	2.30 ±0.02	0.35 ±0.02	1.50 ±0.005	0.35 ±0.004	0.99 ±0.02	0.04 ±0.005	8.81 ±0.02
2F	47.20 ±0.03	12.90 ±0.02	15.96 ±0.01	9.60 ±0.01	2.30 ±0.02	0.35 ±0.02	1.50 ±0.005	0.35 ±0.004	0.99 ±0.02	0.04 ±0.005	8.81 ±0.02
2G	54.30 ±0.03	14.07 ±0.02	6.16 ±0.01	5.97 ±0.01	3.18 ±0.02	1.44 ±0.02	1.85 ±0.005	0.28 ±0.004	0.74 ±0.02	0.05 ±0.005	11.96 ±0.02
3A	54.30 ±0.03	14.07 ±0.02	6.16 ±0.01	5.97 ±0.01	3.18 ±0.02	1.44 ±0.02	1.85 ±0.005	0.28 ±0.004	0.74 ±0.02	0.05 ±0.005	11.96 ±0.02
4A	47.20 ±0.03	17.90 ±0.02	15.96 ±0.01	12.60 ±0.01	2.30 ±0.02	0.35 ±0.02	1.50 ±0.005	0.35 ±0.004	0.99 ±0.02	0.04 ±0.005	8.81 ±0.02
5A	49.50 ±0.03	17.50 ±0.02	8.72 ±0.01	10.10 ±0.01	1.38 ±0.02	0.45 ±0.02	1.73 ±0.005	0.25 ±0.004	1.00 ±0.02	0.04 ±0.005	9.33 ±0.02
6A	54.30 ±0.03	14.07 ±0.02	6.16 ±0.01	5.97 ±0.01	3.18 ±0.02	1.44 ±0.02	1.85 ±0.005	0.28 ±0.004	0.74 ±0.02	0.05 ±0.005	11.96 ±0.02
6B	54.30 ±0.03	14.07 ±0.02	6.16 ±0.01	5.97 ±0.01	3.18 ±0.02	1.44 ±0.02	1.85 ±0.005	0.28 ±0.004	0.74 ±0.02	0.05 ±0.005	11.96 ±0.02
7A	47.50	10.90	19.50	8.16	2.30	0.40	1.50	0.40	1.00	0.04	8.3

	±0.03	±0.02	±0.01	±0.01	±0.02	±0.02	±0.005	±0.004	±0.02	±0.005	±0.02
8A	47.50 ±0.03	10.90 ±0.02	19.50 ±0.01	8.16 ±0.01	2.30 ±0.02	0.40 ±0.02	1.50 ±0.005	0.40 ±0.004	1.00 ±0.02	0.04 ±0.005	8.3 ±0.02
8B	46.10 ±0.03	10.25 ±0.02	23.15 ±0.01	7.56 ±0.01	1.90 ±0.02	0.50 ±0.02	1.62 ±0.005	0.45 ±0.004	1.05 ±0.02	0.04 ±0.005	7.38 ±0.02
8C	46.10 ±0.03	10.25 ±0.02	23.15 ±0.01	7.56 ±0.01	1.90 ±0.02	0.50 ±0.02	1.62 ±0.005	0.45 ±0.004	1.05 ±0.02	0.04 ±0.005	7.38 ±0.02
9A	46.10 ±0.03	10.25 ±0.02	23.15 ±0.01	7.56 ±0.01	1.90 ±0.02	0.50 ±0.02	1.62 ±0.005	0.45 ±0.004	1.05 ±0.02	0.04 ±0.005	7.38 ±0.02
10A	47.20 ±0.03	12.90 ±0.02	15.96 ±0.01	9.60 0.01	2.30 ±0.02	0.35 ±0.02	1.50 ±0.005	0.35 ±0.004	0.99 ±0.02	0.04 ±0.005	8.81 ±0.02
10B	47.20 ±0.03	12.90 ±0.02	15.96 ±0.01	9.60 ±0.01	2.30 ±0.02	0.35 ±0.02	1.50 ±0.005	0.35 ±0.004	0.99 ±0.02	0.04 ±0.005	8.81 ±0.02
$LET_{av}(i)$ ($MeV.g^{-1}.cm^{-2}$)	1.71	1.67	1.54	1.66	1.70	1.65	1.61	1.69	1.58	1.50	2.03

*Calculated mass fraction.

The k_α-value, which is the ratio between the ED_β and the ED_α,was calculated as 0.100±0.015 (~0.1) for all studied bricks. The *q* factor values were calculated on the basis Table 4 data for all dated bricks (0.99-1.01). The mass fractions of ^{238}U and ^{232}Th measured by γ spectrometry, the K2O concentration (%), the average archaeological dose (paleodose) and annual dose, and the corresponding date (age) are presented in Table IV.15.

Table IV.15: γ-spectrometry analysis results, measured paleodose and annual dose, and the corresponding determined date (age) of the studied bricks

Zone	**Sample N°**	**Mass fraction and concentration**			**Dose**		**Date (A.D.±SD*)**
		U ($mg\ kg^{-1}$)	**Th ($mg\ kg^{-1}$)**	**$K_2O^{\#}$ (%)**	**Average Paleodose (Gy)**	**Average annual dose (mGy)**	
1	1A	2.15±0.08	7.9±0.20	1.08±0.05	5.90±0.25	3.54±0.15	352±30
	1B	2.15±0.08	7.9±0.20	1.08±0.05	5.91±0.20	3.54±0.15	349±27
	1C	2.15±0.08	7.9±0.20	1.08±0.05	5.92±0.18	3.54±0.15	346±25
2	2A	2±0.08	7.8±0.20	1.73±0.05	5.60±0.22	3.48±0.12	409±30
	2B	2±0.008	7.8±0.20	1.73±0.05	5.62±0.22	3.48±0.12	404±30
	2C	1.95±0.08	7.8±0.20	1.50±0.05	5.75±0.19	3.48±0.12	365±25
	2D	1.95±0.08	7.8±0.20	1.50±0.05	5.80±0.30	3.48±0.12	352±30
	2F	1.95±0.08	7.8±0.20	1.50±0.05	5.78±0.29	3.48±0.12	358±30
	2G	2.2±0.08	8±0.20	1.85±0.05	5.85±0.20	3.54±0.15	366±28
3	3A	2.2±0.08	8±0.20	1.85±0.05	6.03±0.22	3.54±0.15	316±25
4	4A	1.9±0.08	7.85±0.20	1.50±0.05	5.95±0.34	3.47±0.12	304±28
5	5A	2±0.008	7.8±0.20	1.73±0.05	6.39±0.34	3.48±0.12	182±16
6	6A	2.2±0.08	7.8±0.20	1.85±0.05	6.38±0.32	3.51±0.14	201±18

	6B	2.2±0.08	8±0.20	1.85±0.05	6.35±0.29	3.54±0.15	225±20
7	7A	1.95±0.08	7.75±0.20	1.50±0.05	6.36±0.29	3.47±0.12	186±15
8	8A	1.95±0.08	7.75±0.20	1.50±0.05	6.67±0.44	3.47±0.12	97±10
	8B	1.92±0.08	7.75±0.20	1.62±0.05	6.65±0.40	3.48±012	108±10
	8C	1.92±0.08	7.75±0.20	1.62±0.05	6.55±0.36	3.48±0.12	137±12
9	9A	1.92±0.08	7.75±0.20	1.62±0.05	5.75±0.27	3.48±0.12	367±30
10	10A	1.95±0.08	7.8±0.20	1.50±0.05	6.40±032	3.48±0.12	180±15
	10B	1.95±0.08	7.8±0.20	1.50±0.05	6.60±0.32	3.48±0.12	122±10

[#] the concentration of ^{40}K is 0.01167% in natural Potassium K, [*] SD: standard deviation

From the above obtained data (Table IV.15), the city construction and development timeline map is established (Fig.IV.16).

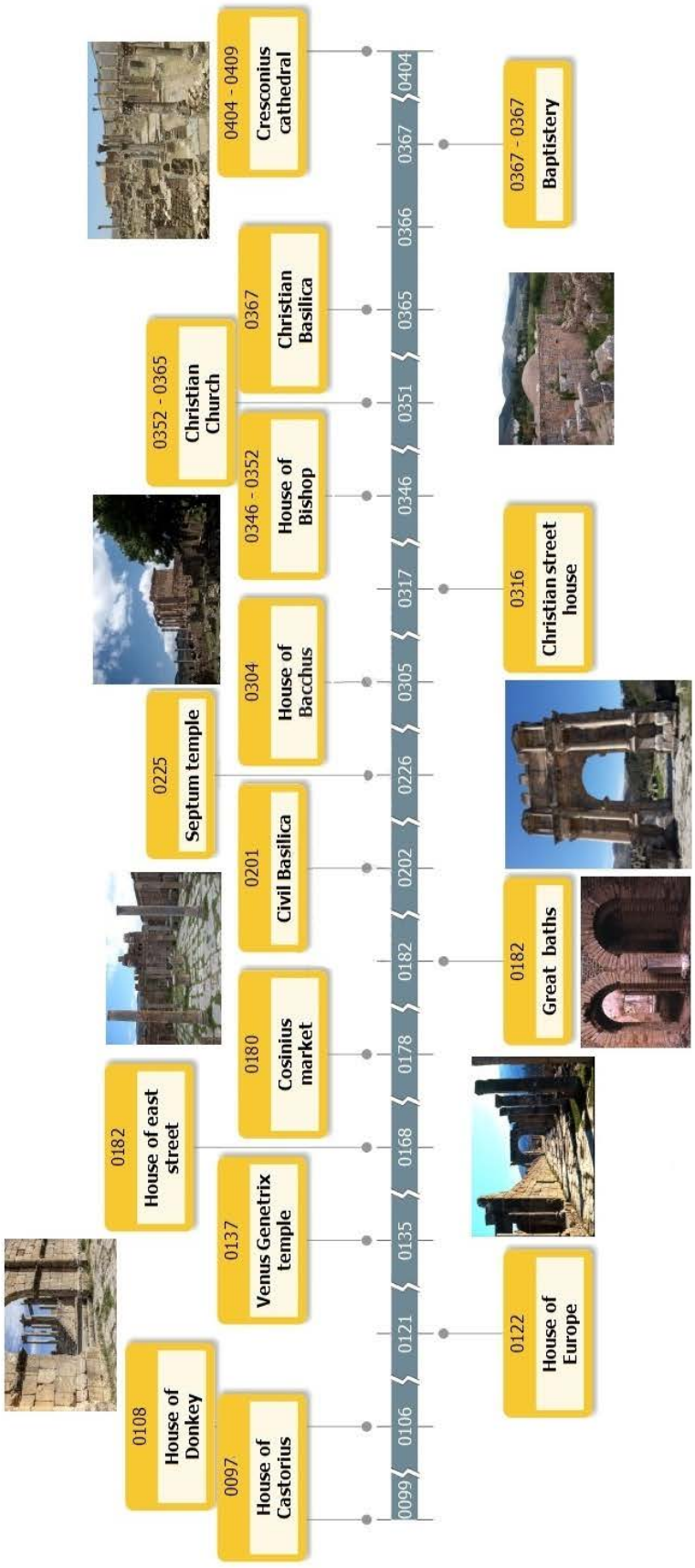

Fig. IV.16:Estblished timeline map of *Cuicul* constrcution development showing main dated places, monuments and buildings (all dates are A.D.)

The established timeline map with the different mentioned dates gives satisfaction because it fits well with some historically known periods and events which closely related to some building and temples construction. It is very important to mention, that with the assistance of archeologists, the selection of dated bricks was thoroughly performed by ensuring that there is no doubt about their original fixation on the walls. Despite all our precautions, few selected samples (bricks) gave not consistent dates with the aforementioned period and were therefore excluded from this study. The non-consistency is maybe due to some well-done recent site restoration with non-original bricks. No evidence was found concerning the reuse of bricks from destructed walls in the construction of new ones during the city life.

The timeline map demonstrates that the veteran's houses, which constitute the primitive colony, were constructed until the end of the first century at the east of the main cardo down street. At the beginning of the second century, to the first modest veteran's houses succeeded much larger houses equipped with baths, fountains, and moldings in mosaics such as the house of the Donkey (108 A.D.) and the house of Europe (122 A.D.). The city was also centered on some kind forum sometimes called the old forum (square between zone 8 and 10 of Fig.IV.15). The square place serving as forum was all surrounded by public buildings such as the Curia, the temple with triple sanctuaries, the basilica of justice and civil affairs, the temple of Venus Genetrix (137 A.D.), and the Cosinius brothers' market (180 A.C.). The city then grew and developed through its extension to the south along three main axes: Central (main cardo), Eastern, and Western. One house of the eastern street is dated in 186 A.D.. Thus, with the increase in the population, the southern suburban area was being built, and the center of urban activity tended to move towards the South. This movement resulted in the construction of a new forum. The monument and building dated in this aera, Septum temple (225 A.D.), reveals that the construction of this forum was mainly during the first third of the third century. Here, it is very important to mention that civil basilica is dated 202 A.D. although it is known that this basilica is of 4th century. This disparity is due to the fact that, according to some historical studies and results of archaeological excavations [44-45], the civil basilica was built at the end of the 4th century on the remains of an old temple dedicated to Frugifer God which was built in the same period as Septum temple. Thus, it is possible that same bricks were reused in the new construction or the dated wall was kept from the first construction. These assumptions need to be confirmed by deeper studies.

If the dates already determined seem to follow certain logic in the development of the city, the construction date of the great baths is problematic. Indeed, the determined date (182 A.D.) is countered because the baths are located at a distance from the south limit of the old center of the city. This implies that the great baths were built before the new forum of the city and that an area between the thermal baths and the old city was left empty as Louis Leschi indicated in his historical study on the site in 1950 [44]. This controversy remains inexplicable in the context of this study because it is not acceptable to consider any reuse of bricks for the construction of all these baths. However, it is just possible to consider that these baths are built before the new forum for reasons depending on its location which should be better for the connection of the baths to the underground water and for water evacuation after use. A second possible reason is regarding the existence of a pre-established plan for the development of the city involving certain priorities in the construction of buildings and monuments, and therefore the choice of their implementation places. It should be reminded that *Cuicul* was constructed on a spur of land created by two mountain rivers and surrounded by rolling hills with some irregularities making the availability and the choice of construction areas difficult. Finally, at the southeastern end of the city was the last phase of the city construction which coincides with the Christian period. All dated house and building (House of Bacchus, House of Bishop, Private house, Church, Basilica and Baptistery) are between 304 A.D. and 409 A.D. The Christian basilica (367 A.D.) was first constructed at the west limit of the western street (zone N°9) just before the ramparts. According to our study results, the *Cresconius* cathedral was constructed between 404 A.D. and 409 A.D. at the northern limit of the Christian street probably because of the designation of the bishop and the increase of the Christian population. *Cresconius* was the Catholic bishop who represented *Cuicul* at the Council of Carthage (411 A.D.) between Catholic and Donatist bishops [46]. This conference was held on the 1st of June 411 A.D., with a view of uniting the Donatists to the Church, and convincing them of the necessity of seeking salvation in the Catholic Church. In 411 Donatism was declared a heresy by Emperor *Honorius* who endorsed the outcome of a council held at Carthage [46]. In this context *Cresconius*, Bishop of Cuicul, decided to build a very large church where all the Christians of the town could gather. Although the TL dated construction period of this new basilica (404-409 A.D.) is slightly before this construction decision date (411), the TL dating results remain very accurate and significative with such known and confirmed historical events [46].

IV.4.5 Conclusions

In this work, a timeline map was established presenting construction dates of the major parts of *Cuicul* (Djémila) roman city by thermoluminescence technique. Accurate construction dates were obtained through the optimization of the different dating steps starting from bricks selection and quartz separation until TL signal reading and TL growth curves establishment. By ensuring the supralinearity of TL growth curves and also by perfoming all the necessary corrections on dose, the determined ages and dates were with acceptable standards deviations. The strategy of dividing the site into different zones was carefully carried out based on topographical observations and by consulting expert archaeologists. The importance of this study is related to fact that it was made possible to place the different phases of *Cuicul* construction in a scientifically proven chronological order. The dating result obtained for the civilian basilica of the 4th century, may give us an evidence about the reuse of construction material during the city life of *Cuicul*. Further investigation will be necessary conducted in the futur in order to clarfy this point. This will certainly allow archaeologists and historians to confirm or to reject certain hypotheses in relation with the construction of certain buildings during the whole development of the city between the first and fifth centuries.

References

[1] Aitken MJ (1974) Physics and archaeology, Oxford: 26-84.

[2] Zimmerman DW (1971) Thermoluminescent dating using fine grains from pottery. Archaeometry 13: 29–52.

[3] Wright AG (2017) The Photomultiplier Handbook. Masters Oxford University Press, Oxford.

[4] Zimmerman DW, Huxtable J (1969) Recent Applications and Developments in Thermoluminescent Dating. Archaeometry 11:105-108

[5] Aitken, MJ (1985) Thermoluminescence Dating. Academic Press, London.

[6] Mejdahl V (1979) Thermoluminescence dating: beta dose attenuation in quartz grains.

[7] Mejdahl V (1987) Internal radioactivity in quartz and feldspar grains. Ancient TL, 5 (2): 10-17

[8] Furetta C (2003) Handbook of Thermoluminescence. World Scientific Publishing.

[9] Bøtter-Jensen L (2000) Development of Optically Stimulated Luminescence Techniques using Natural Minerals and Ceramics, and their Application to Retrospective Dosimetry. Dissertation, University of Copenhagen.

[10] Jain M, Booetten-Jensen L, Singhvi AK (2003) Dose evaluation using multiple aliquot quartz OSL: test of methods and new protocol for improved accuracy and precision. Radiation measurements 37:67-80

[11] Richter D (2007) Advantages and Limitations of Thermoluminescence Dating of Heated Flint from Paleolithic Sites. Geoarchaeology 22(6) : 671–683

[12] Felix C, Singhvi AK (1997) Study of non-linear luminescence-dose growth curves for the estimation of paleodose in luminescence dating: results of Monte Carlo simulations. Radiation Measurements 27:599

[13] Fleming SJ (1970) Thermoluminescent dating: refinement of quartz inclusion method. Archaeometry 12(2): 133-146

[14] Murray AS, Wintle AG (2000) Luminescence dating of quartz using an improved single-aliquot regenerative-dose protocol. Radiation Measurements 32(1):57–73

[15] Sanzelle S, Miallier D, Pilleyre T, Faïn J, Montret M (1996) A new slide technique for regressing TL/ESR dose response curves. Radiation Measurements 26: 631-638.

[16] Aitken MJ (1974) Physics and archaeology, Oxford: 26-84

[17] Zimmerman DW (1971) Thermoluminescent dating using fine grains from pottery. Archaeometry 13: 29–52

[18] Jain M, Booetten-Jensen L, Singhvi AK (2003) Dose evaluation using multiple aliquot quartz OSL: test of methods and new protocol for improved accuracy and precision. Radiation measurements 37:67-80

[19] Richter D (2007) Advantages and Limitations of Thermoluminescence Dating of Heated Flint from Paleolithic Sites. Geoarchaeology 22(6) : 671–683

[20] Felix C, Singhvi AK(1997) Study of non-linear luminescence-dose growth curves for the estimation of paleodose in luminescence dating: results of Monte Carlo simulations. Radiation Measurements 27:599

[21] Fleming SJ (1970) Thermoluminescent dating: refinement of quartz inclusion method. Archaeometry 12(2): 133-146

[22] Aitken, MJ (1985) Thermoluminescence Dating. Academic Press, London.

[23] Mejdahl V (1979) Thermoluminescence dating: beta dose attenuation in quartz grains. Archaeometry 21: 61-72.

[24] Mejdahl V (1987) Internal radioactivity in quartz and feldspar grains. Ancient TL, 5 (2): 10-17

[25] Pilleyre T(1991) Datation par thermoluminescence : Application à la chronologie des retombées volcaniques. Thèse de doctorat de l'université Blaise Pascal - Clermont II, Clermont-Ferrand, France.

[26] Bassinet C (2007) Datation par luminescence : recherches méthodologiques et applications au volcanisme dans l'environnement de Laschamp.Thèse de doctorat de l'université Blaise Pascal- Clermont-Ferrand II, Françe. tel-00171318

[27] Prescott JR, Hutton JT (1994) Cosmic ray contributions to dose rates for luminescence and ESR dating: Large depths and long-term time variations. Radiation Measurements, 23:497-500.

[28] Pilleyre T, Montret M, Fain J, Miallier D, Sanzelle S (1992) Attempts at dating ancient volcanoes using the red TL of quartz. Quaternary Science Reviews, 11: 13-17

[29] Leydier-Bareil AM (2006) Les arcs de triomphe dédiés à *Caracalla* en Afrique romaine. Doctorat histoire de l'art et archéologie, Université de Nancy 2, France. LN006/26-2 bis.

[30] Lourenço PB, Fernandes FM, Castro F (2010) Handmade Clay Bricks: Chemical, Physical and Mechanical Properties. International Journal of Architectural Heritage DOI: 10.1080/15583050902871092

[31] Akli Ikherbane M (2003) Le site archéologique de Djemila, l'antique *Cuicul*: Éventail d'actions possibles. Les Dossiers d'archéologie (Dijon) A286:26-31

[32] Allais Y (1953) Le quartier à l'Est du Forum des Sévères. Revue Africaine XCVII: 48-65

[33] Allais Y (1971) Le quartier Occidental de Djemila (Cuicul). Antiquités Africaines, 5: 95-119

[34] Aitken MJ (1970) Dating by Archaeomagnetic and Thermoluminescent Methods. Philosophical Transactions of the Royal Society of London. Series A, Mathematical and Physical Sciences, A Symposium on the Impact of the Natural Sciences on Archaeology Vol. 269, No. 1193: 77-88

[35] Kharfi F, Boudraa L, Benabdelghani I, Bououden M (2019) TL dating and XRF clay provenance analysis of ancient brick at Cuicul Roman city, Algeria, Journal of Radioanalytical and Nuclear Chemistry 320:395–403

[36] Dessales H (2018) Petit catalogue des techniques de la construction romaine, Ecole Normale Supérieure ENS/CNRS, Paris, France, http://www.archeologiesenchantier.ens.fr/spip.php?article30. Accessed 17 August 2019

[37] Adam JP (2017) la construction romaine- matériaux et techniques. Picard, 7th Ed

[38] Strickland M (2010) Roman Building Materials, Construction Methods, and Architecture: The Identity of an Empire. Thesis, Clemson University. All Theses. 909. https://tigerprints.clemson.edu/all_theses/909. Accessed 17August 2019

[39] Francisco M. Fernandes, Paulo B. Lourenço and Fernando Castro, Ancient Clay Bricks: Manufacture and Properties, in: M. Bostenaru Dan et al. (eds.), Materials, Technologies and Practice in Historic Heritage Structures, DOI 10.1007/978-90-481-2684-2 3, © Springer Science+Business Media B.V. 2009

[40] Stalley, Roger (1999), Early Medieval Architecture. Oxford University Press, USA. pp. 112–14. ISBN 0-19-284223-4.]

[41] Libby W (1946) Atmospheric helium three and radiocarbon from cosmic radiation, Physical Review 69 (11–12): 671–672.

[42] Kharfi F, Ketfi R (2018) Irradiated black pepper identification based on thermoluminescence of silicate minerals. Journal of Radioanalytical and Nuclear Chemistry 315:503–507

[43] Pilleyre T, Montret M, Fain J, Miallier D, Sanzelle S (1992) Attempts at dating ancient volcanoes using the red TL of quartz. Quaternary Science Reviews, 11: 13-17

[44] L. Leschi (1950), Djemila Antique CVICVL, OFALAC, France

[45] A. Eugène (1943) Une nouvelle basilique civile à Cuicul (Djemila). In: Comptes rendus des séances de l'Académie des Inscriptions et Belles-Lettres, 87e année, 3 : 376-386.

[46] Manual of Councils of the Holy Catholic Church -Rev. Edward H, Landon. M.A. https://www.ecatholic2000.com/councils2/untitled-06.shtml. Accessed 5 September 2019

CONCLUSIONS

Conclusions

In this thesis project, the conclusions we would like to formulate concerns three essential points.

First of all, it was well demonstrated that quartz separation procedure must accurately be fulfilled in order to get suitable amount of quartz in terms of purity and grain-sizes for the used thermoluminescence dating method. OSL and TL signals reading must also be performed under specific reading conditions in terms of heating, lighting and controlling atmosphere. The adjustment of the photo-multiplier is also primordial to get suitable TL and OSL signals. Accurate determination of the luminescence signals is essential and closely related to the sample preparation. Thus, the best sample preparation technique, and TL and OSL signals reading were identified allowing the determination of an accurate paleodose.

Secondly, a first scientific study was conducted on the famous archaeological site of *Cuicul* (Djémila) for dating and construction materials origin detemination purposes. The results obtained indicate that the used TL technique is a very suitable dating method, particularly, when samples are well prepared, the supralinearity TL growth is achieved and all correction on dose and TL signal are considered. The fabrication date of studied brick is in good agreement with the known construction phases and the history of *Cuicul* and the *Caracalla* arch reported by many archaeologists and historians. The XRF analysis of the construction materials taken from different clay's deposit sites demonstrates that only one type of clay is close in composition to the terra-cotta of the dated brick and is therfore suitable for its fabrication regarding its characteristics. Indeed, the composition of the used clay was found very suitable for the fabrication of a good quality brick in terms of mechanical properties. This result allowed us to suppose that Roman builders did some simple tests on the construction materials for the selection of the most suitable one. Thus, the results obtained in the framework of this work are very promising and will certainly contribute to put some of the *Cuicul* remains in their real chronological context. These results have, in fact, served to formulate some hypotheses on the manufacture technique as well as the provenance of the construction materials.

Finally, a timeline map was establsihed presenting construction dates of the major parts of *Cuicul* (Djémila) roman city by thermoluminescence technique. Accurtate construction dates were obtained through the optimization of the different dating steps strating from bricks selection and quartz separation until TL signal reading and TL growth curves establisment. By ensuring the supralinearity of TL growth curves and also by perfoming all the necessary

corrections on dose, the determined ages and dates were with acceptable standards deviations. The strategy of dividing the site into different zones was carefully carried out on the basis of topographical observations and by consulting expert archaeologists. The importance of this study is related to fact that it was made possible to place the different phases of *Cuicul* construction in a scientifically proven chronological order. This will certainly allow archaeologists and histoirians to confirm or to reject certain hypothesis in relation with the construction of certain buildings and with the whole development of the city between the first and fifth centuries.

Articles

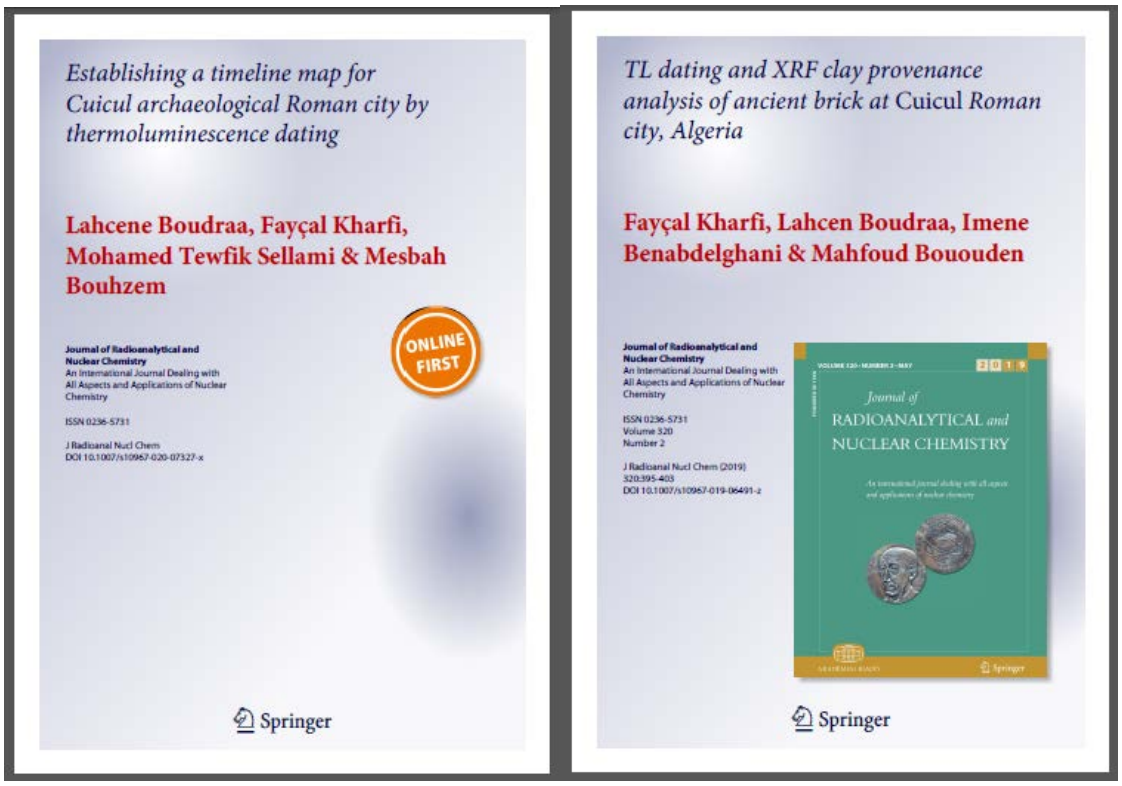

Establishing a timeline map for Cuicul archaeological Roman city by thermoluminescence dating

Lahcene Boudraa, Fayçal Kharfi, Mohamed Tewfik Sellami & Mesbah Bouhzem

ONLINE FIRST

Journal of Radioanalytical and Nuclear Chemistry
An International Journal Dealing with All Aspects and Applications of Nuclear Chemistry

ISSN 0236-5731

J Radioanal Nucl Chem
DOI 10.1007/s10967-020-07327-x

Springer

TL dating and XRF clay provenance analysis of ancient brick at Cuicul *Roman city, Algeria*

Fayçal Kharfi, Lahcen Boudraa, Imene Benabdelghani & Mahfoud Bououden

Journal of Radioanalytical and Nuclear Chemistry
An International Journal Dealing with All Aspects and Applications of Nuclear Chemistry

ISSN 0236-5731
Volume 320
Number 2

J Radioanal Nucl Chem (2019)
320:395-403
DOI 10.1007/s10967-019-06491-z

Journal of RADIOANALYTICAL and NUCLEAR CHEMISTRY

Springer

TL dating and XRF clay provenance analysis of ancient brick at Cuicul *Roman city, Algeria*

Fayçal Kharfi, Lahcen Boudraa, Imene Benabdelghani & Mahfoud Bououden

Journal of Radioanalytical and Nuclear Chemistry
An International Journal Dealing with All Aspects and Applications of Nuclear Chemistry

ISSN 0236-5731
Volume 320
Number 2

J Radioanal Nucl Chem (2019)
320:395-403
DOI 10.1007/s10967-019-06491-z

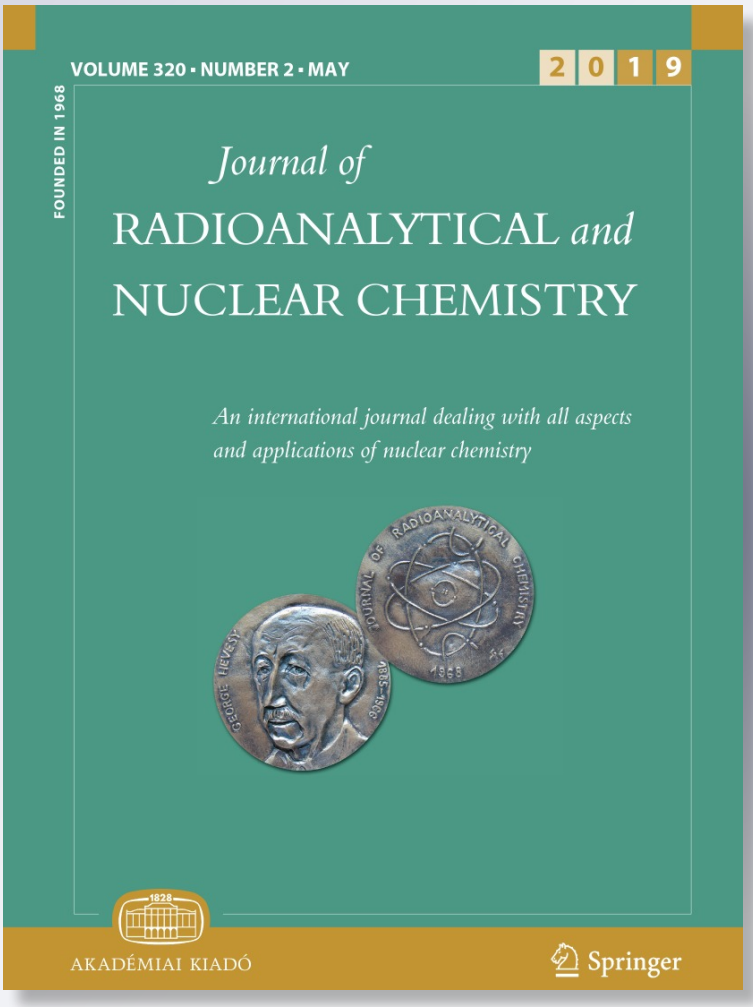

Springer

Journal of Radioanalytical and Nuclear Chemistry (2019) 320:395–403
https://doi.org/10.1007/s10967-019-06491-z

TL dating and XRF clay provenance analysis of ancient brick at *Cuicul* Roman city, Algeria

Fayçal Kharfi[1,2] · Lahcen Boudraa[1,2,3] · Imene Benabdelghani[1] · Mahfoud Bououden[4]

Received: 1 January 2019 / Published online: 26 March 2019

Abstract
In this work, a terra-cotta brick collected from the famous archaeological Roman city *Cuicul*, Algeria, was successfully dated by thermoluminescence. The provenance of the fabrication material was also identified by X-ray fluorescence analysis (XRF). The results obtained show that the brick was probably made in 198 A.D. This date is in good agreement with the history of the dated site and the neighborhood *Caracalla* arch edified in honour to *Caracalla* emperor (211–217 A.D.). The XRF study demonstrates that the raw clay used for the fabrication of the brick is local and well selected by the Roman builders.

Keywords Cuicul · Archaeological dating · Thermoluminescence · Material provenance · X-ray fluorescence

Introduction

Cuilcul is a famous Roman city situated 50 km at the north-east of Setif, Algeria. This ancient city was classified by the UNESCO as world heritage centre in 1982 [1, 2]. *Cuicul* was a colony of Roman veterans built on uneven ground. It is one of the most important Roman cities since the end of the 2nd century A.D., during the reign of Emperor *Nerva* (96–98). The colony of *Cuicul* was built and developed during approximately three centuries around a forum surrounded by public buildings such as the municipal *curia*, the *capitol*, the *judicial basilica* for justice and stock exchange transactions and the *Cosinius* brothers market with its eighteen shops. At the beginning of the third century, it overflowed its ramparts by the creation of the *Septimius Severus* temple, the *Caracalla* arch (211–217 A.D.), the market and the *civil basilica*. Although the historical development of the city has been described by several authors [3–5], no scientific study has been conducted on the site. Spectrometric analysis and archaeological dating using scientific methods are very powerful and more than necessary tools to place all cultural and archaeological vestiges and objects in their real historical context and to avoid any controversy regarding their origin. This work is a contribution aiming the scientific reconstruction of *Cuicul* history by dating a terra-cotta brick and the study of its fabrication material origin. Thus, the TL technique was used for the terra cotta brick dating by and the XRF for clay provenance identification.

✉ Fayçal Kharfi
kharfifaycal@yahoo.com

1 Department of Physics, University of Ferhat Abbas-Setif 1, Campus El-Bèz, 19000 Setif, Algeria

2 Laboratory of Dosing, Analysis and Characterization with High Resolution (DAC), Campus El-Bèz, 19000 Setif, Algeria

3 Nuclear Research Centre of Birine, Birine, Algeria

4 National Public Museum of Setif, Setif, Algeria

Theory

Thermoluminescence dating

Thermoluminescence dating was originally developed by Aitken [6], and Zimmermann and Huxtable [7]. It is a technique widely used in archaeological dating [8–13]. Thermoluminescence is based on the thermal stimulated emission of light from an insulator or a semiconductor following the previous absorption of energy from ionizing radiation. In archaeological dating, TL is used for the determination of the paleodose (D) stocked in the dated artefact through the determination of the equivalent beta dose (ED_β) by additional and artificial exposure to β doses. Indeed, by TL dating, the age of a dated artefact is given by the following formula Eq. (1).

$$Age(y) = \frac{D(Gy)}{D_a(Gy/y)}, \quad (1)$$

where D is the archaeological dose (Paleodose) and D_a is the total annual dose.

The main steps of the dating experimental procedure are the following:

1. Identification of the suitable protocol for measuring the archaeological dose by thermoluminescence,
2. Preparation of the samples,
3. Plateau dose test,
4. TL signals acquisition
5. Archaeological dose determination,
6. Determination of the effective alpha contribution k_α,
7. Measurement of the main radionuclides (U, Th, K) mass fractions in terra-cotta,
8. Study of the radiochemical homogeneity of terra-cotta: microdosimetry considerations,
9. Determination of the annual irradiation dose.

Clay provenance study

Because of the spread availability of clays in nature around cities, it is acceptable to consider that the chemical composition of the brick (terra-cotta) is a good indicator of their provenance. Thus, the comparison between the chemical composition of the terra-cotta of the dated brick and those of certain clay deposit sites allows the determination of which site is the most probable of the clay provenance. In this work, XRF analysis was conducted to compare the chemical oxides compositions of the clay samples collected around the archaeological site with the dated brick's terra-cotta in order to identify the provenance of the construction material. In the followed comparison procedure, oxydes like Na_2O, P_2O_5, and CaO were excluded from the comparison to avoid to consider the contamination and some components elmination due to the fabrication and the archealogical preservation of the brick such as firing conditions, moisture and organic material contents. Thus, the average relative difference in oxides (Δ) and the independent samples student t test (t) for bilateral distribution were considered for this comparison. Δ and t were calculated by the following formulas:

$$\Delta = \frac{\sum_{i=1}^{n} \frac{C_{ox(i)}(brick) - C_{ox(i)}(clay)}{C_{ox(i)}(brick)}}{n}, \tag{2}$$

$$t = \frac{\bar{C}_{clay} - \bar{C}_{brick}}{\sqrt{\frac{S^2}{n}}}, \tag{3}$$

$$S^2 = \frac{\sum_{i=1}^{n} (C_{ox(i)}(clay) - \bar{C}_{clay})^2 - (C_{ox(i)}(brick) - \bar{C}_{brick})^2}{2n-2}, \tag{4}$$

where $C_{ox(i)}(brick)$ is the content of the oxyde i in the brick's terra-cotta, $C_{ox(i)}(clay)$ is the content of the oxyde i in any given clay, $\bar{C}_{clay}$ is the average oxide content in the clay, $\bar{C}_{brick}$ is the average oxide content in the brick, and n is the number of considered oxides. The collected clays came from three (3) different deposit sites around the archaeological city *Cuicul*.

Experimental

Dated brick collection

In this work, a terra-cotta brick fragment taken from a separation wall located at approximately 25 m (east) from the *Caracalla* arch of *Cuicul* Roman archaeological city was dated by TL technique (Fig. 1).

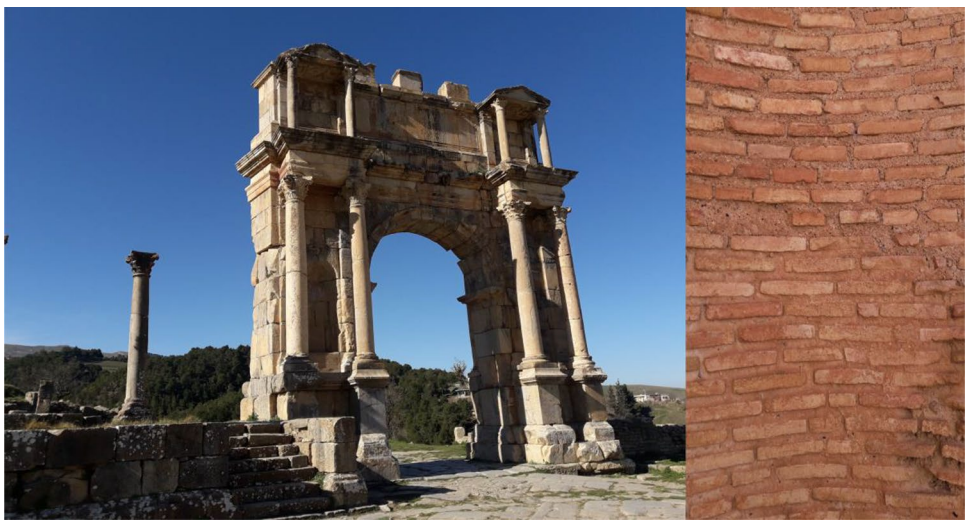

Fig. 1 The *Caracalla* arch and the separation wall of the dated brick

Fig. 2 Google map photo showing the dated site (white circle) and the localizations of the identified clay provenance deposit sites (S01, S02 and S03)

Table 1 Necessary geographic and burial data for cosmic dose

Site	Geographic Coordinates and burial depth of the brick	
Cuicul (Djémila), Setif, Algeria	Latitude	36.3°
	Longitude	5.7°
	Altitude	900 m
	Burial depth	0 m

The local clay materials used for the fabrication of the dated brick were possibly collected from the neighbourhood of *Cuicul* archaeological city. In order to confirm if local construction material was used and from which deposit site it was probably collected, we have first identified all the old clay' deposit sites around the city (Fig. 2), and then we have analyzed the clay's composition by XRF. The different clays compositions were then compared to the terra-cotta composition of the dated brick.

The necessary geographic coordinates of the archaeological site and the burial depth of the dated brick requested for cosmic dose determination are presented in Table 1.

Determination of the paleodose

For the terra-cotta, the paleodose dose is stocked in many minerals mainly the quartz and feldspar. Natural TL in quartz results from continuous exposure to nuclear radiation from uranium and thorium impurities within the sample itself, from uranium and thorium in distant grains, from potassium and from cosmic radiation. In this work, a mixed additive and regeneration method similar to that described by Sanzelle et al. [14] is used. This method is based on TL multi-aliquots additive dose standard protocol (MAAD) and fine grains technique [15, 16]. The Paleodose dose was determined by measuring on several identical treated aliquots in terms of mineral phase separation (quartz), separated grains size and deposited quantity on each disk, the TL signals of natural plus artificial beta doses (1st glows) and the TL signals for different only additive beta doses after natural TL removing (2nd glows). To ensure that all aliquots are identical, the normalization procedures described by Jain et al. [17] and Richter [18] were followed. The considered normalization procedures were the weight normalization (WN) and the glow growth curves matching by the observation if the two curves match well when one of the two curves is shifted towards the other. The measurement protocol was also optimized in terms of errors and checked in terms of extrapolation procedures according to Felix and Singhvi review [19]. Thus, on the obtained line back to the abscissa axis representing dose yields the equivalent beta dose (ED_β). The natural TL growth curve was also measured from the origin using the same samples (2nd glows) and the supralinearity intercept, I, is then determined. The Paleodose is then taken to be equal to the sum of the absolute values of ED_β and I by assuming that the measured 2nd glow growth curve is identical to the natural glow growth curve. This assumption was experimentally checked in many thermoluminescence dating works. Indeed, many dating experiences showed that the intercept, I, does not generally change between 1st and 2nd glows, particularly if the 1st and 2nd glows slopes are parallel in the linear region (above the supralinear knee) such as our case [16–20]. In the used method, TL measurements were made on a number of separated quartz grains deposited on many TL reading stainless steel disks. Two sets of disks were necessary: the first set is used for the natural plus additive β doses TL signal reading (1st glow) and the second set for TL signal reading due to different β doses after natural signal removing (2nd glow). The difference between the two obtained TL growth curves must be uniform and gives the paleodose. In this method it is assumed that the dating clock was set to zero at the time of the brick's baking.

For the sample preparation, the outer layers were removed by 2 mm, then the sample was crushed and sieved and the fraction below 40 µm was selected. Next, the following, etching procedures were performed: 10% (v/v) HCl for 1 h to remove the carbonate, 10% (v/v) H_2O_2 for 48 h to remove the organic component, 1% (v/v) HF for 1 h to remove clay and 10% (v/v) HCl for 30 min to eliminate fluorosilicates that had possibly formed. Through a time controlling grain sedimentation procedure in acetone (~0.8 g/cm^3), polymineral fine grains fraction in the range of 1–8 µm were separated and then deposited onto stainless steel disks.

Table 2 Conditions of TL signals reading

Luminescence reading mode	Thermoluminescence
Maximum reading temperature	450 °C
Heating rate	5 °C/s
Preheating	230°/10 s
TL signal sampling	250 points over the range 0–450 °C
Analyzed sample weight	2 mg
Regeneration	2 h at 450 °C

The necessary artificial thermoluminescence signals were induced by the ^{90}Sr–^{90}Y calibrated beta source integrated in the Risø system delivering 0.1 Gy/s. A plateau test was also performed in order to determine the temperature interval where the TL signal must be considered. In this test two aliquots of the quartz grains are TL tested, one after additional exposure to beta dose and the other one without additional exposure. Ratio of the two TL curves obtained should provide a plateau in the TL range.

In this work, the RisøTL/OSL-DA-20 luminescence reader was used [21]. The TL signals were all collected under the same experimental conditions presented in Table 2.

Determination of the annual dose

The annual dose, D_a, is the natural radioactivity contribution in TL essentially of by the nuclear radiation from Potassium ^{40}K(β and γ emitter),Thorium(α-emitter), and Uranium (α-emitter) plus its additional β and γ radiation which is emitted along the decay chains. Minor contributions yield from rubidium contamination (β-emitter) and cosmic radiation. It is expressed according to the relation: $D_a = k_\alpha D_\alpha + D_\beta + D_\gamma + I_{cosmic}$. Thus, the annual dose rate was calculated from the activity and the mass fractions of the relevant α, β, and γ emitting radionuclides which have been determined by γ-spectrometry. The natural radionuclides providing the annual dose have very long half-lives and therefore the annual dose rate is assumed to be constant. Generally, when considering the fine grain protocol of Zimmerman, such as our case, the alpha particles do not have the same efficiency to contribute to the annual dose. This is why some studied aliquots were also exposed to different alpha doses (3, 6, and 12 Gy) delivered by a calibrated ^{241}Am alpha source (45 mGy/s) for the determination of the effective alpha contribution k_α. k_α is determined as a ration of the equivalent beta dose (ED_β) to the equivalent alpha dose (ED_α). The equivalent alpha dose was determined by the same manner as the equivalent beta dose. The annual α, β, and γ corrected doses were calculated by the following expressions [16, 22–26].

$$D_\beta = q(1-h)\left[0.146 \times 0.940 \times \mu_U \times C(U) + 0.273 \times 0.915 \times \mu_{Th} \times C(Th) + 0.649 \times \mu_{K_2O} \times C\left(K_2O\right)\right], \quad (5)$$

Table 3 The attenuation factors μ_i of the β outer dose

μ_U	μ_{Th}	μ_{K2O}
0.83	0.77	0.91

$$D_\gamma = q(1-h)\left[0.113 \times C(U) + 0.0476 \times C(Th) + 0.202 \times C\left(K_2O\right)\right], \quad (6)$$

$$D_\alpha = k_\alpha[2.78 \times C(U) + 0.732 \times C(Th)], \quad (7)$$

where $C(x)$ are the mass fraction expressed in mg kg^{-1} for Uranium (U) and Thorium (Th) and in % for K_2O, h is the relative water content, k_α is the effective alpha contribution obtained by comparing TL produced per unit of beta and alpha doses. The used attenuation factors μ_x of the β outer dose corresponding to the grain size interval of the dated brick varying, by microscopy observation, from 200 µm–315 µm are given in Table 3 [25].

q is a correction factor that takes into account the fact that requested doses for age calculation are those delivered to the quartz and not to whole sample matrix and is given by:

$$q = \frac{LET_{av}(Quartz)}{LET_{av}(Humid\ matrix)} = \frac{LET_{av}\left(SiO_2\right)}{\sum_i \rho_i LET_{av}(i)}, \quad (8)$$

where LET_{av} is the average linear energy transfer, ρ_i is the mass fraction of any given oxide i in the matrix.

The experimental procedure for determining the relative water content h of the sample is as follows: a portion of the raw sample is weighed, and then it is put in the oven at 110 °C until full dry. This portion is then weighted again. By convention, water that is removed at 110 °C is called free water. h is then obtained by taking the weight ratio of the free water and the same sample before drying.

The determination of the annual dose rate requests the determination of the Uranium-238 (^{238}U), the Thorium-232 (^{232}U) and Potassium-40 (^{40}K) mass fractions in the matrix (terra-cotta) and the main oxides weight fractions in the sample. High resolution gamma spectrometry was used to determine the radionuclides mass fractions in the matrix in which the quartz grains were separated. A brick sample (powder) of 10 g of weight was dried at 110 °C for 20 h and crushed to less than 100 µm and then packaged in an airtight PETP (Polyethylene Terephthalate) tube. This material prevents losses of Radon (^{222}Rn), element of short half life (3.8 days), and thus guarantees γ spectrometric measurements under secular equilibrium conditions. A delay of 15 days is respected between the setting in tube and the measurement in order to ensure the radioactive equilibrium between this gas and its descendants. The detector containing the sample was placed in a lead

enclosure with low activity to reduce the count of γ-rays in the environment. The γ-photons produced during the decay of the U, Th and K elements are detected by a Canberra High-Purity Germanium (HPGe) well detector with a relative efficiency of 40%. The determination of the mass fractions of the different radionuclides is carried out by comparing the intensities of the lines with those obtained for standards. The gamma spectrometer thus makes it possible to separately obtain the uranium, thorium and potassium contents of our brick sample.

Cosmic dose varies with longitude, latitude, altitude and burial depth and was calculated using the equations given by Prescott and Hutton [27]. In-situ annual dose rate was also determinate by the use of three TLD-200 (CaF_2: Dy) dosimeters positioned inside the wall for 6 month and at the exact position from where the dated brick was taken. The TLDs were covered by the remaining brick fragments not used for TL signal reading in order to reproduce the same exposure conditions.

Determination of clay and terra-cotta chemical composition

In this work, a Rigaku ZSX primus wave diffractive X-ray Fluorescence spectrometer was used for the elemental analysis of the sample and thus the determination of the mass fraction of the main oxides. Thus, after a drying phase at 100 °C for 24 h, the samples were ground and screened at ~ 50 µm. To analyze powder samples, the briquette method was used, in which the obtained powder is pressed at 200 kilonewtons to make a disk which is suitable for the undertaken XRF analysis (Fig. 3).

Results and discussion

The ED_α and I values of the dated brick were determined using TL measurements. Three fragments of the same brick were separately used for the separation of quartz grains and the establishment of the necessary glow growth curves for the determination of the paleodose. From each fragment, 18 aliquots were prepared and grouped into six groups for measuring the necessary TL signals. Two (2) additional aliquots were used for the plateau test. Established glow growth curves of the first fragment (Frag.1) were found as the most suitable for the paleodose determination in terms of minimum error, supralinearity and parallel growth of the two glow curves. The necessary collected TL signals of Frag.1 corresponding to natural plus beta doses (1st glow) and corresponding to only beta doses (2nd glow) with additive beta doses varying from 2 to 12 Gy are given in triplicate aliquots in Figs. 4 and 5. The plateau dose was also checked by the comparison of TL curves due the paleodose and to an additive beta dose of 6 Gy and shows that TL signals must be considered within the interval 265 °C–365 °C.

On the basis of the TL signals obtained, the dose response curves were then established allowing the determination of the equivalent dose (ED_β) and the dose intercept (I) (Fig. 6).

From results presented in Fig. 6, the paleodose was determined as 6.48 ± 0.20 Gy. The X-ray fluorescence analysis

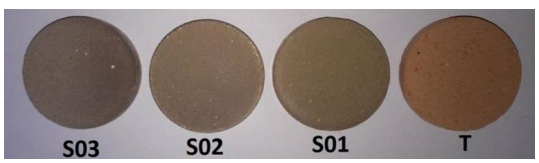

Fig. 3 Prepared XRF samples of the brick's terra-cotta (T) and collected clays (S01, S02 and S03)

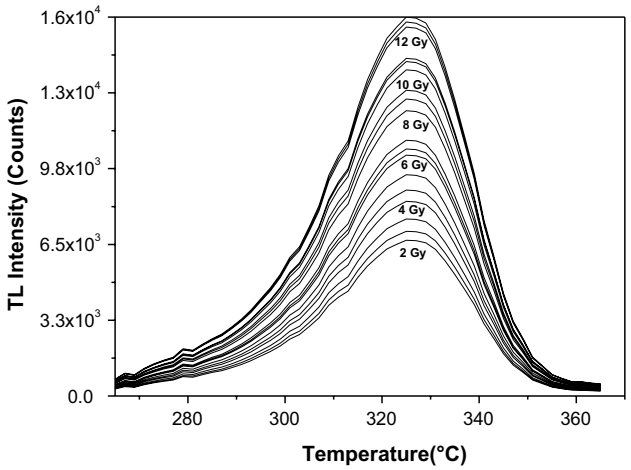

Fig. 4 TL signals induced by natural plus additive beta doses (1st glow)

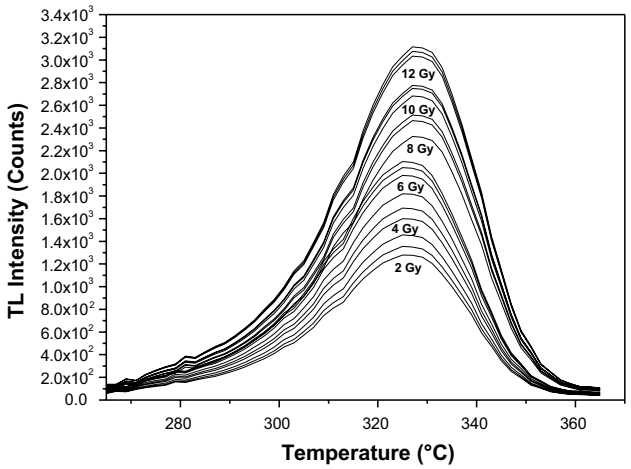

Fig. 5 TL Signals induced by additive beta doses only (2nd glow)

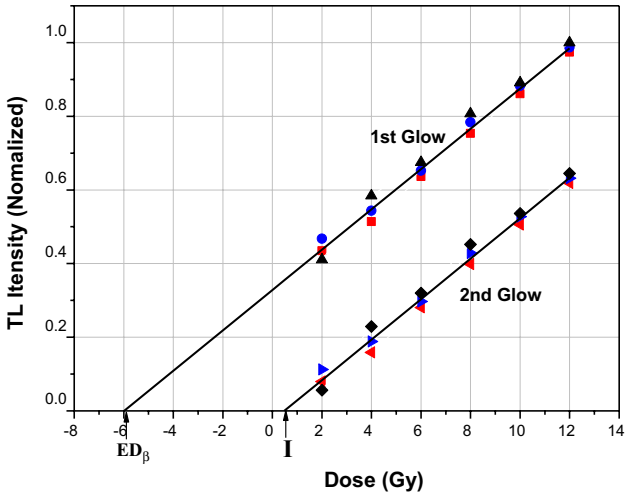

Fig. 6 Requested TL growth curves as a function of dose allowing the determination of the equivalent dose (ED_β) and the intercept dose (I) and therefore the paleodose ($ED_\beta + I$)

data requested for the determination of the annual dose are presented in Table 4. *LET* data are taken from Ref. [28].

The determined equivalent alpha dose (ED_α) is 58.72 Gy. Thus, k_α-value, which is the ration between the ED_β (5.99 ± 0.20 Gy) and the ED_α (58.72 ± 6.80 Gy), was calculated as 0.102 ± 0.015 (~0.1). Because the brick fragment is found on the ground (burial depth equal to 0 m) and because some radioisotopes mass fractions are very low, the contributions of ^{226}Ra, ^{222}Rn and ^{87}Rb in the annual dose were considered as negligible. The mass fractions of ^{238}U and ^{232}Th measured by γ spectrometry are presented in Table 5 with the main used factors and the corresponding specific and total annual doses.

From the above obtained data on paleodose and annual dose resumed in Table 6, the age and thus the fabrication date of the studied brick were estimated. A value of the age of 1820 ± 127 years was found dating back the fabrication of the brick to the year 198 A.D.

The dated brick was taken from a separation double-walled brick wall. The wall location is almost 25 meters at the east of the *Caracalla* arch overlooking the southern forum. The construction period of the *Caracalla* arch is known by the emperor *Caracalla* titulature: 211–217 A.D. Given the proximity of the wall to the arch of *Caracalla*, it is possible to assume that the wall was built during the same period as the arch. According to the epigraphic table (Fig. 7), the arch was erected probably in 217 in honour of the Emperor *Caracalla*, his mother *Julia Domna* and his deceased father *Septimius Severus* [29]. Thus, the determined date by TL method gives satisfaction because it fits well in the historical context of the construction period and is conform to the development of the city. As the text is very discreet about the event which is at the origin of the

Table 4 X-ray fluorescence analysis results and used *LET*s for *q* factor calculation

Element	SiO_2	Al_2O_3	Fe_2O_3	CaO	MgO	Na_2O	K_2O	P_2O_5	TiO_2	MnO	H_2O^a
Mass fraction (%)	54.30 ± 0.03	14.07 ± 0.02	6.16 ± 0.01	5.97 ± 0.01	3.18 ± 0.02	1.44 ± 0.02	1.85 ± 0.005	0.28 ± 0.004	0.74 ± 0.02	0.05 ± 0.005	11.96 ± 0.02
$LET_{av}(i)$ (MeV.g^{-1} cm^{-2})	1.71	1.67	1.54	1.66	1.70	1.65	1.61	1.69	1.58	1.50	2.03

[a]Calculated mass fraction

Table 5 γ-spectrometry analysis results, correction factors and annual doses

	U	Th	K_2O[a]
Mass fraction and concentration	2.24 ± 0.08 mg kg^{-1}	8.00 ± 0.20 mg kg^{-1}	1.85 ± 0.05%
h	0.12		
q	1		
$q(1-h)$	0.88		
Specific annual Dose (mGy/y)	1.07 ± 0.02	2.49 ± 0.02	0.013 ± 0.001
Total annual dose (mGy/y)	3.57 ± 0.05		

[a]The concentration of ^{40}K is 0.01167% in natural Potassium K

Table 6 Measured Paleodose, annual dose and the corresponding age

Sample	Frag.1[a]	Frag.2	Frag.3
Paleodose (Gy)	**6.48 ± 0.20**	6.57 ± 0.75	6.42 ± 0.87
Cosmic dose rate (calculated)	0.34 ± 0.02 mGy/y		
Annual α, β and γ dose	3.57 ± 0.05 mGy/y		
Total environmental annual dose	3.91 ± 0.07 mGy/y		
In-situ average annual dose measured by TLD-200	3.21 ± 0.20 mGy/y		
Average annual dose	3.56 ± 0.14 mGy/y		
Age (year)	**1820 ± 127**	1822 ± 21(SD[b])	

[a]The best in terms of minimum error glow growth curves quality (parallel growth and supralinearity)

[b]Standard deviation

Fig. 7 The epigraphic table of the Caracala arch of *Cuicul* Roman city

Table 7 XRF analysis and comparison between clays of the studied three deposit sites and the brick terra-cotta

Oxyde		SiO_2	Al_2O_3	Fe_2O_3	CaO	MgO	Na_2O	K_2O	P_2O_5	TiO_2	MnO
Mass fraction (%)		Terra-Cotta of the dated brick									
		54.30	14.07	6.16	5.97	3.18	1.44	1.85	0.28	0.74	0.05
		Clays from deposit sites									
	S01	55.50	16.90	7.67	12.10	1.79	0.18	1.15	0.37	1.02	0.04
	Δ	0.26 ± 0.14					*t* test	0.36			
	S02	47.90	19.10	8.72	19.90	1.58	0.47	1.71	0.26	0.99	0.04
	Δ	0.29 ± 0.16					*t* test	0.97			
	S03	46.40	19.10	8.96	20.60	1.31	0.36	1.50	0.33	0.99	0.04
	Δ	0.32 ± 0.16					*t* test	0.85			

construction, it remains to suppose an intervention of the municipality in relation with the great works undertaken during this period for the development of the southern forum and on the juxtaposing constructions like the wall from which the brick's fragment is taken.

The XRF analysis results and the comparison results of the clay materials taken from the three considered deposit sites around the city are presented in Table 7.

From the obtained XRF results, it is obvious that S01 is close in composition to the terra-cotta of the dated brick.

Thus, the dated brick material comes from S01 although it is relatively difficult to access. The S01 clay is essentially a silicon-aluminous one with lower carbonates contents. The brick fabricated from this clay sintered generallly at 900 °C and is of good quality regarding the technical properties actually required in the manufacture of terra-cotta products [30]. Thus, it is possible that Roman builders did some simple tests on the brick in order to select the most suitable clay to be used. Thus, we can assume that the Roman construction knowledge was not limited in the architecture aspect but it was possibly extended to some construction material selection mastering. These assumptions have to be confirmed by further investigations and multidisciplinary studies.

Conclusions

In this work, a first scientific study was conducted on the famous archaeological site of *Cuicul* (Djémila) for dating and construction materials origin detemination purposes. This site has been included in the UNESCO list of World Heritage Sites since 1982. The results presented in this work indicate that the used TL technique is a suitable dating method, particularly, when samples are well prepared, the supralinearity TL growth is achieved and all correction on dose and TL signal are considered. The fabrication date of studied brick is in good agreement with the known construction phases and the history of *Cuicul* and the *Caracalla* arch reported by many archaeologists and historians [3–6, 29]. The XRF analysis of the construction materials taken from different clay's deposit sites demonstrates that only S01 clay is close in composition to the terra-cotta of the dated brick and is suitable for its fabrication regarding its characteristics. Indeed, the composition of the used clay was found very suitable for the fabrication of a good quality brick in terms of mechanical properties. This result allows us to suppose that Roman builders did some simple tests on the construction materials for the selection of the most suitable one. In conclusion, the results obtained in the framework of this work are very promising and will certainly contribute to put some of the *Cuicul* remains in their real chronological context. These results have, in fact, served to formulate some hypotheses on the manufacture technique as well as the provenance of the construction materials.

References

1. https://whc.unesco.org/fr/list/191. Accessed 19 March 2018
2. UNESCO (2000) Roman Art in Africa, World Heritage N°16
3. Akli Ikherbane M (2003) Le site archéologique de Djemila, l'antique *Cuicul*: Éventail d'actions possibles. Les Dossiers d'archéologie (Dijon) A286:26–31
4. Allais Y (1953) Le quartier à l'Est du Forum des Sévères. Revue Africaine XCVII:48–65
5. Allais Y (1971) Le quartier Occidental de Djemila (Cuicul). Antiquités Africaines 5:95–119
6. Aitken MJ (1970) Dating by archaeomagnetic and thermoluminescent methods. Philos Trans R Soc Lond Ser A 269(1193):77–88
7. Zimmerman DW, Huxtable J (1969) Recent applications and developments in thermoluminescent dating. Archaeometry 11:105–108
8. Veronese I, Goksu HY, Schwenk P, Herzig F (2008) Thermoluminescence dating of a mikveh in Ichenhausen, Germany. J Environ Radioact 99:621–630
9. Kondopoulou D, Aidona E, Ioannidis N, Polymeris GS, Tsolakis S (2015) Archaeomagnetic study and thermoluminescence dating of Protobyzantine kilns (Megali Kypsa, North Greece). J Archaeol Sci Rep 2:156–168
10. Yeea KP, Mob RH (2018) Thermoluminescence dating of stalactitic calcite from the early Palaeolithic occupation at Tongamdong site. J Archaeol Sci Rep 19:405–410
11. Sears DWG, Sears H, Sehlke A, Hughes SS (2018) Induced thermoluminescence as a method for dating recent volcanism: Hawaii County, Hawaii, USA. J Volcanol Geoth Res 349:74–82
12. Sabtu SN (2015) Thermoluminescence dating analysis at the site of an ancient brick structure at Pengkalan Bujang, Malaysia. Appl Radiat Isot 105:182–187
13. Temaa E, Polymerisc G, Moralesd J, Goguitchaichvilid A, Tsaknakie V (2015) Dating of ancient kilns: a combined archaeomagnetic and thermoluminescence analysis applied to a brick workshop at Kato Achaia, Greece. J Cult Herit 16:496–507
14. Sanzelle S, Miallier D, Pilleyre T, Faïn J, Montret M (1996) A new slide technique for regressing TL/ESR dose response curves. Radiat Meas 26:631–638
15. Aitken MJ (1974) Physics and archaeology. Clarendon Press, Oxford, pp 26–84
16. Zimmerman DW (1971) Thermoluminescent dating using fine grains from pottery. Archaeometry 13:29–52
17. Jain M, Booetten-Jensen L, Singhvi AK (2003) Dose evaluation using multiple aliquot quartz OSL: test of methods and new protocol for improved accuracy and precision. Radiat Meas 37:67–80
18. Richter D (2007) Advantages and limitations of thermoluminescence dating of heated flint from paleolithic sites. Geoarchaeology 22(6):671–683
19. Felix C, Singhvi AK (1997) Study of non-linear luminescence-dose growth curves for the estimation of paleodose in luminescence dating: results of Monte Carlo simulations. Radiat Meas 27:599
20. Fleming SJ (1970) Thermoluminescent dating: refinement of quartz inclusion method. Archaeometry 12(2):133–146
21. Kharfi F, Ketfi R (2018) Irradiated black pepper identification based on thermoluminescence of silicate minerals. J Radioanal Nucl Chem 315:503–507
22. Aitken MJ (1985) Thermoluminescence dating. Academic Press, London
23. Mejdahl V (1979) Thermoluminescence dating: beta dose attenuation in quartz grains. Archaeometry 21:61–72
24. Mejdahl V (1987) Internal radioactivity in quartz and feldspar grains. Ancient TL 5(2):10–17
25. Pilleyre T(1991) Datation par thermoluminescence: application à la chronologie des retombées volcaniques. Thèse de doctorat de l'université Blaise Pascal—Clermont II, Clermont-Ferrand, France
26. Bassinet C (2007) Datation par luminescence : recherches méthodologiques et applications au volcanisme dans l'environnement de Laschamp. Thèse de doctorat de l'université Blaise Pascal- Clermont-Ferrand II, Françe
27. Prescott JR, Hutton JT (1994) Cosmic ray contributions to dose rates for luminescence and ESR dating: large depths and long-term time variations. Radiat Meas 23:497–500

28. Pilleyre T, Montret M, Fain J, Miallier D, Sanzelle S (1992) Attempts at dating ancient volcanoes using the red TL of quartz. Quat Sci Rev 11:13–17
29. Leydier-Bareil AM (2006) Les arcs de triomphe dédiés à *Caracalla* en Afrique romaine. Doctorat histoire de l'art et archéologie, Université de Nancy 2, France. LN006/26-2 bis
30. Lourenço PB, Fernandes FM, Castro F (2010) Handmade clay bricks: chemical, physical and mechanical properties. Int J Archit Herit. https://doi.org/10.1080/15583050902871092

Establishing a timeline map for Cuicul archaeological Roman city by thermoluminescence dating

Lahcene Boudraa, Fayçal Kharfi, Mohamed Tewfik Sellami & Mesbah Bouhzem

Journal of Radioanalytical and Nuclear Chemistry
An International Journal Dealing with All Aspects and Applications of Nuclear Chemistry

ISSN 0236-5731

J Radioanal Nucl Chem
DOI 10.1007/s10967-020-07327-x

Springer

Journal of Radioanalytical and Nuclear Chemistry
https://doi.org/10.1007/s10967-020-07327-x

Establishing a timeline map for Cuicul archaeological Roman city by thermoluminescence dating

Lahcene Boudraa[1,2,3] · Fayçal Kharfi[1,2] · Mohamed Tewfik Sellami[4] · Mesbah Bouhzem[4]

Received: 2 December 2019

Abstract
In this work, a timeline map regarding the construction and the development of the archaeological Roman city *Cuicul*, Algeria, was established by thermoluminecence dating technique. The city was first subdivided into 10 main zones according to the observable architecture similarities and extensions. Already tested thermoluminescence dating procedure (Kharfi et al. in J Radioanal Nucl Chem 320:395–403, 2019) was used for the average age determination. The established timeline map fit well with the globally known history of the city and its development between the 1st and the 5th centuries except for the case of the great baths where an expectable date was determined (182 A.D.) which requires more studies.

Keywords Cuicul · Terra-cotta brick · X-ray fluorescence · Thermoluminescence dating · Timeline map

Introduction

Cuical is an ancient Roman city which was classified by the UNESCO as world heritage centre in 1982 [1, 2]. *Cuicul*, with its more than 500 years of history, is one of the most famous archaeological sites in Algeria. This Roman colony of veterans was founded on the site of an existing village already known as *Cuicul*. It was located in Numidia near the border with Mauretania Caesariensis. The first excavations at the site were undertaken in 1909 and the site has not revealed all these secrets so far as few scientific studies have been conducted on. In this work and after a successful thermoluminescence dating of a brick's wall near the Caracalla arch [3], a big project was conducted, just after this first achievement, aiming the reconstruction of an accurate timeline map of the whole city by the same dating technique. This project was conducted in four (4) major phases: (1) Historical study on the site, (2) site subdivision and dated terra-cotta bricks collection, (3) thermoluinescence dating, (4) data analysis and timeline map establishment. In the present work and in addition to thermolumienscence technique many others scientific techniques were used, such as X-ray fluorescence and γ-spectrometry, for the collection of requested dating data.

Theory

The known history of the city

The common and widely admitted hsitroy of *Cuicul* inform us that in 96 AD Emperor Nerva founded a Roman colony of veterans on the site of an existing village already known as *Cuicul* [4–6]. *Cuicul* is thus a Roman colony built and developed during approximately five centuries. The main buildings of *Cuicul* are a forum surrounded by public buildings such as the municipal curia, the capitol, the judicial basilica for justice and stock exchange transactions and the *Cosinius* brothers market with its eighteen shops. At the beginning of the third century, it overflowed its ramparts by the creation of the Septimius Severus temple, the Caracalla arch, the market and the civil basilica. At the beginng of the 4th century after the conversion of Rome to Christianity, many Christian neighborhoods with religious constructions were built under the reign of the Emperor Constantin. This was the case of *Cuicul* with a new extension toward the south

✉ Fayçal Kharfi
kharfifaycal@yahoo.com

1 Department of Physics, Ferhat Abbas-Setif1 University, Campus El-Bèz, 19000 Sétif, Algeria

2 Laboratory of Dosing, Analysis and Characterization in High Resolution (DAC), Campus El-Bèz, 19000 Sétif, Algeria

3 Nuclear Research Centre of Birine, 17200 Djelfa, Algeria

4 Djemila Archaeological Museum, 19000 Sétif, Algeria

Published online: 06 August 2020

carrying the new Christian character. Although the historical development of the city has been described by several authors [7–9], no scientific study has been conducted on the site. Indeed, the historical studies are not completed and not accurate in terms of accurate city construction chronology.

Brick fabrication and construction technique

Cuicul has known during the ancient period several construction phases. At the beginning the choice and the construction of the site were based on military considerations and then the city starting to be populated by the veteran soldiers and the civilians coming from different regions. Thus, the city lived an exemplary stability and was developed to become a small city with all the roman conveniences of the time. During the next Byzantine period many maintenance and restitution works were carried out. Several construction techniques were used in the construction of this city. Brick's samples dated in the framework of this work were collected from walls constructed by two different techniques. The first technique is the so-called *Opus Testaceum* and the second one is the *Opus mixtum* technique. In *Opus Testaceum* technique only terra-cotta bricks are used with a lime mortar. This technique has been used since the beginning of the 1st century and has gradually replaced other techniques, thanks to its strength and ease of use [10, 11]. The *Opus mixtum* is a technique of wall constrcution with both brick and stone facing. This techique became common in the 1st and 2nd centuries AC. In the *opus mixtum* technique, panels of shaped stones were separated by bands of brick facing. This technique saved on manpower and on bricks which were relatively expensive at the time. Finally, it is important to mention that brick is a reused construction material and therefore erroneous dating may come from the reutilization of bricks from older destroyed walls voluntary or because of earthquake [12–14].

Site subdivision and sampling strategy

By taking into consideration the possible modifications on the site due to restauration works as well as lootings by vandals and other invaders, an adequate city subdivision in urban area (zones) was carried out by targeting the existence of at least one building constructed with the *Opus Testaceum* or *Opus Testaceum* techniques and not seeming to undergo any modification. The city has been divided into 10 separated urban zones that have some similarities. The city subdivision was performed from the south to the north according to the observable architecture harmony and by making cross-checks with the historical texts although little informative on the exact period of construction (Fig. 1). The operation of brick's samples collection (Table 1) was conducted with the assistance of experienced archaeologists

Table 1 Site subdivision into main urban zones and collected brick samples with construction technique

Zone N°	Name	Sample no	Origin of the sample	Construction technique
1	Christian Street: Bishop house.	1A	Wall of the house of Bishop	*Opus Testaceum*
		1B	Wall of the house of Bishop	*Opus Testaceum*
		1C	Wall of the house of Bishop	*Opus Testaceum*
2	Christian Street: Church, Cathedral and Baptistery	2A	Wall of the Cresconius cathedral	*Opus Testaceum*
		2B	Crypt of the Cresconius cathedral	*Opus Testaceum*
		2C	Wall of the Church	*Opus Testaceum*
		2D	Foundation of Church	*Opus Testaceum*
		2F	Wall of the Church underground chamber	*Opus Testaceum*
		2 g	Walls of the Baptistery: east, south and west sides	*Opus Testaceum*
3	Christian Street: Houses	3A	Walls of a Christian neighbourhood house	*Opus Testaceum*
4	Bacchus House	4A	Walls of the house of Bacchus	*Opus Testaceum*
5	Great baths	5A	Walls of the baths	*Opus Testaceum*
6	Severian place	6A	Wall of civil basilica	*Opus Testaceum*
		6B	Wall near the Septum temple	*Opus Testaceum*
7	Eastern street	7A	Wall of the house with bath	*Opus Testaceum*
8	Top of the Cardo Maxium	8A	Wall of the house of Castorius	*Opus mixtum*
		8B	Wall of the house of the Donkey	*Opus mixtum*
		8C	Venus Genetrix Temple	*Opus mixtum*
9	Western street	9A	Christian basilica	*Opus mixtum*
10	Down of the Cardo Maximus:	10A	Cosinius market: east wall	*Opus mixtum*
		10B	Walls of the house of Europe	*Opus mixtum*

Fig. 1 Google map photo showing the dated site, subdivision zones and examples of walls from where dated bricks were taken

and museum's technicians to avoid samples selection from recent restored places.

Brick identification and comparison

The chemical composition of the brick (terra-cotta), particularly the oxides fraction (%) is a good indicator for their identification and comparison. Thus, the comparison between the chemical composition of the terra-cotta of the dated brick allows the determination the origin of the brick and if it was taken from another place and resued or not. In this work, XRF analysis was conducted to compare the chemical oxides compositions of the dated brick's terra-cotta collected from different places of the archaeological site for their classification. In the followed comparison procedure, oxides mass fraction was considered. Oxides mass fraction will be also used for the determination of q correction factor that takes into account the fact that requested doses for age calculation are those delivered to the quartz and not to whole sample matrix.

Thermoluminescence dating

Aitken, and Zimmermann are the most relevant works behind the discovery and the utilisation of the development of thermoluminescence dating [15, 16]. It is a technique widely used in archaeological dating [17–22]. In archaeological dating, thermoluminescence is used for the

determination of the paleodose (D) stocked in the dated artefact through the determination of the equivalent beta dose (ED_β) by additional and artificial exposure to β doses. The age of a dated artefact is given by the following formula Eq. (1).

$$Age(y) = \frac{D(Gy)}{D_a(Gy/y)}, \tag{1}$$

where D is the archaeological dose (Paleodose) and D_a is the total annual dose.

In this work the method is based on TL multi-aliquots additive dose standard protocol (MAAD) and fine grains technique [23, 24] is used. The Paleodose dose was determined by measuring the TL signals of natural plus artificial beta doses (1st glows) and the TL signals for different only additive beta doses after natural TL removing (2nd glows). From the obtained growth curves the equivalent beta dose (ED_β) and supralinearity intercept, I, ware determined allowing the determination of the Paleodose as their sum. TL measurements were made on sufficient quantity of separated quartz grains deposited on many TL reading stainless steel disks. The annual dose, D_a, is the natural radioactivity contribution in TL essentially calculated from the activity and the mass fractions of the relevant α, β, and γ emitting radionuclides which have been determined by γ-spectrometry and by minor contribution yield from cosmic radiation It is expressed according to the relation: $D_a = k_\alpha D_\alpha + D_\beta + D_\gamma + I_{cosmic}$. With the fine grain protocol of Zimmerman, used in this work, the alpha particles do not have the same efficiency to contribute to the annual dose. This is why some studied aliquots were also exposed to different alpha doses. The equivalent alpha dose was determined by the same manner as the equivalent beta dose. The annual α, β, and γ corrected doses were calculated by the following expressions [24–29].

$$\begin{aligned} D_\beta = q(1-h)\big[&0.146 \times 0.940 \times \mu_U \times C(U) \\ &+0.273 \times 0.915 \times \mu_{Th} \times C(Th) + 0.649 \times \mu_{K_2O} \\ &\times C\big(K_2O\big)\big], \end{aligned} \tag{2}$$

$$D_\gamma = q(1-h)\big[0.113 \times C(U) + 0.0476 \times C(Th) + 0.202 \times C\big(K_2O\big)\big], \tag{3}$$

$$D_\alpha = k_\alpha[2.78 \times C(U) + 0.732 \times C(Th)], \tag{4}$$

where $C(x)$ are the mass fraction expressed in mg kg^{-1} for Uranium (U) and Thorium (Th) and in % for K_2O, h is the relative water content, k_α is the effective alpha contribution obtained by comparing TL produced per unit of beta and alpha doses.The used attenuation factors μ_x of the β outer dose corresponding to the grain size interval of the dated brick varying, by microscopy observation, from 200 µm-315 µm are given in reference [3]. q is a correction factor given by:

$$q = \frac{LET_{av}(Quartz)}{LET_{av}(Humid\ matrix)} = \frac{LET_{av}\left(SiO_2\right)}{\sum_i \rho_i LET_{av}(i)}, \tag{5}$$

where LET_{av} is the average linear energy transfer, ρ_i is the mass fraction of any given oxide i in the matrix.

The theory and practice of the used dating procedure is completely described in our previous work [3].

Experimental

Samples collection and dating by thermoluminescence

In this work, a terra-cotta brick fragment taken from different areas from *Cuicul* Roman archaeological city was dated by TL technique. The necessary geographic coordinates of the archaeological site and the burial depth of the dated brick requested for cosmic dose determination are presented in Table 2.

For the samples preparation, the same experimental procedure based on the use of HCl, H_2O_2 and HF, described in our previous work, is used [3]. Time controlling grain sedimentation procedure in acetone (~0.8 g/cm^3) allow separation of polymineral fine grains fraction in the range of 1–8 µm which were deposited onto stainless steel disks. The necessary artificial thermoluminescence signals were induced by the ^{90} sr-^{90}Y calibrated beta source integrated in the Risø system delivering 0.1 Gy/s. In this work, the RisøTL/OSL-DA-20 luminescence reader was used [30]. The TL signals were all collected under the same experimental conditions presented in Table 3.

The experimental procedure for determining the relative water content h was also described in kharfi el al. [3]. For the determination of the effective alpha contribution k_α the used grain disks for beta equivalent dose determination (ED_β) are exposed to 3, 6, and 12 Gy alpha dose delivered by a calibrated ^{241}Am alpha source (45 mGy/s). Thus k_α is determined as a ration of the equivalent beta dose (ED_β) to

Table 2 Necessary geographic and burial data for cosmic dose

Site	Geographic Coordinates and burial depth of the brick	
Cuicul (Djémila), Setif, Algeria	Latitude	36.3°
	Longitude	5.7°
	Altitude	900 m
	Burial depth	0 m

Table 3 Conditions of TL signals reading

Luminescence reading mode	Thermoluminescence
Maximum reading temperature	450 °C
Heating rate	5 °C/s
Preheating	230°/10 s
TL signal sampling	250 points over the range 0 to 450 °C
Analyzed sample weight	2 mg
Regeneration	2 h at 450 °C

the equivalent alpha dose (ED_α). However, the determination of the Uranium-238 (^{238}U), the Thorium-232 (^{232}U) and Potassium-40 (^{40}K) mass fractions in the matrix (terra-cotta) was performed by high resolution gamma spectrometry following the same procedure described in [3]. Indeed, a Canberra High-Purity Germanium (HPGe) well detector with a relative efficiency of 40% was used for γ-photon detection.

Finally, in-situ annual dose rate was also determinate by the use of TLD-200 (CaF_2: Dy) dosimeters positioned inside the wall for six month and at the exact position from where the dated bricks were taken. The TLDs were covered by the remaining brick fragments not used for TL signal reading in order to reproduce the same exposure conditions.

Brick's terra-cotta chemical composition determination

In this work, a Rigaku ZSX primus wave diffractive X-ray fluorescence spectrometer was used for the elemental analysis of the sample and thus the determination of the mass fraction of SiO_2 and the oters necessary oxydes. Thus, after a drying phase at 100 °C for 24 h, the samples were ground and screened at ~ 50 µm. To analyze powder samples, the briquette method was used, in which the obtained powder is pressed at 200 kN to make a disk which is suitable for the undertaken XRF analysis.

Results and discussion

For each dated brick, three fragments were separately used for the separation of quartz grains and the establishment of the necessary glow growth curves for the determination of the paleodose after determination of the ED_α and I values. Thus, three dates were separately determined and the average value its standard deviation (SD) is reported for each dated brick. Thus, after quartz separation 18 aliquots, subdivided into six (6) groups, were used for the determination of the paleodose through TL signals collection and growth curves establishment. The plateau test was performed using two (2) additional aliquots. The TL growth curves were obtained by varying the additive Beta dose between 2 and 12 Gy with a 2 Gy step. The checked plateau for an additive Beta dose of 6 Gy demonstrates well that it is necessary to consider the TL glows in the temperature interval of 260–370 °C and this for the growth curves establishment and therefore for the determination of the paleodose. The X-ray fluorescence analysis data requested for the determination of the annual dose are presented in Table 4. *LET* data are taken from reference [31].

The k_α-value, which is the ration between the ED_β and the ED_α, was calculated as 0.100 ± 0.015 (~ 0.1) for all studied bricks. The q factor values were calculated on the basis Table 4 data for all dated bricks (0.99–1.01). The mass fractions of ^{238}U and ^{232}Th measured by γ spectrometry, the K2O concentration (%), the average archaeological dose (paleodose) and annual dose, and the corresponding date (age) are presented in Table 5.

From the above obtained data (Table 5), the city construction and development timeline map is established (Fig. 2).

The established time lie map with the different mentioned dates gives satisfaction because it fits well with some historically known period and events which closely related to some building and temples construction. It is very important to mention, that with the assistance of archeologists, the selection of dated bricks was thoroughly performed by ensuring that there is no doubt about their original fixation on the walls. Although all our precautions, few selected samples (bricks) gave not consistent dates with the aforementioned period and were therefore excluded from this study. The non-consistency is maybe due to some well-done recent site restoration with non-orginal bricks. No evidences were found concerning the reuse of bricks from destructed walls in the construction of a new ones during the city life.

The timeline map demonstrates that the veteran's houses, which constitute the primitive colony, were constructed until the end of first century at the east of main cardo down street. At the beginning of the second century, to the first modest veterans houses succeeded much larger houses equipped with baths, fountains, and moldings in mosaics such as the house of the Donkey (108 A.D.) and the house of Europe (122 A.D.). The city was also centered on some kind forum sometimes called the old forum (square between zone 8 and 10 of Fig. 1). The square place serving as forum was all surrounded by public buildings such as the Curia, the temple with triple sanctuaries, the basilica of justice and civil affairs, the temple of Venus Genetrix (137 A.D.), and the Cosinius brothers market (180 AC). The city then grew and developed through its extension to the south along three main axes: Central (main cardo), Eastern, and Western. One house of the eastern street is dated in 186 A.D.. Thus, with the increase in the population, the southern suburban area was being built, and the center of urban activity tended to move towards the South. This movement resulted in the

Table 4 X-ray fluorescence analysis results and used *LET*s for *q* factor calculation

Sample	Oxide mass fraction (%)										
	SiO_2	Al_2O_3	Fe_2O_3	CaO	MgO	Na_2O	K_2O	P_2O_5	TiO_2	MnO	H_2O^*
1A	53.50 ± 0.03	11.80 ± 0.02	13.67 ± 0.01	7.10 ± 0.01	2.89 ± 0.02	0.25 ± 0.02	1.08 ± 0.005	0.39 ± 0.004	1.00 ± 0.02	0.04 ± 0.005	8.28 ± 0.02
1B	53.50 ± 0.03	11.80 ± 0.02	13.67 ± 0.01	7.10 ± 0.01	2.89 ± 0.02	0.25 ± 0.02	1.08 ± 0.005	0.39 ± 0.004	1.00 ± 0.02	0.04 ± 0.005	8.28 ± 0.02
1C	53.50 ± 0.03	11.80 ± 0.02	13.67 ± 0.01	7.10 ± 0.01	2.89 ± 0.02	0.25 ± 0.02	1.08 ± 0.005	0.39 ± 0.004	1.00 ± 0.02	0.04 ± 0.005	8.28 ± 0.02
2A	49.50 ± 0.03	17.50 ± 0.02	8.72 ± 0.01	10.10 ± 0.01	1.38 ± 0.02	0.45 ± 0.02	1.73 ± 0.005	0.25 ± 0.004	1.00 ± 0.02	0.04 ± 0.005	9.33 ± 0.02
2B	49.50 ± 0.03	17.50 ± 0.02	8.72 ± 0.01	10.10 ± 0.01	1.38 ± 0.02	0.45 ± 0.02	1.73 ± 0.005	0.25 ± 0.004	1.00 ± 0.02	0.04 ± 0.005	9.33 ± 0.02
2C	47.20 ± 0.03	12.90 ± 0.02	15.96 ± 0.01	9.60 ± 0.01	2.30 ± 0.02	0.35 ± 0.02	1.50 ± 0.005	0.35 ± 0.004	0.99 ± 0.02	0.04 ± 0.005	8.81 ± 0.02
2D	47.20 ± 0.03	12.90 ± 0.02	15.96 ± 0.01	9.60 ± 0.01	2.30 ± 0.02	0.35 ± 0.02	1.50 ± 0.005	0.35 ± 0.004	0.99 ± 0.02	0.04 ± 0.005	8.81 ± 0.02
2F	47.20 ± 0.03	12.90 ± 0.02	15.96 ± 0.01	9.60 ± 0.01	2.30 ± 0.02	0.35 ± 0.02	1.50 ± 0.005	0.35 ± 0.004	0.99 ± 0.02	0.04 ± 0.005	8.81 ± 0.02
2G	54.30 ± 0.03	14.07 ± 0.02	6.16 ± 0.01	5.97 ± 0.01	3.18 ± 0.02	1.44 ± 0.02	1.85 ± 0.005	0.28 ± 0.004	0.74 ± 0.02	0.05 ± 0.005	11.96 ± 0.02
3A	54.30 ± 0.03	14.07 ± 0.02	6.16 ± 0.01	5.97 ± 0.01	3.18 ± 0.02	1.44 ± 0.02	1.85 ± 0.005	0.28 ± 0.004	0.74 ± 0.02	0.05 ± 0.005	11.96 ± 0.02
4A	47.20 ± 0.03	17.90 ± 0.02	15.96 ± 0.01	12.60 ± 0.01	2.30 ± 0.02	0.35 ± 0.02	1.50 ± 0.005	0.35 ± 0.004	0.99 ± 0.02	0.04 ± 0.005	8.81 ± 0.02
5A	49.50 ± 0.03	17.50 ± 0.02	8.72 ± 0.01	10.10 ± 0.01	1.38 ± 0.02	0.45 ± 0.02	1.73 ± 0.005	0.25 ± 0.004	1.00 ± 0.02	0.04 ± 0.005	9.33 ± 0.02
6A	54.30 ± 0.03	14.07 ± 0.02	6.16 ± 0.01	5.97 ± 0.01	3.18 ± 0.02	1.44 ± 0.02	1.85 ± 0.005	0.28 ± 0.004	0.74 ± 0.02	0.05 ± 0.005	11.96 ± 0.02
6B	54.30 ± 0.03	14.07 ± 0.02	6.16 ± 0.01	5.97 ± 0.01	3.18 ± 0.02	1.44 ± 0.02	1.85 ± 0.005	0.28 ± 0.004	0.74 ± 0.02	0.05 ± 0.005	11.96 ± 0.02
7A	47.50 ± 0.03	10.90 ± 0.02	19.50 ± 0.01	8.16 ± 0.01	2.30 ± 0.02	0.40 ± 0.02	1.50 ± 0.005	0.40 ± 0.004	1.00 ± 0.02	0.04 ± 0.005	8.3 ± 0.02
8A	47.50 ± 0.03	10.90 ± 0.02	19.50 ± 0.01	8.16 ± 0.01	2.30 ± 0.02	0.40 ± 0.02	1.50 ± 0.005	0.40 ± 0.004	1.00 ± 0.02	0.04 ± 0.005	8.3 ± 0.02
8B	46.10 ± 0.03	10.25 ± 0.02	23.15 ± 0.01	7.56 ± 0.01	1.90 ± 0.02	0.50 ± 0.02	1.62 ± 0.005	0.45 ± 0.004	1.05 ± 0.02	0.04 ± 0.005	7.38 ± 0.02
8C	46.10 ± 0.03	10.25 ± 0.02	23.15 ± 0.01	7.56 ± 0.01	1.90 ± 0.02	0.50 ± 0.02	1.62 ± 0.005	0.45 ± 0.004	1.05 ± 0.02	0.04 ± 0.005	7.38 ± 0.02
9A	46.10 ± 0.03	10.25 ± 0.02	23.15 ± 0.01	7.56 ± 0.01	1.90 ± 0.02	0.50 ± 0.02	1.62 ± 0.005	0.45 ± 0.004	1.05 ± 0.02	0.04 ± 0.005	7.38 ± 0.02
10A	47.20 ± 0.03	12.90 ± 0.02	15.96 ± 0.01	9.60 ± 0.01	2.30 ± 0.02	0.35 ± 0.02	1.50 ± 0.005	0.35 ± 0.004	0.99 ± 0.02	0.04 ± 0.005	8.81 ± 0.02
10B	47.20 ± 0.03	12.90 ± 0.02	15.96 ± 0.01	9.60 ± 0.01	2.30 ± 0.02	0.35 ± 0.02	1.50 ± 0.005	0.35 ± 0.004	0.99 ± 0.02	0.04 ± 0.005	8.81 ± 0.02
$LET_{av}(i)$ (MeV g^{-1} cm^{-2})	1.71	1.67	1.54	1.66	1.70	1.65	1.61	1.69	1.58	1.50	2.03

*Calculated mass fraction

Table 5 γ-spectrometry analysis results, measured paleodose and annual dose, and the corresponding determined date (age) of the studied bricks

Zone	Sample no	Mass fraction and concentration			Dose		Date (A.D.±SD*)
		U (mg kg^{-1})	Th (mg kg^{-1})	$K_2O^{\#}$ (%)	Average paleodose (Gy)	Average annual dose (mGy)	
1	1A	2.15 ± 0.08	7.9 ± 0.20	1.08 ± 0.05	5.90 ± 0.25	3.54 ± 0.15	352 ± 30
	1B	2.15 ± 0.08	7.9 ± 0.20	1.08 ± 0.05	5.91 ± 0.20	3.54 ± 0.15	349 ± 27
	1C	2.15 ± 0.08	7.9 ± 0.20	1.08 ± 0.05	5.92 ± 0.18	3.54 ± 0.15	346 ± 25
2	2A	2 ± 0.08	7.8 ± 0.20	1.73 ± 0.05	5.60 ± 0.22	3.48 ± 0.12	409 ± 30
	2B	2 ± 0.008	7.8 ± 0.20	1.73 ± 0.05	5.62 ± 0.22	3.48 ± 0.12	404 ± 30
	2C	1.95 ± 0.08	7.8 ± 0.20	1.50 ± 0.05	5.75 ± 0.19	3.48 ± 0.12	365 ± 25
	2D	1.95 ± 0.08	7.8 ± 0.20	1.50 ± 0.05	5.80 ± 0.30	3.48 ± 0.12	352 ± 30
	2F	1.95 ± 0.08	7.8 ± 0.20	1.50 ± 0.05	5.78 ± 0.29	3.48 ± 0.12	358 ± 30
	2 g	2.2 ± 0.08	8 ± 0.20	1.85 ± 0.05	5.85 ± 0.20	3.54 ± 0.15	366 ± 28
3	3A	2.2 ± 0.08	8 ± 0.20	1.85 ± 0.05	6.03 ± 0.22	3.54 ± 0.15	316 ± 25
4	4A	1.9 ± 0.08	7.85 ± 0.20	1.50 ± 0.05	5.95 ± 0.34	3.47 ± 0.12	304 ± 28
5	5A	2 ± 0.008	7.8 ± 0.20	1.73 ± 0.05	6.39 ± 0.34	3.48 ± 0.12	182 ± 16
6	6A	2.2 ± 0.08	7.8 ± 0.20	1.85 ± 0.05	6.38 ± 0.32	3.51 ± 0.14	201 ± 18
	6B	2.2 ± 0.08	8 ± 0.20	1.85 ± 0.05	6.35 ± 0.29	3.54 ± 0.15	225 ± 20
7	7A	1.95 ± 0.08	7.75 ± 0.20	1.50 ± 0.05	6.36 ± 0.29	3.47 ± 0.12	186 ± 15
8	8A	1.95 ± 0.08	7.75 ± 0.20	1.50 ± 0.05	6.67 ± 0.44	3.47 ± 0.12	97 ± 10
	8B	1.92 ± 0.08	7.75 ± 0.20	1.62 ± 0.05	6.65 ± 0.40	3.48 ± 012	108 ± 10
	8C	1.92 ± 0.08	7.75 ± 0.20	1.62 ± 0.05	6.55 ± 0.36	3.48 ± 0.12	137 ± 12
9	9A	1.92 ± 0.08	7.75 ± 0.20	1.62 ± 0.05	5.75 ± 0.27	3.48 ± 0.12	367 ± 30
10	10A	1.95 ± 0.08	7.8 ± 0.20	1.50 ± 0.05	6.40 ± 032	3.48 ± 0.12	180 ± 15
	10B	1.95 ± 0.08	7.8 ± 0.20	1.50 ± 0.05	6.60 ± 0.32	3.48 ± 0.12	122 ± 10

[#]The concentration of ^{40}K is 0.01167% in natural Potassium K

**SD* standard deviation

construction of a new forum. The monument and building dated in this aera, Septum temple (225 A.D.) and civil basilica (201 A.D.), reveals that the construction of this forum was mainly during the first third of the third century. If the dates already determined seem to follow certain logic in the development of the city, the construction date of the great baths is problematic. Indeed, the determined date (182 A.D.) is countered because the baths are located at a distance from the south limit of the old center of the city. This implies that the great baths were built before the new forum of the city and that an area between the thermal baths and the old city was left empty. This controversy remains inexplicable in the context of this study because it is not acceptable to consider any reuse of bricks for the construction of all these baths. However, it is just possible to consider that these baths are built before the new forum for reasons depending on its location which should be better for the connection of the baths to the underground water and for water evacuation after use. A second possible reason is regarding the existence of a pre-established plan for the development of the city involving certain priorities in the construction of buildings and monuments, and therefore the choice of their implementation places. It should be reminded that *Cuicul* was constructed on a spur of land created by two mountain rivers and surrounded by rolling hills with some irregularity making the availability and the choice of construction areas difficult. Finally, at the southeastern end of the city was the last phase of the city construction which coincides with the Christian period. All dated house and building (House of Bacchus, House of Bishop, Private house, Church, Basilica and Baptistery) are between 304 A.D. and 409 A.D.. The Christian basilica (367 A.D.) was first constructed at the west limit of the western street (zone N°9) just before the ramparts. According to our study results, the *Cresconius* cathedral was constructed between 404 A.D. and 409 A.D. at the northern limit of the Christian street probably because of the designation of the bishop and the increase of the Christian population. *Cresconius* was the Catholic bishop who represented *Cuicul* at the Council of Carthage (411 A.D.) between Catholic and Donatist bishops [32]. This confence held on the 1st of June 411 A.D., with a view of uniting the Donatists to the Church, and convincing them of the necessity of seeking for salvation in the Catholic Church. In 411 Donatism was declared a heresy by Emperor *Honorius* who endorsed the outcome of a council held at Carthage [32]. In this context *Cresconius*, Bishop of Cuicul, decided to build a

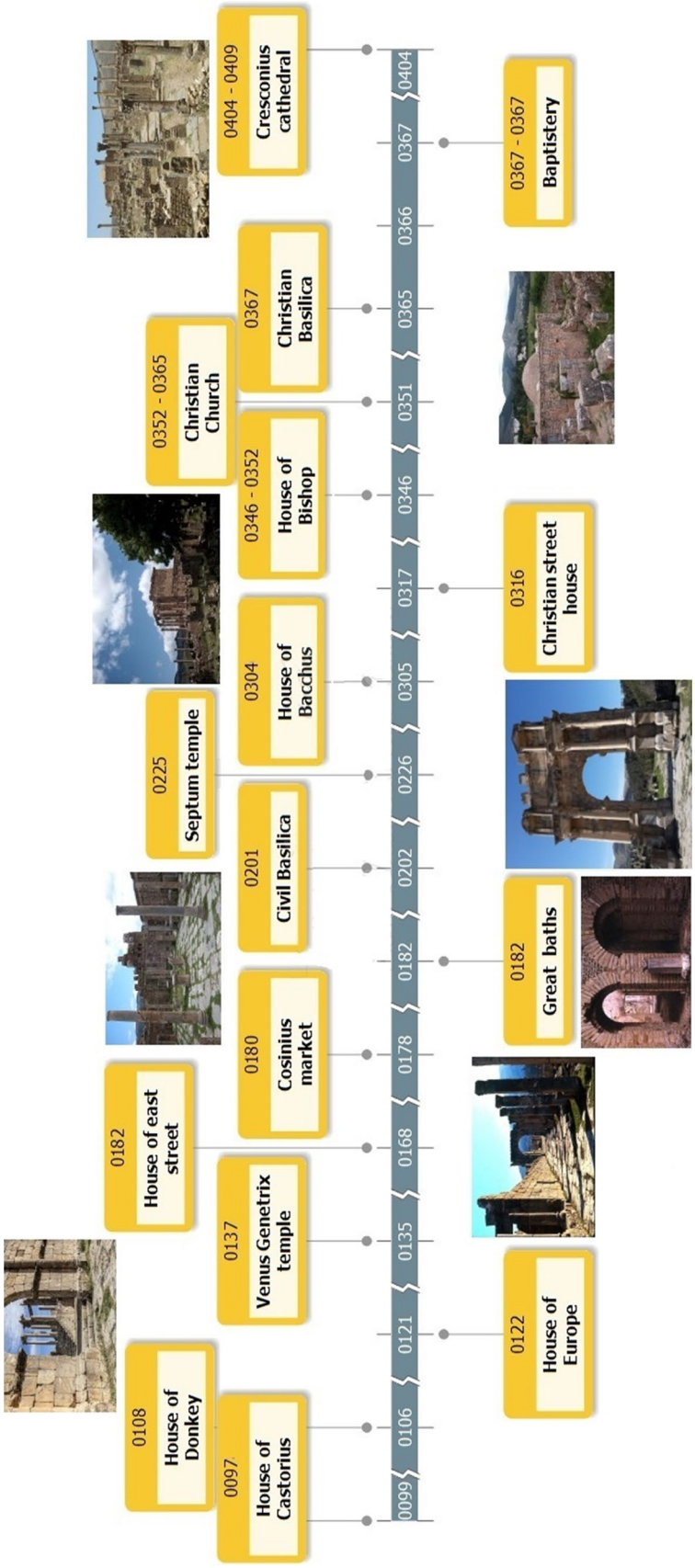

Fig. 2 Fig. 2 Estblished timeline map of *Cuicul* constrcution development showing main dated places, monuments and buildings (all dates are A.D.)

very large church where all the Christians of the town could gather. Allthough the TL dated construction period of this new basilica (404–409 A.D.) is slightly before this construction decision date (411), the TL dating results remain very accurate and significative with such known and confirmed historical events [32].

Conclusions

In this work, a timeline map was establsihed presenting construction dates of the major parts of *Cuicul* (Djémila) roman city by thermoluminescence technique. Accurtate construction dates were obtained through the optimization of the different dating steps strating from bricks selection and quartz separation until TL signal reading and TL growth curves establisment. By ensuring the supralinearity of TL growth curves and also by perfoming all the necessary corrections on dose, the determined ages and dates were with acceptable standards deviations. The strategy of dividing the site into different zones was carefully carried out on the basis of topographical observations and by consulting expert archaeologists. The importance of this study is related to fact that it was made possible to place the different phases of *Cuicul* construction in a scientifically proven chronological order. This will certainly allow archaeologists and histoirians to confirm or to reject certain hypothesis in relation with the construction of certain buildings and with the whole development of the city between the first and fifth centuries.

Acknowledgements Pr. F. Kharfi, the principal investigator of this project, and his team would like to thank the Director of Djelima Museum and his staff for their kind assistance in the achievement of this project. We also thank the general direction of scientific research and technological development (DGRSDT) of the Algerian higher education and scientific research ministry. This research was undertaken in the framework of a university research and formation project (PRFU: B00L02UN190120190008).

Compliance with ethical standards

Conflict of interest The authors declare that they have no conflict of interest.

References

1. https://whc.unesco.org/fr/list/191/. Accessed 19 March 2018
2. UNESCO (2000) Roman Art in Africa, World Heritage N°16
3. Kharfi F, Boudraa L, Benabdelghani I, Bououden M (2019) TL dating and XRF clay provenance analysis of ancient brick at Cuicul Roman city, Algeria. J Radioanal Nucl Chem 320:395–403
4. Dussaud R, Louis L (1954) Djemila, antique Cuicul. In: Syria, Tome 31, fascicule 3–4: 338–339
5. Dupuis X (2001) Les origines de la colonie de Cuicul. In: Bulletin de la Société Nationale des Antiquaires de France, 2001/2006: 151–161. https://doi.org/10.3406/bsnaf.2006.10521
6. Cagnat R (1916) Djemla colonnie militaire de Nevra, CRAI: 593–599
7. Akli Ikherbane M (2003) Le site archéologique de Djemila, l'antique *Cuicul*: Éventail d'actions possibles. Les Dossiers d'archéologie (Dijon) A286:26–31
8. Allais Y (1953) Le quartier à l'Est du Forum des Sévères. Revue Africaine XCVII: 48–65
9. Allais Y (1971) Le quartier Occidental de Djemila (Cuicul). Antiquités Africaines 5:95–119
10. Dessales H (2018) Petit catalogue des techniques de la construction romaine, Ecole Normale Supérieure ENS/CNRS, Paris, France. http://www.archeologiesenchantier.ens.fr/spip.php?article30. Accessed 17 Aug 2019
11. Adam JP (2017) la construction romaine- matériaux et techniques, 7th edn. Picard, Paris
12. Strickland M (2010) Roman building materials, construction methods, and architecture: the identity of an empire. Thesis, Clemson University. All Theses. 909. https://tigerprints.clemson.edu/all_theses/909. Accessed 17 Aug 2019
13. Fernandes FM, Lourenço PB, Castro F (2009) Ancient clay bricks: manufacture and properties. In: Bostenaru Dan M et al (eds) Materials, technologies and practice in historic heritage structures. Springer, Berlin. https://doi.org/10.1007/978-90-481-2684-2
14. Stalley R (1999) Early Medieval Architecture. Oxford University Press, USA, pp 112–114. ISBN 0-19-284223-4.]
15. Aitken MJ (1970) Dating by archaeomagnetic and thermoluminescent methods. Philos Trans R Soc Lond Ser A Math Phys Sci 269(1193):77–88
16. Zimmerman DW, Huxtable J (1969) Recent applications and developments in thermoluminescent dating. Archaeometry 11:105–108
17. Veronese I, Goksu HY, Schwenk P, Herzig F (2008) Thermoluminescence dating of a mikveh in Ichenhausen, Germany. J Environ Radioact 99:621–630
18. Kondopoulou D, Aidona E, Ioannidis N, Polymeris GS, Tsolakis S (2015) Archaeomagnetic study and thermoluminescence dating of Protobyzantine kilns (Megali Kypsa, North Greece. J Archaeol Sci Rep 2:156–168
19. Yeea KP, Mob RH (2018) Thermoluminescence dating of stalactitic calcite from the early Palaeolithic occupation at Tongamdong site. J Archaeol Sci Rep 19:405–410
20. Sears DWG, Sears H, Sehlke A, Hughes SS (2018) Induced thermoluminescence as a method for dating recent volcanism: Hawaii County, Hawaii, USA. J Volcanol Geotherm Res 349:74–82
21. Sabtu SN (2015) Thermoluminescence dating analysis at the site of an ancient brick structure at Pengkalan Bujang, Malaysia. Appl Radiat Isot 105:182–187
22. Temaa E, Polymerisc G, Moralesd J, Goguitchaichvilid A, Tsaknakie V (2015) Dating of ancient kilns: a combined archaeomagnetic and thermoluminescence analysis applied to a brick workshop at Kato Achaia, Greece. J Cult Heritage 16:496–507
23. Aitken MJ (1974) Physics and archaeology. Clarendon Press, Oxford, pp 26–84
24. Zimmerman DW (1971) Thermoluminescent dating using fine grains from pottery. Archaeometry 13:29–52
25. Aitken MJ (1985) Thermoluminescence dating. Academic Press, London
26. Mejdahl V (1979) Thermoluminescence dating: beta dose attenuation in quartz grains. Archaeometry 21:61–72
27. Mejdahl V (1987) Internal radioactivity in quartz and feldspar grains. Ancient TL 5(2):10–17

28. Pilleyre T (1991) Datation par thermoluminescence: Application à la chronologie des retombées volcaniques. Thèse de doctorat de l'université Blaise Pascal - Clermont II. Clermont-Ferrand, France
29. Bassinet C (2007) Datation par luminescence: recherches méthodologiques et applications au volcanisme dans l'environnement de Laschamp. Thèse de doctorat de l'université Blaise Pascal- Clermont-Ferrand II, Françe. tel-00171318
30. Kharfi F, Ketfi R (2018) Irradiated black pepper identification based on thermoluminescence of silicate minerals. J Radioanal Nucl Chem 315:503–507
31. Pilleyre T, Montret M, Fain J, Miallier D, Sanzelle S (1992) Attempts at dating ancient volcanoes using the red TL of quartz. Quatern Sci Rev 11:13–17
32. Manual of Councils of the Holy Catholic Church -Rev. Edward H, Landon MA https://www.ecatholic2000.com/councils2/untitled-06.shtml. Accessed 5 Sept 2019

Abstract: The main objectives of this thesis project are the thermoluminecence dating and the reconstruction of a chronological map (timeline map) relating to the construction of the ancient Roman city "*Cuicul-Djemila*" located at about fifty kilometers north-east of the city of Setif. The archaeological dating was carried out by the technique of thermoluminecence on terra-cotta bricks. The source of the raw material used in the manufacture of bricks (clay) taken from a wall near the famous Caracalla's arch was also studied using the X-ray Fluorescence technique (XRF). The dating results reveal dates that fit well into the historical context of construction and development of the city between the second and the sixth centuries before falling into oblivion from the middle of the 6th century (A.D.). The statistical comparison of the XRF data between the compositions of the terra-cotta used in the manufacture of a brick with the clays of deposits located around the city allows the identification of the deposit probably used for the fabrication of bricks of a wall located at ~25 meters from Caracalla's arch (211-217 A.D.). The same wall was dated by thermoluminecence in 198 A.D. Finally, a construction development timeline map of *Cuicul* was established by thermoluminescence dating.

Keywords: Cuicul, Archaeological dating; Thermoluminescence; Chronological map; Clay.

Résumé : Les principaux objectifs de ce projet de thèse sont la datation par thermoluminecence et la reconstitution d'une carte chronologique relative à la construction de la cité romaine antique « *Cuicul-Djemila* » située à une cinquantaine de kilomètres au nord-est de la ville de Sétif. La datation archéologique a été effectuée par la technique de thermoluminecence sur des briques à base de terre-cuite. La provenance de la matière brute utilisée dans la fabrication des briques (argile) d'un mur, situé à proximité du fameux arc de Caracalla, a été aussi étudiée en utilisant la technique de Fluorescence X (XRF). Les résultats de la datation révèlent des dates qui s'inscrivent bien dans le contexte historique de la construction et du développement de la cité entre le second et cinquième siècle avant de tomber dans l'oubli à partir du milieu du 6ème siècle (ap. J.-C.). La comparaison statistique des données XRF entre la composition de la terre-cuite utilisée dans la fabrication d'une brique avec les argiles de gisements repérés aux alentours de la cité a permis d'identifier le gisement probablement utilisé dans la fabrication des briques du mur situé à ~25 mètres de l'arc de *Caracalla* (211-217 ap. J.-C). Le même mûr est daté par thermoluminescence en 198 ap. J.-C.

Mots-clés : Cuicul, Datation archéologique ; Thermoluminescence ; Carte chronologique ; Argile.

ملخص: أهداف مشروع هذه الأطروحة هي التأريخ عن طريق التوهج الحراري وإعادة بناء خريطة زمنية تتعلق ببناء المدينة الرومانية القديمة "كيوكول - جميلة" الواقعة على بعد حوالي خمسين كيلومترا شمال شرق مدينة سطيف. تم تنفيذ التاريخ الأثري من خلال تقنية التوهج الحراري على الطوب المصنوع من الطين. كما تمت دراسة مصدر المواد الخام المستخدمة في تصنيع الطوب (الطين) لجدار بالقرب من قوس كاراكالا الشهير باستخدام تقنية وميض الأشعة السينية (XRF). تكشف نتائج التاريخ عن تواريخ تتناسب جيدا مع السياق التاريخي لبناء وتطور المدينة بين القرنين الثاني والخامس قبل الوقوع في النسيان ابتدءا من منتصف القرن السادس (ب.م). مكنت المقارنة الإحصائية لبيانات XRF بين تركيبة الطين المستخدمة في تصنيع الطوب مع تركيبة الرواسب الموجودة في جميع أنحاء المدينة المكان المحتمل لاستخراج الطين المستعمل في تصنيع طوب الحائط الموجود على بعد حوالي 25 مترا من قوس كاراكالا (211-217 ب.م). يعود تاريخ نفس الحائط المحدد بالتوهج الحراري الى 198 ب. م.

كلمات مفتاحيه : كويكول، التأريخ الأثري، التوهج الحراري، خريطة زمنية ، طين.